# ELECTRICAL BREAKDOWN CHARACTERISTICS OF SULFUR HEXAFLUORIDE

by

TOHEI NITTA

Central Research Laboratory

Mitsubishi Electric Corporation

CORRECTIONS IN "ELECTRICAL BREAKDOWN CHARACTERISTICS OF SULRUR HEXAFLUORIDE"

| page | line | wrong | correct |
|---|---|---|---|
| i | 24 | concerns | is concerned |
| 2 | 13 | convention | convection |
| 5 | 5 | that of | those of |
| 7 | 5 | a certain | certain |
| 10 | 4 | regardless | regardless of |
| 11 | 11 | criterion 10 | criterion in equation 10 |
| 16 | 1 | sphere gap | sphere gaps |
| 24 | Title | EXPERIMENTS [45] | EXPERIMENTS [47] |
| 30 | 2 | discharge voltage | discharge voltages |
| 35 | 20 | Fig. 1-7 | Fig. 1-6 |
| 36 | 13 | Corona Stabilized | corona stabilized |
| 41 | 10 | exceed | exceeds |
| 49 | 30 | the order of two | three or four times |
| 50 | 1 | the number of weak points is | these irregularities are |
| 51 | 3-4 | of the order of two | three or four times |
| 53 | 19 | As the | As a |
| 55 | 20 | constant | a given |
| 56 | 11 | seems | seem |
| 57 | 3 | protrusion | protrusions |
| 57 | 5 | protrusion | protrusions |
| 59 | 23 | weight | weights |
| 66 | Fig. 43, | bottom picture | (b) Gap E |
| 70 | 8 | about the order of two | three or four times |
| 72 | Title | IN $SF_6$ | IN SF6 [83, 85] |
| 73 | 21 | concerns | is concerned |
| 81 | 14 | various pressure | various pressures |
| 82 | 32 | phenomena | phenomenon |
| 83 | 20 | weak point | weak points |
| 86 | 12 | pressure | pressures |
| 89 | 19 | Fig. 60 is | Fig. 60 Shows |
| 91 | 8 | Gap E | Gap G |
| 91 | 9 | strength | strength of this gap |
| 98 | 11 | phenomena | phenomenon |
| 103 | 4-5 | phenomena | phenomenon |
| 103 | 13 | substation | substaions |
| 109 | 29 | coroan | corona |
| 117 | 5 | characteristic | characteristics |
| 119 | 1 | presented | which is presented |
| 129 | 6 | polots | plots |
| 131 | 14 | phenomena | phenomenon |
| 131 | 18 | concerns | is concerned |
| 145 | 6 | Kyot | Kyoto |
| 149 | 24 | coincide | coincides |
| 161 | 6 | differentiate | differentiating |
| 162 | 10 | differentiate | differentiating |
| 166 | 1 | satisfy | satisfies |

# ELECTRICAL BREAKDOWN CHARACTERISTICS OF SULFUR HEXAFLUORIDE

by

TOHEI NITTA

Central Research Laboratory
Mitsubishi Electric Corporation

August 1974

## ABSTRACT

Breakdown characteristics of compressed $SF_6$ are studied theoretically and experimentally. The results are formulated so that they are useful in the insulation design of $SF_6$ gas insulated equipments.

In Chapter II, the distinguishing traits of the ionization processes in $SF_6$ are briefed and the criterion of the electrical discharge of the gas is formulated based on the single avalanche streamer mechanism. Strong dependence of the ionization and electron attachment coefficients of $SF_6$ on electric field simplifies the formulation very much. As a result of the simplification, the maximum field strength at the discharge inception or the breakdown of an arbitrary gap in $SF_6$ is expressed as a simple function of gas pressure and the geometrical shape of the gap. Some important properties which characterize $SF_6$ gas out of common gases such as air and nitrogen, are deduced theoretically by this formulation of the discharge criterion.

In Chapter III, these theoretical conclusions on the discharge characteristics of $SF_6$ are compared with the results of ac and dc experiments. It was shown that the theory explains the experimental results very well at low gas pressures where the discharge characteristic is a pure representative of the property of sample gas. At high gas pressures, however, the discharge characteristic is governed not only by the property of $SF_6$ gas but also, more or less, by the property of electrode. Experimental breakdown voltage is lower than the theoretical estimation under the effect of the electrode. The discharge characteristics at this high pressure condition are found to be influenced by the surface roughness and the area of the negative electrode.

The effect of electrode surface is studied in Chapter IV. Microscopic irregularities or protrusions on the electrode enhance the electric field at the very vicinities of them. As far as the electron multiplication process in the enhanced field concerns, the effect of the protrusions on the breakdown voltage is appreciable only when the height of the protrusion exceeds a critical value of the order of $10\mu$ which is a function of the gas pressure. When the effect of the electrode surface is appreciable on the discharge characteristics of a gap, very low prebreakdown dark current of the order of $10^{-9}$ to $10^{-5}$ A is observed experimentally dependeing on the gap condition. Breakdown of the gap under the effect of electrode follows one of the pulsative dark current which attributed to the effect of a protrusion on the electrode. Since large electrode has more irregularities

statistically, the effect of the area of the stressed part of the electrode on the breakdown characteristics is suggested in this chapter.

The result of the study on the statistical distribution of the breakdown voltages and the effect of the electrode area are presented in Chapter V. Statistical distribution of the breakdown voltages of $SF_6$ obeys Weibull distribution rather than normal distribution under the effect of the electrode surface. The fact shows that the breakdown is governed by the statistical properties of the weak points in the gap, as expected. The critical condition whether the breakdown characteristic of a gap is influenced by the electrode or not is determined as a function of gas pressure and the area of the stressed part of the negative electrode. As the result of the statistical study of the area effect of $SF_6$, the reduction of the breakdown voltage from the theoretical estimation is explained quantitatively so that the insulation design of a practical gas insulated equipment could be done using the results of small scale laboratory experiments.

In Chapter VI, voltage-time characteristic of the breakdown in $SF_6$ is studied for impulse and switching surge applied voltages. The characteristic is classified into three patterns depending on the gap configuration and gas pressure. The criterion that the breakdown characteristic of a gap is classified into one of these patterns and the detailed properties of the V–t characteristic of each of these patterns are presented. The results are generalized as a semi-empirical formula which will be useful in the quantitative evaluation of the insulation co-ordination and the abnormal voltage protection of $SF_6$ gas insulated power equipments.

CONTENTS

ABSTRACT

CONTENTS

# I. INTRODUCTION

## §1. $SF_6$ as Gaseous Dielectric

Sulfur hexafluoride ($SF_6$) was first introduced by Moissan and Lebeau in 1900 when they burned sulfur in fluorine. [1] The sulfur burned with a "livid flame", and the gas product was found not to attack glass in spite of its rich fluorine content. Studies showed that the gas is quite stable chemically and does not react even if it is heated in the presence of various materials. The gas was only partly destroyed by electric arcing.

It was not until 1937, though, that Charlton and Cooper pointed out the high dielectric strength of the gas. [2] In 1938, Cooper applied for U.S. pattent on the use of $SF_6$ as a gaseous dielectric. [3] $SF_6$ gas has been produced commercially since 1947 in the United States and later in many other countries.

Gases with high molecular weight usually have high dielectric strength. [4] However, whether or not a gas is suitable for electric insulating purposes does not only depend on its dielectric strength but on the following physical and chemical properties. [5, 6]

a. Chemical inertness

The gas should be chemically inert. At least it should not attack the materials commonly used in high voltage equipments up to the highest possible temperature.

b. Low condensation temperature

Condensation temperature of the gas must be low or the vapor pressure at the operating temperature must be high, so that the gas can be used at elevated pressures with high dielectric strength.

c. Non-toxicity

The gas and its chemical products under the normal and abnormal conditions should be non-toxic to assure the safty of the equipment in which the gas is utilized.

d. Thermal conductivity

The gas should have high heat transfer coefficient so as to the heat production in the equipment is effectively removed by the gas.

e. Availability

Of course, the gas has to be readily available and not too expensive.

Among many gases having high dielectric strength, $SF_6$ has almost all the favorable properties as gaseous dielectric and has widely accepted for the insulation of high voltage equipments. [7] The dielectric strength of $SF_6$ is the order of three times higher than that of common gases such as air and nitrogen. The gas is very inert up to 200°C in contact with most materials in high voltage equipments. The vapor pressure is above 7 atm at −20°C. The high vapor pressure at low temperature allows the insulation of an equipment at high gas pressure.

$SF_6$ is non-toxic. However, care must be taken to the decomposition products by electric arcing in the gas. They have moderate toxicity but can be removed effectively by some absorbent. [5]

Most of gases do not transfer heat as well as liquid. Moreover, gases of low molecular weight usually have much higher thermal conductivity than those with high molecular weight. However, $SF_6$ transfers heat mostly by convention and overall heat transfer coefficient is known to be greater than that of helium and hydrogen. [8]

## §2. Applications of $SF_6$ in Power Equipments

The earliest application of compressed $SF_6$ gas insulation was in electrostatic generators and X-ray machines. [9] Then the application is extended to electronics and power industries. [5, 10]

The gas has been widely used over the last 20 years in power circuit breakers. In the application, $SF_6$ gas is used as an insulant as well as an arc quenching medium. As the same kind of application, $SF_6$ lightning arrester is also developed and introduced in the field quite recently. [11]

The gas proved its supreme importance by the recent introduction of high voltage gas insulated power substations. [12–16] While the principal advantage of the gas insulated substations is their compactness, the prefabrication in the factory reduces field installation cost and they may be more economical than conventional stations even exclusive of the saving in space. [17] A great number of $SF_6$ gas insulated substations are now in operation in Japan at the voltage ranging from 60 to 500 kV. [18]

Gas insulated power transmission system is another promissing application of the gas as a dielectric. [19] The system is expedient for very high power transmission. Though the development first started in Japan, [20, 21] the application is particularly accepted

and several systems are in operation in the United States. [22–24]

So far, it can be seen every indication that the demand for all of these gas insulated power systems will continue to increase in the future in Japan and all over the world.

## §3. Scope of the Present Work

These high voltage power systems have been insulated by mineral oil and atmospheric air in conjunction with solid insulation for many years. And as a matter of course, they are designed to give full play to the merits of these insulating materials. Correspondingly, new designs of $SF_6$ gas insulated systems have to be coordinative with the peculier discharge characteristics of compressed $SF_6$ gas arising as a result of the strong electron affinity of the gas ——— the tendency to attach free electrons to form heavy negative ions. Compressed $SF_6$ gas insulation is also special to the old air insulation scheme because the high dielectric strength, hence the high electric field at the electrode surface yields a strong electrode effect on the breakdown characteristics of the medium.

To attain well refined insulation design of these power systems to take the advantage of the properties of $SF_6$, the electrical breakdown of $SF_6$ have been studied experimentally in many laboratories on various electrode configurations.

In the first stage of the study, a great deal of the efforts were stressed on the characteristics of very nonuniform field gaps, whose breakdown voltage has unusual negative slope upon gas pressure. [5, 10, 25–31] Breakdown field strength of uniform field gaps in SF6 were, of course, another point of interest as a basic insulation property of the gas. [32, 33]

Research efforts were extended to more general factors which influence the breakdown characteristics of the gas, such as the shape of the electrode, electrode materials, impurities, applied voltage wave form, breakdown time lags etc. [34–38] A number of data of large scale experiments up to the extra-high-voltage level are now available in public. [39–42]

In spite of all of these research efforts, the understanding of the breakdown characteristics of $SF_6$ is still far from complete. Although a few attempts to formulate breakdown voltages of simple gaps as a function of the geometrical configuration and gas pressure, [43–49] very little has been done to understand and formulate the characteristics of the gas in more general form to be applicable for practical insulation design, neither

on theoretical nor on empirical basis.

The first aim of the present work is to formulate theoretically the electrical discharge characteristics of $SF_6$ in a simple form, so that we can foretell the breakdown characteristics of a given gap of arbitrary geometry. The results of the theoretical approach were testified by laboratory experiments in various test conditions.

The results of the small scale laboratory experiments and their theoretical formulation usually fails to explain the breakdown characteristics of large practical gas insulated equipments. Because of this scale effect, the design of the practical equipments have had to be done by full scale model experiments, although most of these developmental tests are usually not reported in public.

The second aim of the present work is to clarify the basic law which governs the scale effect of the discharge characteristics of $SF_6$ and obtain a theoretical basis to the interpretation of the breakdown characteristics in actual application condition in terms of small scale laboratory test data. The effect of microscopic irregularities which are inevitable on the surface of the electrode are discussed quantitatively by the aid of Weibull statistics as the origin of the scale effect of electrode.

Thirdly, time factor involved in the breakdown process in $SF_6$ is studied as the voltage-time characteristic for impulse and switching surge applied voltages. The results are generalized as a semi-empirical formula which will be useful in the quantitative evaluation of insulation coordination and abnormal voltage protection of $SF_6$ gas insulated power systems.

As a whole, the present work is devoted to formulate the breakdown characteristics of $SF_6$ to be useful for practical application. The mechanism of the breakdown in $SF_6$ is out of the reach of the work and only taken into consideration as the basis of the above formulation.

There are many factors other than the gas and electrodes which will be important in gas insulation, such as the dust particles unavoidable in the enclosure, [50–55] the solid insulating support to hold the live part mechanically from the ground. [38, 40, 56–59] However, the interest of the present work is limited to the breakdown characteristics of pure $SF_6$ without any detectable foreign particles or solid insulation. In the practical design of gas insulated equipments, special care must be taken of these factors.

## II. DISCHARGE PHENOMENA IN $SF_6$ [47]

### §1. Introduction

Gas molecules which have halogen atoms in their structure generally have strong tendency to attach free electrons to form negative ions. Because of this electron affinity, electrical discharge characteristics of $SF_6$ are different from that of common gases.

The primary ionization process in a common gas dielectric is ionization by collision between neutral gas molecules and free electrons accelerated by the applied field. The number of new electron ion pairs increases quite rapidly by this process building up an avalanche of electrons. In an electronegative gas with strong electron affinity, the electrons produced in this collision process are attached by neutral moleculres very easily. Several investigators have studied on the negative ion formation in $SF_6$, a detailed summary is presented by Naidu and Prasad. [60] Most abundant species produced by the attachment process are $SF_6^-$, $SF_5^-$ and $F^-$. $SF_6^-$ is formed as a result of resonance capture process which forms excited ions $(SF_6^-)^*$ which is then stabilized by a collision with a neutral molecule.

$$e + SF_6 \rightleftharpoons (SF_6^-)^* \xrightarrow[SF_6]{} SF_6^-$$

The formation of $SF_5^-$ is by mean of a dissociative attachment process of the form;

$$e + SF_6 \longrightarrow SF_5^- + F$$

The ion $F^-$ is formed in dissociative capture of the type as;

$$e + SF_6 \longrightarrow (SF_5 + F^-),\ (SF_4 + F + F^-)$$

Once the electrons are captured to form these negative ions, they can not gain sufficient energy to ionize neutral molecules. Thus the attachment removes the electrons from the discharge process and tends to prevent the growth of the avalanche.

Geballe and Reeves [33] applied Townsend's mechanism to the breakdown of electronegative gases such as $SF_6$ and obtained the criterion of uniform field breakdown as;

$$\frac{\gamma a}{a - \eta} \left[ exp \left\{ (a - \eta)\, d \right\} - 1 \right] = 1 \qquad (1)$$

From this equation, they showed that the uniform field breakdown voltage has an asymptotic value of E/p and the limiting value is given by the condition;

$$a = \eta \qquad (2)$$

where E is the applied electric field, p gas pressure, $a$ the Townsend's first ionization coefficient, $\eta$ the attachment coefficient of the gas and $\gamma$ is the probability per positive ion of liberating an electron from the cathode. The condition has been verified experimentally by Geballe and Reeves [33], Crowe and Devins [61], Bhalla and Craggs [62] and other people for low pd region, where d is the electrode separation of the gap. It is known that the criterion does not hold at high pd region. The disagreement is explained as the effect of the field emission of electrons from the asperities on the surface of electrode, [62, 63] and very slight field enhancement at the rounded edge of the electrode. [64, 65]

Recently, Perdersen extended the criterion in equation 2 to the non-uniform field gaps and obtained the following equation as the criterion for the Townsend breakdown of an electronegative gas. [45]

$$\gamma \int_0^d exp \left[ \int_0^x (a - \eta)\, dx \right] dx = 1 \qquad (3)$$

The secondary process in Townsend's mechanism will be very sensitive to the condition of the electrode and gas impurity and the above criterion will only be well defined under carefully controlled laboratory conditions. However, the breakdown of $SF_6$ under practical conditions will be explained by streamer mechanism rather than the Townsend's generation mechanism. The streamer theory assumes that the growth of a single electron avalanche results in the formation of the fast moving streamer from the avalanche head.

Though quantative theory of streamer formation has not yet been well established, Meek [66] and Reather [67] assumed that the criterion of streamer formation is fulfilled when the space charge field at the head of an avalanche is sufficiently high to produce secondary avalanches in the enhanced field. This criterion is equivalent to the condition that the number of electrons in an avalanche reaches to a certain critical value. They applied the criterion to non-attaching gases and proved to be in good agreement with experiments for relatively high pd region.

The criterion is applied to the discharge in $SF_6$ by Takuma, [46] Pedersen [45] and the present author [47], independently. The present author showed that the strong electron affinity and other physical properties of the gas simplify the formulation of discharge voltage for uniform and non-uniform field gaps very much. [47] The criterion explained the experiments well for a certain limited conditions. It is shown in this chapter how the criterion is applied to the electrical discharge of $SF_6$. Some of the peculier breakdown characteristics of $SF_6$ are explained theoretically using the above formulation of the breakdown or discharge inception voltage of the gas in the last part of the chapter.

## §2. Discharge Criterion in $SF_6$

### 2-1 Electron Avalanche in $SF_6$

Electron multiplication process by collision ionization in electronegative gases takes place in the region where the ionization coefficient $\alpha$ exceeds the electron attachment coefficient $\eta$. When an initiation electron of an avalanche starts from the most favorable position, the average number of electrons in the avalanche N is given by the following relation.

$$ln\ N = \int_0^{x_c} (\alpha - \eta)\ dx \tag{4}$$

Here x (cm) is the distance from the surface of the electrode which gives the maximum electric field $E_{max}$ and $x_c$ is the value of x where $\alpha=\eta$. In case that the relation $\alpha>\eta$ hold in every part of the gap, $x_c$ is the spacing of the gap.

Values of $\alpha/p$ and $\eta/p$ for $SF_6$ as functions of E/p have been measured by Geballe and Harrison [68] and Bhalla and Graggs. [62] Figure 1 is the result of the measurement by Bhalla and Craggs at 5 mmHg pressure. Because of the practical difficulty, there is no experimental data available on the relation at the pressures higher than atmospheric. But, in principle, the relation has little dependence on gas pressure.

It should be noted that the values of $\alpha/p$ and $\eta/p$ in Figure 1 are approximated as the following linear relations at around the cross point of the two curves.

$$\begin{aligned} \alpha/p &= 23\ (E/p) - 1250 \qquad (cm^{-1} \cdot atm^{-1}) \\ \eta/p &= -4\ (E/p) + 1150 \qquad (\quad " \quad) \end{aligned} \tag{5}$$

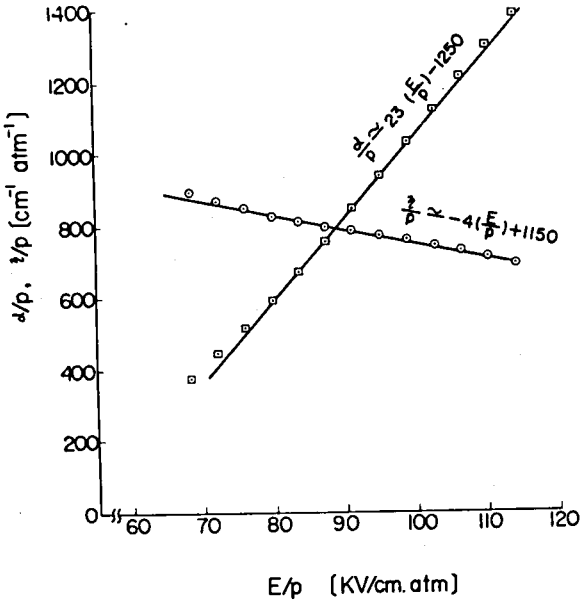


Fig. 1 Ionization and Attachment Coefficients of $SF_6$ as the Function of Electric Field

The relation between $(\alpha - \eta)$ and E/p for $SF_6$ is compared with that of air in Figure 2. The value of E/p at $\alpha = \eta$ for $SF_6$ is about 3 times that for air. This comes from the fact that the value of $\eta$ of $SF_6$ is extraordinarily large whereas $\alpha$ is not so different from that of air. The start of an electron avalanche naturally requires $\alpha$ to exceed $\eta$, at least in a certain part of the gap. This is the simplest reasoning for the high dielectric strength of $SF_6$.

Attention must be paid to the gradient K of these linear relations at the point of $\alpha = \eta$. The value of K for $SF_6$ is several tens of times larger than that for air. The fact means that the value of N in equation 4 is large enough to satisfy the criterion of streamer formation, when E/p slightly exceeds the critical value $(E/p)_{crit}$ – the value of E/p at $\alpha = \eta$.

From equation 5, the relation of $(\alpha - \eta)/p$ vs. E/p for $SF_6$ can be approximated by the linear relation;

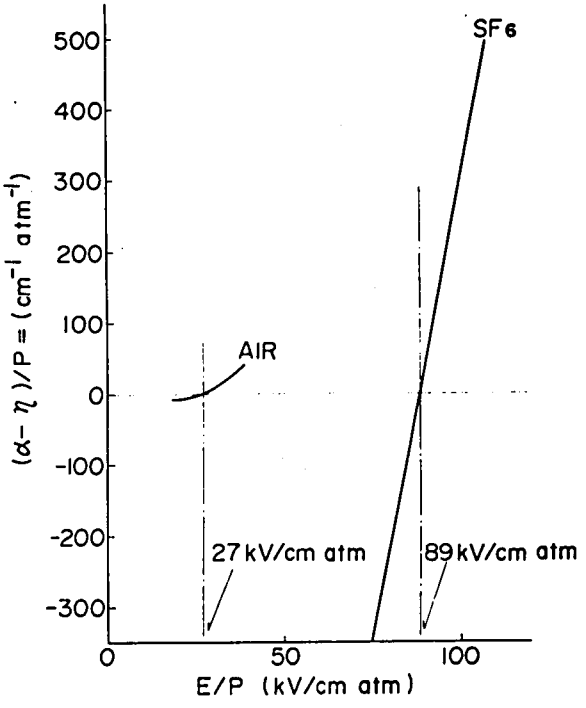


Fig. 2 $(\alpha - \eta)/p$ vs. E/p Characteristics of $SF_6$ and Air

$$\frac{\alpha - \eta}{p} = K\left\{ E/p - (E/p)_{crit} \right\} \ (cm^{-1}\,atm^{-1})$$

$$K = 27 \ (kV^{-1}) \qquad (6)$$

$$(E/p)_{crit} = 89 \ (kV/cm \cdot atm)$$

Substitution of equation 6 to equation 4 gives the number of electrons in an avalanche in $SF_6$ as;

$$ln\ N = K \left[ \int_o^{Xc} E\,(x)\,dx - (E/p)_{crit} \cdot p \cdot x_c \right] \qquad (7)$$

## 2-2. Formulation of Discharge Criterion of $SF_6$

Criterion of electrical discharge in $SF_6$ by streamer theory is fulfilled when N reaches a critical value $N_{crit}$. Raether showed that the value of $N_{crit}$ is scarcely dependent on the kind of gas and has the value of order of $10^8$, regardless the uniformity of the distribution of electric field. [67]

Application of this criterion to the breakdown of an arbitrary gap claims the knowledge on the electric field distribution in the gap. The simplest example is an uniform field gap in which E is constant throughout the gap and $x_c$ is equal to the gap spacing d. In this case, equation 7 is simplified as;

$$ln\ N = K\ [\ E - (E/p)_{crit} \cdot p\ ]\ d$$

Putting $N = N_{crit}$, breakdown field strength $E_d$ is obtained as;

$$E_d/p = \frac{ln\ N_{crit}}{K \cdot p \cdot d} + (E/p)_{crit} \tag{8}$$

Hence, the breakdown voltage $V_d$ is expressed as a function of pd as;

$$V_d = \frac{ln\ N_{crit}}{K} + (E/p)_{crit} \cdot p \cdot d \tag{9}$$

The breakdown voltage for uniform field gap is expressed as a function of pd and the relation corresponds to Paschen's law of breakdown voltage for large pd region whose discharge characteristics are governed by the streamer theory.

For a nonuniform field gap, breakdown voltage can be obtained by solving the following equations simultaneously, provided the electric field distribution function E(x) of the gap is known.

$$\frac{E(x_c)}{p} = (E/p)_{crit}$$

$$\int_o^{x_c} E(x)\ dx = \frac{ln\ N_{crit}}{K} + (E/p)_{crit} \cdot p \cdot x_c \tag{10}$$

$$V_d = \int_o^d E(x)\ dx$$

The equations have been solved for a few simple nonuniform field gaps by the aid of electronic computers and the results explained the experimental results very well at relatively low gas pressure. [45, 46, 48] However, the direct solution of eqution 10 for an arbitrary nonuniform field gap with complicated field distribution is not easy even with the aid of an electronic computer. The calculation includes the electric field analysis which gives precise function of E(x) of the gap and the solution of the integral equation 10.

Fig.3 is two examples of the numerical calculation of $\int_o^x (\alpha - \eta)\, dx$ at breakdown or discharge inception voltage for 5 cm diameter sphere to sphere gap at the spacing of d = 0.5 cm and pressure of 1 and 2 atm (absolute), respectively. [45] At atmospheric pressure, the breakdown criterion 10 is fulfilled at the voltage of 45.2kV and the avalanche leading to breakdown crosses the whole gap. This type of breakdown is called streamer mechanism I. On the other hand, for the pressure of 2 atm, the breakdown equation is satisfied at the voltage of 89.4kV for an avalanche length of only a fraction of the spacing. This type of breakdown is called as streamer mechanism II.

The gap whose breakdown is caused by streamer mechanism I is limited to fairly uniform field gaps in $SF_6$. As far as the breakdown voltage concerns, the gap can be

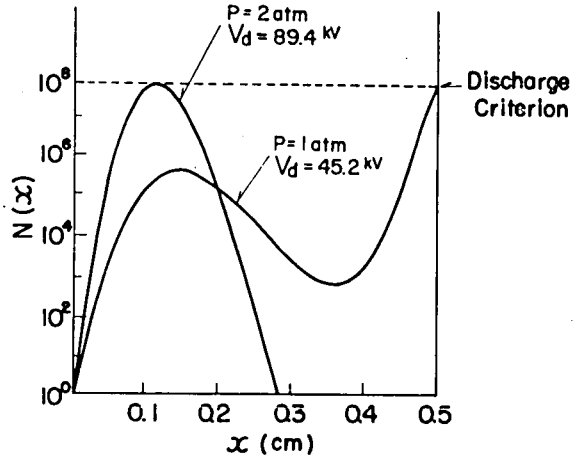


Fig.3 Two Types of Streamer Mechanism of Non-Uniform Field Breakdown in $SF_6$ [45]

looked upon as an uniform field gap of the same gap spacing with sufficient accuracy. The uniform field breakdown voltage by equation 9 at 1 atm pressure is 45.3kV instead of 45.2kV cited above. From this point of view, any non-uniform field gap breakdown in $SF_6$ can be considered as in streamer mechanism II.

This property of $SF_6$ qualifies a very simple approximation in solving equation 10 for an arbitrary non-uniform field gap. The approximation formulation of the breakdown or discharge inception voltage of a non-uniform gap in $SF_6$ is discussed in the followings.

When discharge voltage is applied to a given nonuniform field gap, the axial field strength near the tip of the electrode is supposed to be as in Figure 4. Since the value of K in equation 6 is very large for $SF_6$ in comparison with that of common gases, it is easily understood that N reaches the value required for streamer formation, $N_{crit}$ when $E_{max}/p$ exceeds $(E/p)_{crit}$ by a very small amount and $\Delta E/p$ in Figure 4 is small in comparison with $(E/p)_{crit}$. From this reason, the distance $x_c$ is small for most nonuniform field gaps of interest, and the field distribution E(x) is effective only in the vicinity of the tip of the electrode for the streamer formation criterion in equation 10.

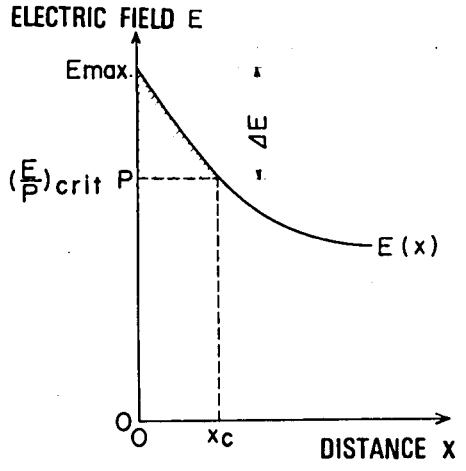


Fig.4 Electric Field Distribution in the Vicinity of $E_{max}$

The electrode surface which gives the maximum field is supposed to be smooth and the radii of curvatures in two directions orthogonal to each other are to be $R_1$ and $R_2$. In the vicinity of the electrode tip, electric flux is approximated to flow in the direction perpendicular to the electrode surface. Then the electric field strength at the point x(cm) distant from the tip ($x << R$) is approximated by the following equation as shown in Figure 5.

$$E(x) = \frac{E_{max}}{(1 + \frac{x}{R_1})(1 + \frac{x}{R_2})} \qquad (11)$$

Since $x_c$ is generally very small compared with $R_1$ and $R_2$ in $SF_6$, equation 11 can be approximated as in equation 12 in the range of $0 < x < x_c$.

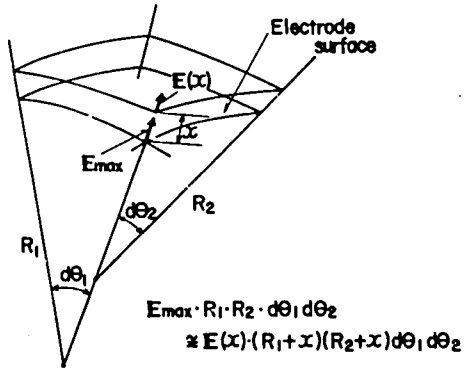


Fig.5 Field Strength in the Vicinity of Electrode Surface

$$E(x) = \frac{E_{max}}{(1 + \frac{x}{R})^2} \tag{12}$$

Here;

$$\frac{1}{R} = \frac{1}{2}\left(\frac{1}{R_1} + \frac{1}{R_2}\right) \tag{13}$$

Substituting equation 12 to the first relation in equation 10, the value of $x_c$ is given as;

$$x_c = R\left(\sqrt{\frac{E_{max}}{(E/p)_{crit}\cdot p}} - 1\right) \tag{14}$$

Substitution of equations 12 and 14 to the second relation in equation 10 yields;

$$\frac{(E_{max})_d}{p} = \left(\frac{E}{p}\right)_{crit}\left(1 + \frac{k}{\sqrt{R\cdot p}} + \frac{k^2}{4R\cdot p}\right) \tag{15}$$

$$k = \sqrt{\frac{4\ ln\ N_{crit}}{K\cdot(E/p)_{crit}}} = 0.175\ (atm^{1/2}\cdot cm^{1/2})$$

In most of the practical electrode configurations, the value of $k/\sqrt{R\cdot p}$ is small in comparison with unity and equation 15 is approximated as;

$$\frac{(E_{max})_d}{p} = \left(\frac{E}{p}\right)_{crit}\left(1 + \frac{k}{\sqrt{R \cdot p}}\right) \tag{16}$$

Equation 15 or 16 shows the maximum field in the gap at the start of an electrical discharge expressed as a function of gas pressure and the equivalent radius of curvature of the electrode R.

Discharge inception or breakdown voltage of the gap is obtained using the utilization factor u — the ratio of the average field $E_{av}$ and the maximum field $E_{max}$ of the gap — as in equation 17.

$$V_d = (E_{av})_d \cdot d = (E_{max})_d \cdot u \cdot d$$

$$u = \frac{E_{av}}{E_{max}} \tag{17}$$

Putting equation 16 and 17 together;

$$V_d = \left(\frac{E}{p}\right)_{crit} \cdot u \cdot p \cdot d \cdot \left(1 + \frac{k}{\sqrt{R \cdot p}}\right) \tag{18}$$

Since $(E/p)_{crit}$ and k are the constants inherent to the gas, discharge voltage of an arbitrary nonuniform field gap is given by the knowledge of the utilization factor of the gap.

## §3. Basic Discharge Characteristics of $SF_6$

Some of the important discharge properties which characterize $SF_6$ out of common gases such as air are explained theoretically by the formulation of the discharge criterion discussed in the foregoing sections. More detailed experimental studies on the gas will be presented in the succeeding chapters.

### 3-1 Constant $E_d/p$ in Uniform Field Breakdown

The comparison of $E_d/p$ vs pd characteristics of uniform field gap for $SF_6$ and air is shown in Figure 6 after Narbut et al. [36] The theoretical curve by equation 8 is given by dot-dash line for $SF_6$ taking $N_{crit}$ as $10^8$. The coincidence between the experimental results and the theory is very good.

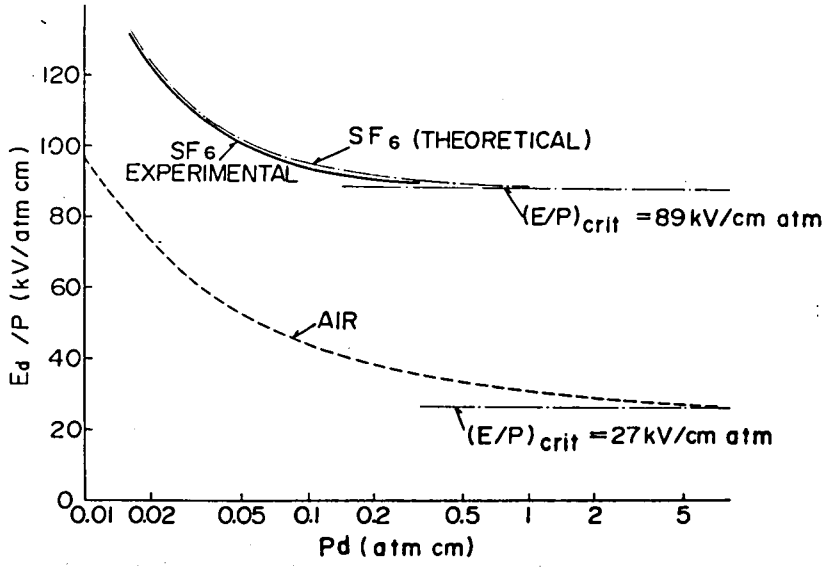


Fig.6 Breakdown Field Strength of Uniform Field Gap in $SF_6$ and Air [36]

One important character special to uniform field breakdown in $SF_6$ comes from the very large value of K in equation 8. The first term in equation 8 is less than 5 percent of the second term for the value of pd higher than 0.14 atm·cm. While the corresponding pd value for air is about 1.8 atm·cm. This is the reason why the value of $E_d/p$ for $SF_6$ can be looked upon as constant over the range of pd of practical interest.

3-2 Importance of the Maximum Field Strength

Narbut et al first pointed out experimentally that the discharge voltage of nonuniform field gap is very much dependent on the maximum field strength in the gap. [36] It can be understood from the fact that for relatively large radius of curvature of electrode R and high value of pressure p the second term in the bracket in equation 15 or 16 is negligible.

Then;

$$\frac{(E_{max})_d}{p} = (E/p)_{crit} \tag{19}$$

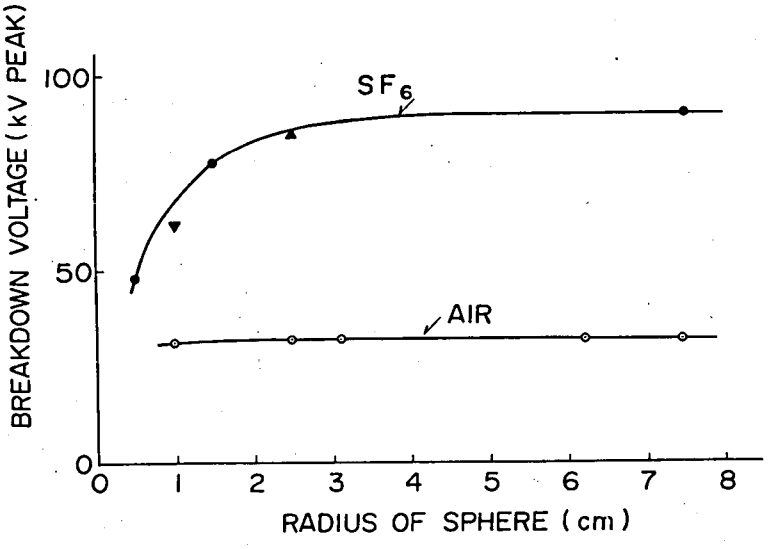


Fig.7 ac Breakdown Voltages of Sphere-Sphere Gap as a Function of Sphere Radius [47]

Figure 7 is the comparison of the breakdown voltages of sphere to sphere gap of various diameters at p = 1 atm and d = 1 cm. The breakdown voltage of air is not so strongly influenced by the nonuniformity of the electric field and keeps an almost constant value down to the sphere radius equal to the spacing of the gap. On the other hand, slight nonuniformity of field distribution reduces the breakdown voltage considerably in $SF_6$. Solid line in the figure is the calculated curve by equation 16.

It should be noted that equation 19 does not coincide to equation 8 for uniform field gap in which R is infinity, since the approximation involved in equation 16 is valid only when $x_c \ll d$.

Equation 19 explains the importance of the maximum field strength, hence the utilization factor of the gap, in the discharge in $SF_6$. Discharge voltage $V_d$ for a given nonuniform field gap of field utilization factor u is approximately given as;

$$V_d = (E/p)_{crit} \cdot u \cdot p \cdot d \qquad (20)$$

From this particular characteristic of $SF_6$, a slightly nonuniform field gap has quite different discharge phenomena from that of uniform field gap. This property is discussed in detail by Pedersen et al. [65]

### 3-3 Saturation of Breakdown Voltage with Gap Spacing

Independent of the electrode configuration, $V_d$ shows very strong saturation tendency with the ratio of the gap spacing d and the radius of curvature of the electrode R. This is one of the most characteristic feature of the breakdown in $SF_6$.

The saturation tendency can be understood from the fact that u decreases with the increase of d/R, and u·d converges to a constant value in equation 18. In the case of a sphere gap of radius R, this situation is easily analyzed as follows. When the gap spacing d of a sphere gap is large enough, the field strength at the electrode surface of potential V converges to the field strength of a conductive sphere of the same potential V in the infinite space. That is;

$$E_{max} \longrightarrow V/R$$

The average field strength $E_{av}$ is given as $E_{av} = V/d$.

$$u \cdot d = \left(\frac{E_{av}}{E_{max}}\right) \cdot d \longrightarrow R$$

Thus, from equation 18, the discharge voltage of a sphere gap of sufficiently large spacing is given as;

$$V_d = (E/p)_{crit} \cdot p \cdot R \left(1 + \frac{k}{\sqrt{p \cdot R}}\right) = V_{\infty,sp} \qquad (21)$$

This brings us to the conclusion that the discharge inception voltage of a sphere gap of radius R converges to $V_{\infty,sp}$ when d tends to infinity. It is noteworthy that $V_{\infty,sp}$ is given as a function of pR and, of course, independent of gap spacing.

When d is not sufficiently large, $V_d$ can be put as;

$$V_d = g \cdot V_{\infty,sp} \qquad (22)$$

Here, g (= ud/R) is a function of only the ratio of d and R, as u is a function of d/R from the similarity relation of the electric field. Using the field calculations of a sphere gap by Ryan and Walley, [69] d/R dependence of g is plotted in Figure 8. It is quite obvious that the d/R dependence of g in the figure brings the saturation tendency of discharge voltage.

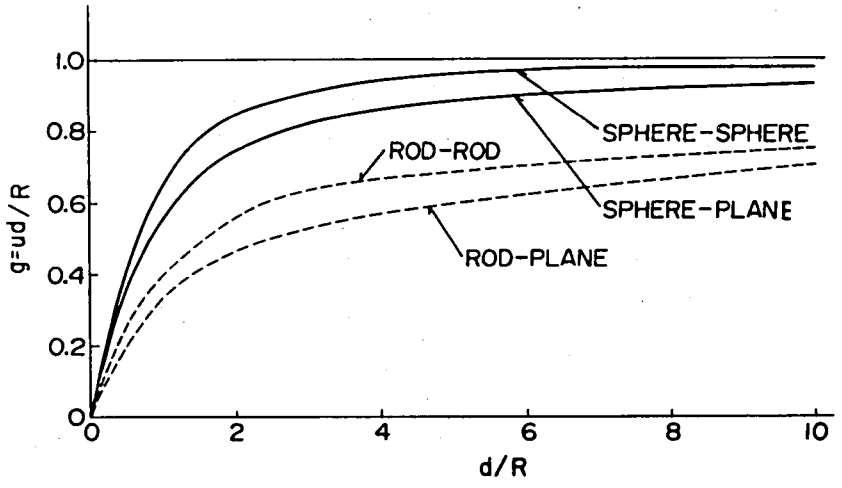


Fig.8 d/R Dependence of g for Sphere and Rod Gaps

A similar discussion can be given for an arbitrary nonuniform field gap. But, for most of nonuniform field gaps, the value of g and the expression of $V_\infty$ can not be obtained analytically. According to the field analysis on rod gap by Abou-Seada and Nasser, [70] the asymptotic value $V_\infty$ for rod gap is about 1.7 times that of sphere gap.

$$V_{\infty,rod} \cong 1.7 \cdot (E/p)_{crit} \cdot R \cdot p \left(1 + \frac{k}{\sqrt{R \cdot p}}\right) \qquad (23)$$

The value of g for rod gap is plotted by dashed lines in Figure 8, using the result of field analysis in Appendix I. The saturation tendency is much stronger for sphere gaps in comparison with that for rod gaps. Similarly, the saturation is stronger for sphere-sphere or rod-rod gaps in comparison with sphere-plane or rod-plane gaps.

### 3-4 Polarity Effect [71]

Pedersen [45] pointed out the fact that the ionization process in asymmetric field gap in $SF_6$ should have polarity effect, since the electron multiplication process of an electron avalanche is different by the direction of the avalanche, whether it is heading from low field to high field region or the opposite, depending on the polarity of applied voltage.

Discharge characteristics expressed by equation 18 have no explicit polarity effect by itself. However, the effect, if any, will be considered as the difference in the value of $N_{crit}$ and hence the difference of k in equation 15 or 16 by the polarity of applied voltage. The polarity effect of the ionization process is analyzed in a generalized form by the light of the formulation in section 2-2 as follows.

Substituting equation 16 to equation 12, the electric field in the vicinity of the electrode ($x \ll R$) is approximated by the next equation, provided $k \ll \sqrt{R \cdot p}$.

$$E(x) \cong \left(\frac{E}{p}\right)_{crit} \cdot p \cdot \left(1 + \frac{k}{\sqrt{R \cdot p}} - \frac{2x}{R}\right) \qquad (24)$$

To generalize the discussion to an arbitrary nonuniform field gap, distance x is normalized by a variable t as;

$$t = \frac{2}{k}\sqrt{\frac{p}{R}} \cdot x \qquad (25)$$

Then, from equation 6, $\alpha - \eta$ in the vicinity of the electrode is expressed as a function of t as:

$$\alpha - \eta = K \cdot \left(\frac{E}{p}\right)_{crit} \cdot k \cdot \sqrt{\frac{p}{R}} \cdot (1 - t) \quad (cm^{-1})$$

or

$$\alpha - \eta = K \left(\frac{E}{p}\right)_{crit} \cdot k^2 \cdot \frac{1 - t}{2} \quad \text{(per unit t)} \qquad (26)$$

By this normalization of distance by t, $t = 0$ corresponds to the surface of the electrode that gives the maximum field, $t = 1$ and $t = 2$ correspond to the point of $\alpha = \eta$ and the point where the integral of $\alpha - \eta$ is reduced to unity and any ionization process stops, respectively, independent on the field distribution of the gap.

For positive applied voltage, the avalanche starts at around the point of $t = 1$ and proceeds toward $t = 0$. The number of electrons in an avalanche changes with t as;

$$N_p(t) = exp \int_1^t \left\{ -(\alpha - \eta) \frac{k}{2} \sqrt{\frac{R}{P}} \right\} dt$$

$$= exp \left\{ K \cdot \left(\frac{E}{p}\right)_{crit} \cdot \frac{k^2}{4} \cdot (1 - t)^2 \right\}$$

By the definition of k in equation 15, $N_p(t)$ is;

$$N_p(t) = N_{crit}^{(1-t)^2} \qquad (0 \leqslant t \leqslant 1) \tag{27}$$

In the case of negative applied voltage, avalanche starts at t = 0 and proceeds to t = 2.

$$N_n(t) = exp \int_0^t (a - \eta) \frac{k}{2} \sqrt{\frac{R}{p}} \cdot dt$$

$$= N_{crit}^{t(2-t)} \qquad (0 \leqslant t \leqslant 2) \tag{28}$$

It is very interesting that the number of electrons in an avalanche is expressed as functions of generalized variable t independent of the field distribution of the gap.

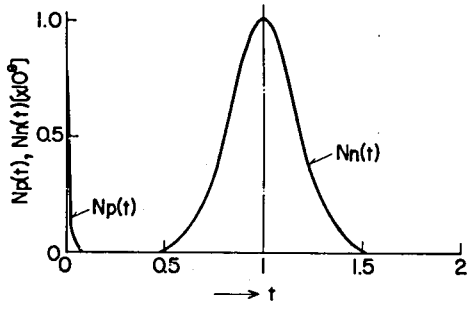


Fig.9 Number of Electrons in an Avalanche

Fig.9 shows $N_p(t)$ and $N_n(t)$ per unit t. In spite of the same field distribution, the distribution of the number of electrons in an avalanche is completely different depending on the polarity of applied voltage. The distribution of positive, negative and net ion densities left in the gap by an avalanche are simply given by multiplying $a$, $\eta$ and $a - \eta$ to $N_p(t)$ or $N_n(t)$.

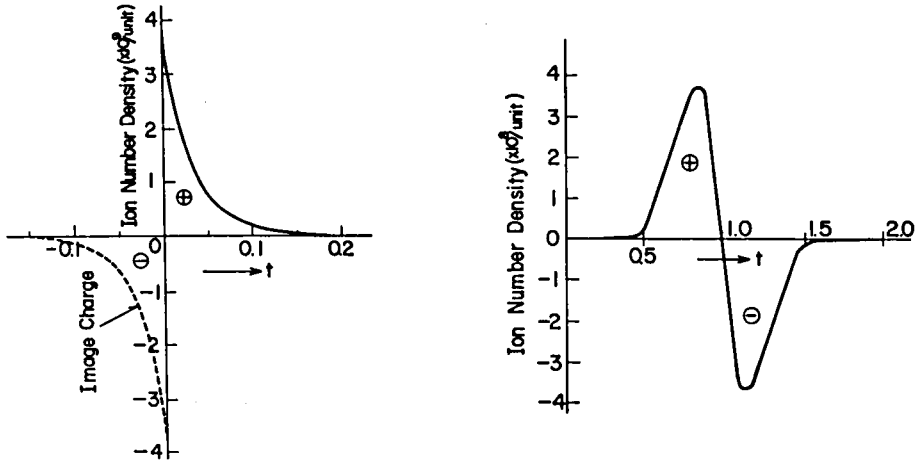


(a) Positive Polarity (b) Negative Polarity

Fig.10 Distributions of Net Charge Density per Unit t

Fig.10(a) and (b) show the examples of net charge distribution per unit t for positive and negative polarity, respectively. The net charge density for positive polarity is more than one order of magnitude larger than the negative one, and distributed in a very small region.

Converting the variable from t to x, the difference in the distribution of ions by an electron avalanche are summalized as follows:

(1) Major part of the positive ions produced by positive applied voltage distributes in the range of x of 0 to $\frac{k}{16}\sqrt{\frac{R}{p}}$ (cm), depending on the shape of the electrode and gas pressure. This positive charge will induce negative image charge of the same amount and opposite polarity inside the electrode.

(2) Positive and negative ions produced by negative applied voltage distribute around the range of x of $\frac{k}{4}\sqrt{\frac{R}{p}}$ to $\frac{k}{2}\sqrt{\frac{R}{p}}$ (cm) and $\frac{k}{2}\sqrt{\frac{R}{p}}$ to $\frac{3k}{4}\sqrt{\frac{R}{p}}$ (cm), respectively.

(3) This means the spread of the distributed charge for negative applied voltage is about 4 times larger than that of positive case.

(4) Charge density per $\frac{k}{2}\sqrt{\frac{R}{p}}$ (cm) distance produced by positive polarity applied voltage is one order of magnitude higher than that of the negative at the same voltage level.

In formulating the discharge criterion of $SF_6$ in Section 2-2, we postulated a constant value of $N_{crit}$, independent of the polarity of applied voltage. However, the above explained difference may introduce a disparity in the values of $N_{crit}$ for positive and negative polarity applied voltages. If the critical condition of streamer formation is the charge density of ions, as proposed by Pedersen, [45] the value of $N_{crit}$ for positive applied voltage will be lower than that of negative polarity for one order of magnitude. Other possible critical condition of streamer formation is the local field distribution due to the charge separation in the gap. In the case of positive polarity, image charge shown by dashed line in Fig.10(a) has to be taken into account. Becaue of the linear relation between $\alpha - \eta$ and the electric field as expressed in equation 6, the contribution of the local field to the ionization process which will be taken place after the avalanche is formed should be determined by the integral of the local field strength through the avalanche head.

If we look the charge separation upon as a dipole, the integral of the local field is the potential difference between the both ends of the real charge distribution which is proportional to the dipole moment of the charge separation for negative polarity and, because of the imaginary negative charge, one half of the corresponding value for positive polarity. Because of the very narrow spread of the net charge, the value of the dipole moment for positive polarity is smaller than that for negative polarity as will be seen in (a) and (b) of Fig.10.

The criterion of the discharge due to the space charge dipole field will impose the value of $N_{crit}$ for positive applied voltage to be higher than that for negative polarity for one order of magnitude.

So far we have no way to judge which of these criterions or others on the value of $N_{crit}$ is good to explain the polarity effect of the discharge voltage of $SF_6$. However, the difference of a few orders of magnitude in the value of $N_{crit}$ results in the change of the value of k in equation 15 for several percent. This means the difference in discharge volt-

ages due to the polarity of applied voltage is theoretically negligible as far as the property of $SF_6$ concerns. The conclusion is not true when the effect of electrode is involved in the process and the characteristic will be discussed in the following chapters.

## §4. Conclusion

Breakdown or discharge inception characteristics of $SF_6$ were theoretically formulated based on single avalanche streamer theory. The formulation is greatly simplified by the strong and approximately linear dependence of $(\alpha - \eta)/p$ upon E/p in $SF_6$. The maximum field strength of an arbitrary gap is expressed in equation 16 as a function of gas pressure and the geometrical shape of the electrode which gives the maximum field in the gap.

The formulation is applied to explain the following basic discharge characteristics of $SF_6$ which characterize the gas out of common gases such as air and nitrogen.

(1) The value of (E/p) at the breakdown of an uniform field gap in $SF_6$ can be looked upon as constant over the wide range of pd.

(2) The maximum field strength in gap is very important in the breakdown of $SF_6$. Because of this property, breakdown voltage of very non-uniform field gap shows strong saturation tendency with regard to gap spacing.

(3) In principle, breakdown characteristics of $SF_6$ should not have any appreciable polarity effect.

# III. AC AND DC DISCHARGE EXPERIMENTS [47]

## §1. Introduction

Many experimental data have been reported on the breakdown characteristics of $SF_6$. Some are relatively large scale experiments aiming at the direct application to the design of high voltage gas insulated apparatus. [39–42] Some experiments are performed on small scale gaps using relatively low applied voltage. [34–38] Even with the refined test conditions of these laboratory experiments, the results are not consistent to each other particularly at high gas pressures.

As discussed in 3-2 of Chapter II, the maximum field is the most important factor that determines the discharge characteristics of a gap in $SF_6$. Many reports do not even include the information on the precise electric field distribution of the gaps tested. Other test conditions such as the finish of electrodes are also important in comparing the test results with the theoretical estimation of the breakdown characteristics.

A series of experiments is planned and performed to test the validity of the discharge criterion and the conclusions of the discussion in Chapter II, using a few simple gaps with various $R \cdot p$ values ranging from an extremely non-uniform field rod to rod gap in which the second term in equation 16 has appreciable effect on the discharge characteristcs of the gap to nearly uniform field large sphere to sphere gap.

Since the discharge criterion in equation 16 includes no time factor in principle, power frequency ac applied voltage is used in the experiments as a typical voltage with low time variance. In order to obtain better understanding of the ac discharge characteristics particularly on the polarity effect, dc discharge characteristics are also studied.

For very non-uniform field gap in low pressure $SF_6$, a discharge started at the point of the highest electric field in the gap does not develop the breakdown of the gap. The discharge produces steady corona. Breakdown voltage of the gap is quite high in this case due to the deconcentration of electric field by the corona discharge. [25, 10] The phenomena is called as "Corona Stabilization". [5] Discussions on the criterion of the corona stabilization is given in the last part of this chapter. In the case of corona stabilized breakdown, corona inception voltage is the discharge voltage in equation 18. The term "breakdown voltage" is used to denote the voltage of the total breakdown of the gap, at which the applied voltage collapses drastically to zero.

## §2. Test Conditions

A sphere gap, the diameter of which is 15 cm (Gap A) was used as a representative of rather uniform field gap configuration. In air, sphere gap of this size is usually considered as a gap which gives fairly uniform field for the spacing of several centimeters tested in the present experiment. This is not true in $SF_6$ because of the strong dependence of the breakdown criterion on the maximum field as discussed in Section 3-2 in Chapter II.

As representatives of non-uniform field gap,two rod-rod gaps, having spherically rounded tips, whose diameters are 3 cm (Gap B) and 1 cm (Gap C) are used.

These electrodes are made of stainless steel (SUS–27) and polished in glassy surface. The roughness of the surface of the electrodes is the order of ± 0.5$\mu$. The surface of the electrode is repolished before the start of each test performed under a certain pressure. Parameters of these gaps are summalized in Table 1.

| Gap | Shape | R(cm) | Spacing (cm) | Material |
|---|---|---|---|---|
| A | (15 cmφ Sp-Sp) | 7.5 | 0 ~ 10 | Stainless steel |
| B | (3 cmφ Spherical Rod-Rod) | 1.5 | 0 ~ 20 | 〃 |
| C | (1 cmφ Spherical Rod-Rod) | 0.5 | 0 ~ 20 | 〃 |

Table 1 Three Electrodes used in the Experiment

One of these three electrodes is set in a large metal tank shown in Fig.11. The tank is evacuated and filled with $SF_6$ to a specified pressure. The spacing of the gap can be set mechanically from outside of the tank without breaking the pressure. This function is very important, since the setting of the gap changes by gas pressure due to the mechanical distortion of the tank. Sparking point of the gap can be observed through four viewing windows provided on the side wall of the tank. Lower electrode is insulated from the grounded tank by low voltage bushing so the current flowing into the electrode is measured separately from the current to any other grounded part in the system.

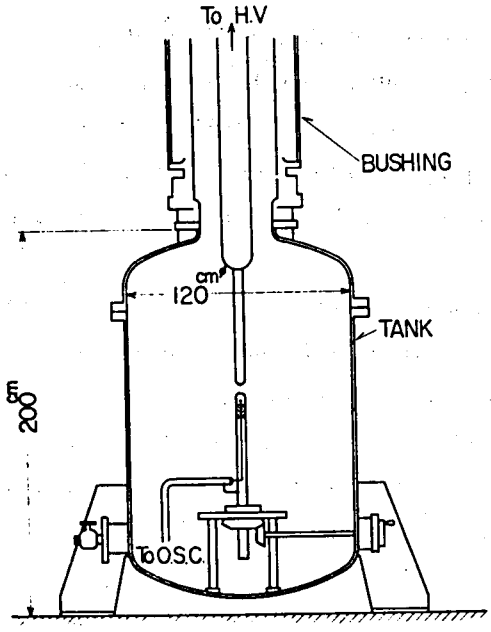


Fig.11 Metal Tank Used in the Experiment

Since the maximum field strength in the gap is the most important factor of the breakdown in $SF_6$, precise field distributions of these gaps in the tank are calculated by over relaxation method, using a digital computer. Details of the calculation are given in Appendix I. Field utilization factor u in equation 17 of rod-rod and sphere-sphere gaps is shown as the field uniformity factor $\xi = 1/u - 1$ in Fig. I–4 in Appendix I. The value of $\xi$ is plotted instead of u simply because of practical convenience. If u is plotted directly, precise determination of u will be difficult for slightly non-uniform field gaps, where u is very close to unity. Because of relatively large size of the tank, the effect of the wall of the tank is limited even in $SF_6$ in most of the gap spacing and gas pressure used in the present experiment, as seen in the filed analysis in Appendix I. [74]

Fig.12 shows a schematic diagram of test circuit. Ac voltage source is a 350 kV testing transformer whose output is applied to the test gap by putting the connecting switches in "a" position. To minimize the energy from the source to the test gap after its breakdown, the source is short circuited right after the breakdown of the test gap within a few micro seconds by ac diverter. [73] The ac diverter is a series of trigger

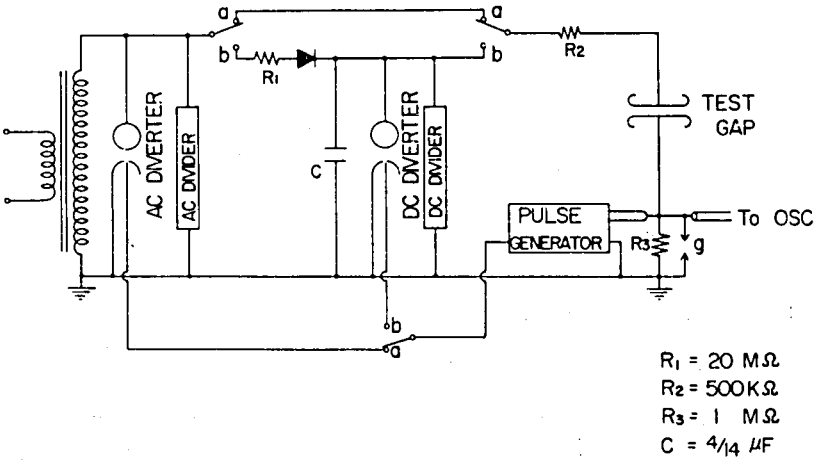


Fig.12 Schematic Diagram of the Test Circuit

gaps works in pressurized nitrogen gas whose working voltage is controled by the gas pressure.

For dc testing, the connecting switches are put in "b" position and the output of the testing transformer is rectified by a series connection of high voltage selenium rectifiers. Smoothing capacitor C is a series connection of 14 units 4 $\mu$F oil-paper capacitors. The large capacitance limited the ripple of dc voltage as low as 0.1% with 300 M$\Omega$ dc voltage divider connected in parallel. Diverter for dc circuit is a series of triggered vacuum gaps. The diverter showed very wide control range and stable operation, however, found out to be applicable only to dc or unipolar surge voltages because of its strong polarity effect.

Voltage across the test gap and the current through the gap are measured in the experiments.

## §3. Discharge Characteristics for ac Applied Voltage

The experimental data of ac discharge voltage of gaps A, B and C are shown in Figures 13, 14 and 15, respectively, together with the theoretical values by equation 18 (solid lines).

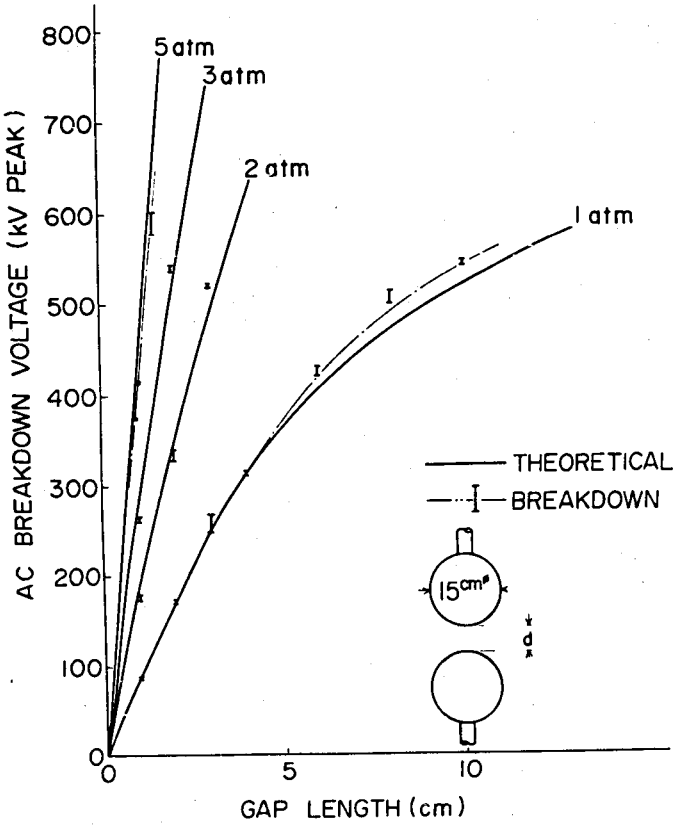


Fig.13 ac Breakdown Voltage for Gap A

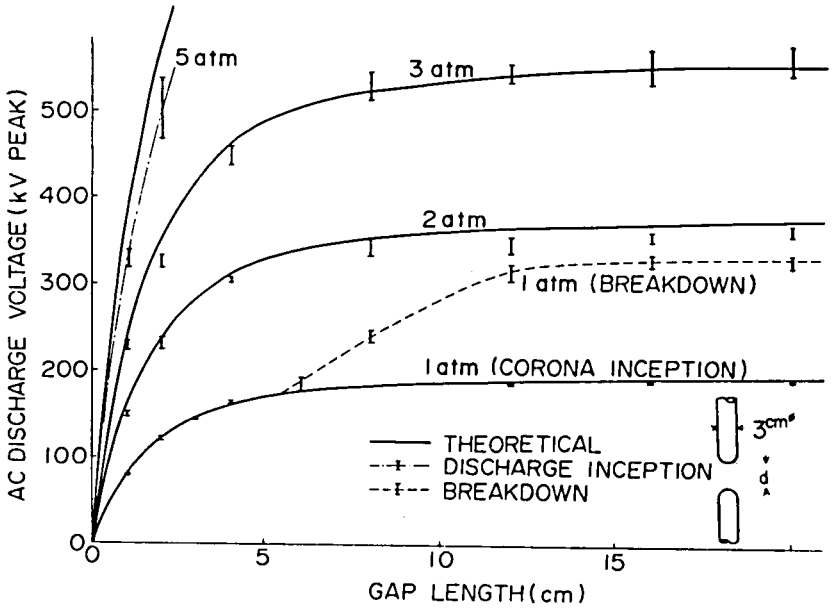


Fig.14 ac Discharge Voltage for Gap B

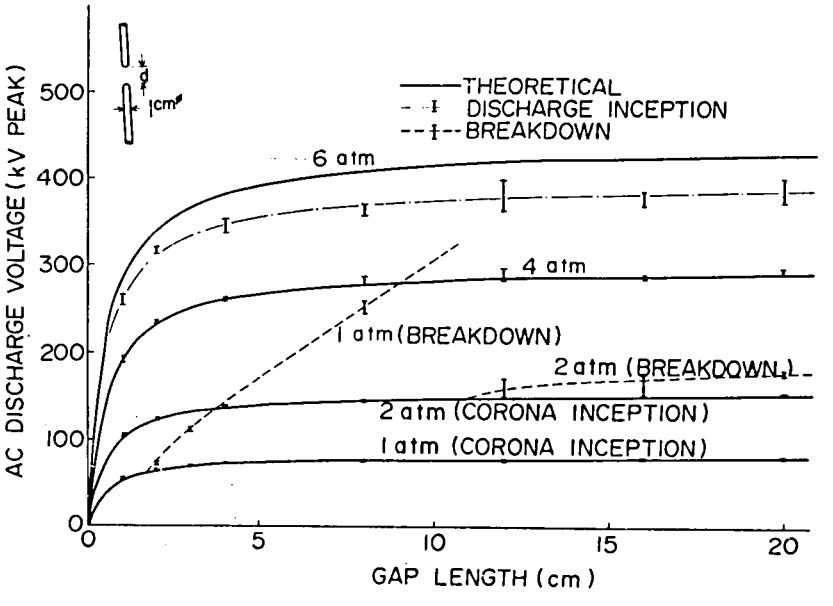


Fig.15 ac Discharge Voltage for Gap C

In the case of corona stabilized breakdown for very non-uniform gap at low pressures, corona inception voltages are plotted as discharge voltage. Corona stabilized breakdown voltages are shown by dashed lines in the figures. The characteristics of the corona stabilized breakdown will be discussed in detail in the last part of this chapter.

At rather low pressure range of less than 4 atm, experimental data show fairly good agreement with the theoretical values for all of the three electrode configurations used. At higher pressures, experimental values are slightly lower than the theoretical values, and the higher the pressure is the more significant the reduction of the breakdown voltage is.

At the pressures of 5 or 6 atmosphere for example, the maximum field strength divided by the pressure $E_{max}/p$ for Gap A and B are about 80 and 83 kV/cm.atm, respectively. These values are much lower than the value $(E/p)_{crit}$ as seen in Fig.2. This means that breakdown occurs even when the maximum electric field strength is less than the value required for $\alpha = \eta$. Under the condition of $\alpha < \eta$, there should not be any electron multiplication process, hence there should not be any discharge in the gap.

Either the dependence of $(\alpha - \eta)/p$ over E/p in Fig.2 or the estimated value of $E_{max}$ itself are incorrect to explain this unexpectedly low breakdown voltage. All of the available data on the relation between $(\alpha - \eta)/p$ and E/p are obtained at the pressure lower than atmospheric. [62] The relation may not be applicable at these high pressures. So far, there is no direct method to testify the relation at high gas pressures.

However, there seems to be some experimental evidence of the enhancement of $E_{max}$ caused by microscopic irregularities on the electrode surface. As an example of the effect of the electrode surface, ac discharge voltage characteristic of Gap C, whose electrode surface is roughened by many breakdown tests, is shown in Fig.16.

The reduction of discharge voltage from the theoretical estimation begins at lower pressure and the rate of the reduction is increased by the roughening of the electrode surface. For carefully polished electrode, the reduction of the discharge voltage calculated from the data in Fig.13 to 15 begins when the surface field strength reaches a critical value of about 400 kV/cm, independent of the electrode shape. For roughened electrode in Fig.16, the critical field strength decreases down to about 150 kV/cm or less.

More detailed discussion on the effect of electrode surface will be given in Chapter IV and V.

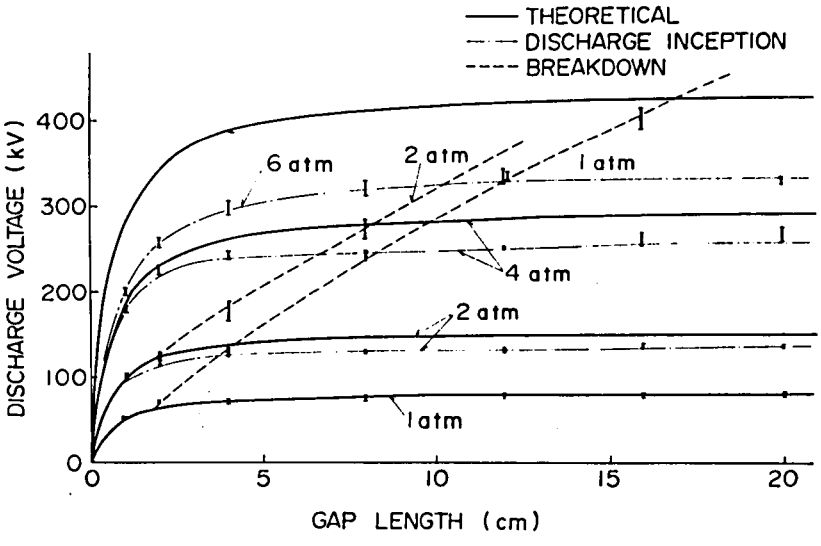


Fig.16 ac Discharge Voltage for Gap C of Roughened Electrodes

## §4. dc Discharge Voltage and Polarity Effect

Theoretical discharge criterion by equation 18 includes no time factor, and to be exact, it should apply to dc voltage. To test the difference between ac and dc voltage and the effect of the polarity of the applied voltage, dc discharge tests have been performed on Gap A, B and C. In Fig.17, 18 and 19, the experimental data of positive and negative dc discharge voltage for these gaps are shown as a function of gas pressure, gap spacing as a parameter. The terms "positive" and "negative" usually denote the polarity of the electrode which gives the maximum electric field. Since the maximum field is produced at the tip of the electrode on which the voltage is applied for all of the gap configurations used in the present experiment, the polarity coincides to the polarity of the applied voltage.

At lower pressures, positive and negative discharge voltages are close to each other and well coincide to the theoretical estimation by equation 18. It is not clearly shown in the figures, but the average values of negative breakdown voltage is a few percent lower than that of positive. Theoretically, it is concluded in Section 3-4 in Chapter II that polarity effect on the discharge inception is negligible. The above mentioned polarity

Fig.17(a)

Positive dc Discharge Voltage for Gap A

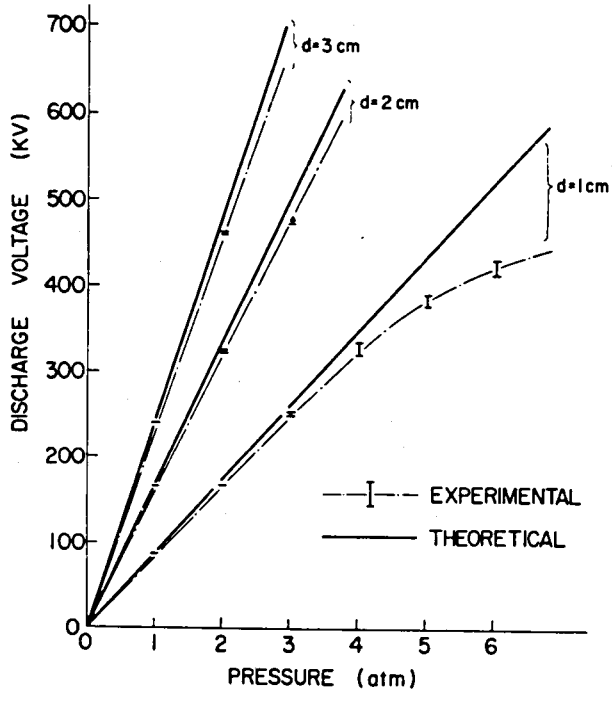


Fig.17(b)

Negative dc Discharge Voltage for Gap A

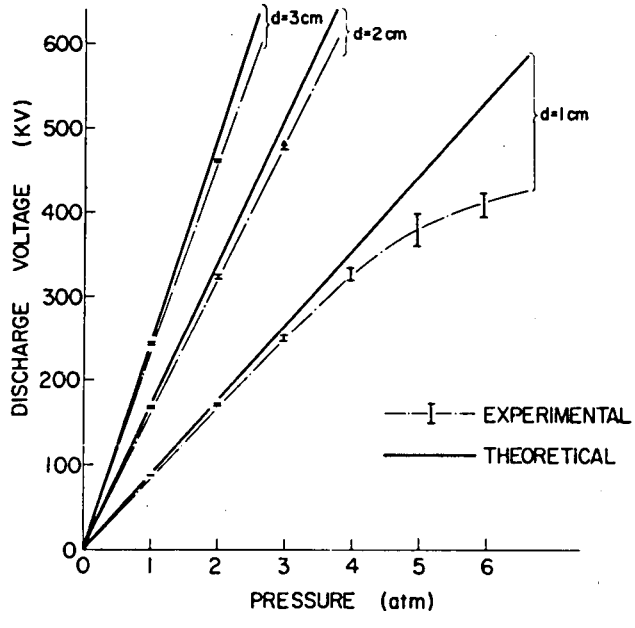

Fig.18(a)

Positive dc Discharge
Voltage for Gap B

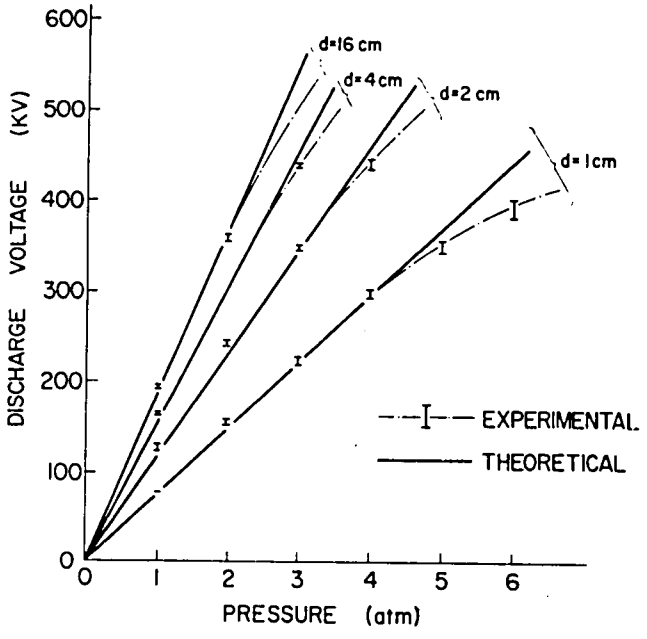


Fig.18(b)

Negative dc Discharge
Voltage for Gap B

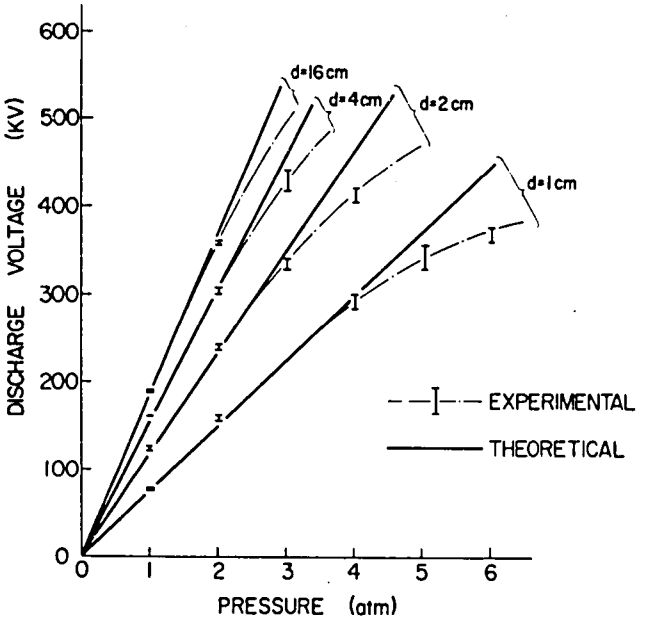

Fig.19(a)

Positive dc Discharge
Voltage for Gap C

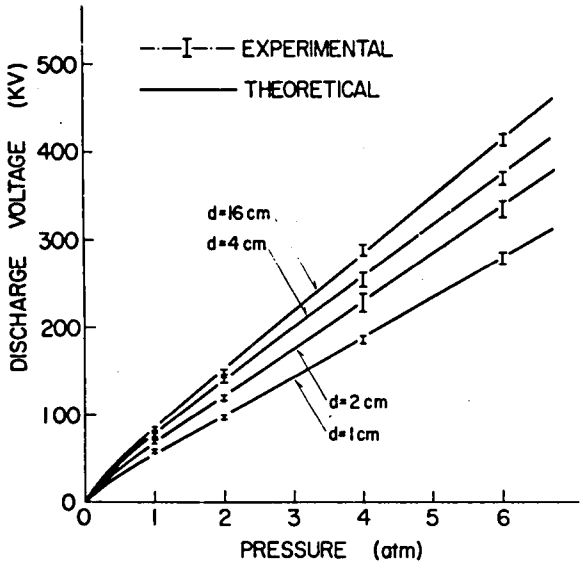


Fig.19(b)

Negative dc Discharge
Voltage for Gap C

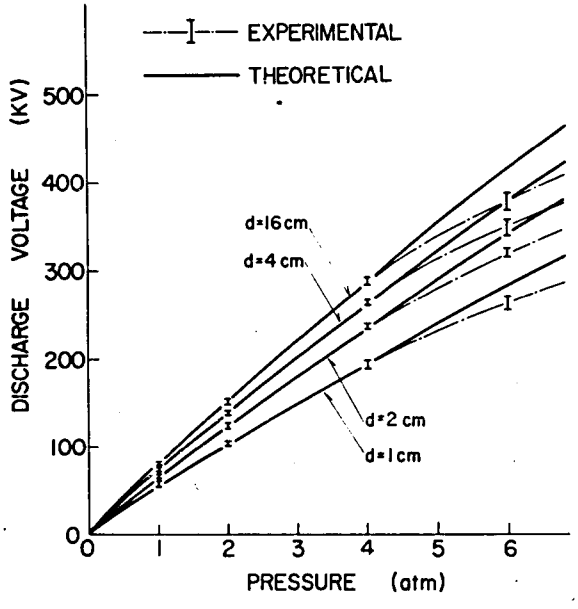

effect seems to be attributable to the different statistical distribution of breakdown voltages. For negative applied voltage, the avalanche that leads to a streamer always starts on the cathode surface while it does in the mid gap for positive polarity. Since there are more initiation electrons on the cathode, average discharge voltage for negative polarity will be lower than that for positive. Slightly larger scattering of discharge voltages for positive applied voltage will support this inference.

At the pressures higher than a certain critical value, hence, when the maximum field strength is higher than a critical value, experimental discharge voltages are lower than the theoretical estimation. The critical field strength for negative polarity coincides to the value for ac applied voltage presented in Section 3. The critical field for positive polarity is always higher than that for negative polarity and the difference between them is larger for more non-uniform field gaps. The characteristic of the critical pressure suggests the effect of the cathode surface for the reduction of the discharge voltage as in the followings.

Field distributions of the gaps used in the present experiment are not symmetric. The maximum field $E_{max}$ on the floating electrode on which voltage is applied is higher than the field at the tip of the grounded opposite electrode $E_{op}$. [74] An example of the distribution for a rod-rod gap whose d/R is 6 is presented in Fig.I-5 in Appendix I. The ratio of $E_{max}$ over $E_{op}$ is close to unity for small d/R and nearly zero for large d/R. The values of $E_{op}/E_{max}$ for sphere-sphere and rod-rod gaps are shown in Fig.I-7 in Appendix I.

If we apply positive voltage on Gap A whose d/R is very small for the spacing tested, field strength on the surface of the cathode $E_{op}$ is very close to $E_{max}$. On the other hand, the field strength on the cathode, $E_{op}$ in the positive discharge process is very low in comparison with $E_{max}$ for larger d/R gaps.

To testify the effect of the cathode surface in the reduction of discharge voltage from the theoretical estimation, the ratio of the experimental and theoretical discharge voltages $V_o/V_d$ are plotted in Fig.20 as a function of the maximum field strength on the cathode, $E^-_{max}$. The value of $E^-_{max}$ is identical to $E_{max}$ for negative applied voltage, while it is equal to $E_{op}$ for positive voltage. The plots for the same gap fall on one curve independent of the polarity of the applied voltage. The same data for roughened electrodes are also shown by dashed lines, although the plots are very limited.

Fig.20 shows the following two properties of the electrical discharge in $SF_6$.

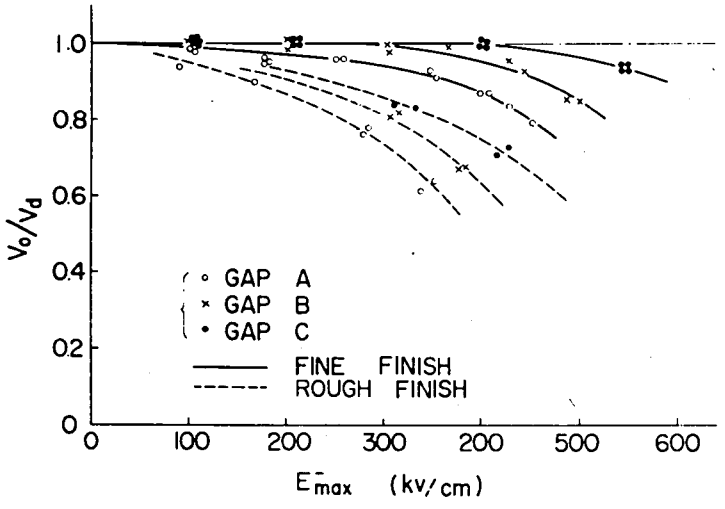


Fig.20 Ratio of the Discharge Voltage over the Theoretical Values as a Function of the Field Strength on the Cathode Surface

(1) The reduction of the discharge voltage from the theoretical estimation at high pressures is caused by the effect of cathode surface. ——— Electrode Surface Effect

(2) The reduction is a function of the size of the electrode.
The reduction is pronounced for larger electrode. ——— Electrode Area Effect

These two points are of the most importance in the practical application of compressed $SF_6$ gas insulation and will be discussed quantitatively in Chapters IV and V.

## §5. Corona Stabilized Breakdown in $SF_6$

### 5-1. Steady Corona and Deconcentration of Electric Field

When the electric field of a gap is extremely non-uniform, the discharge started at the area of the highest electric field in the gap does not always develop the breakdown of the total gap. It produces steady corona discharge in the limited area of the gap. The presence of the corona brings about deconcentration of the electric field stress and hence high breakdown voltage of the gap. This phenomena is called as "Corona Stabilized breakdown" by Camilli, Gordon and Plump. [5]

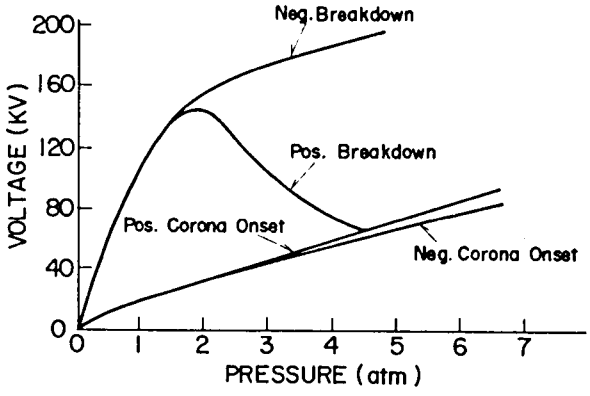


Fig.21 dc Discharge Characteristics of 1.6mm Diameter Hemi-Spherical Point to Plane Gap of 25.4mm Spacing [27]

Fig.21 is an example of the discharge and breakdown characteristics of 1.6mm diameter hemispherical point to plane gap of 25.4mm spacing obtained by Works and Dakin. [27] At low pressures, both positive and negative breakdown voltages are very high showing typical corona stabilized breakdown. However, at the pressures higher than 4 atm, corona stabilization diminishes for positive polarity and positive corona onset voltage coincides to the breakdown voltage of the gap. This produces a well known negative slope in the breakdown voltage vs gas pressure curve in $SF_6$. Corona stabilization for negative applied voltage never diminishes over the range of gas pressure tested in most of the literatures. [5, 25–31]

In the case of the present experiment, very high corona stabilized breakdown voltages are observed for Gap B and C at low gas pressures for both ac and dc applied voltages. Fig.22 and 23 show the relation between the discharge voltage and the corona stabilized breakdown voltage of Gap B and C for dc applied voltage.

For Gap B, the corona stabilization is observed only at 1 atm of pressure for the gap spacing larger than about 6.7 and 4.5 cm for positive and negative polarity, respectively. It is observed at 1 and 2 atm for positive and 1 to 6 atm for negative applied voltage on Gap C. While the corona inception voltage or the discharge voltage for negative polarity is slightly lower than that for positive as pointed out in Section 4 of the present chapter, the corona stabilized breakdown voltage for negative polarity is always

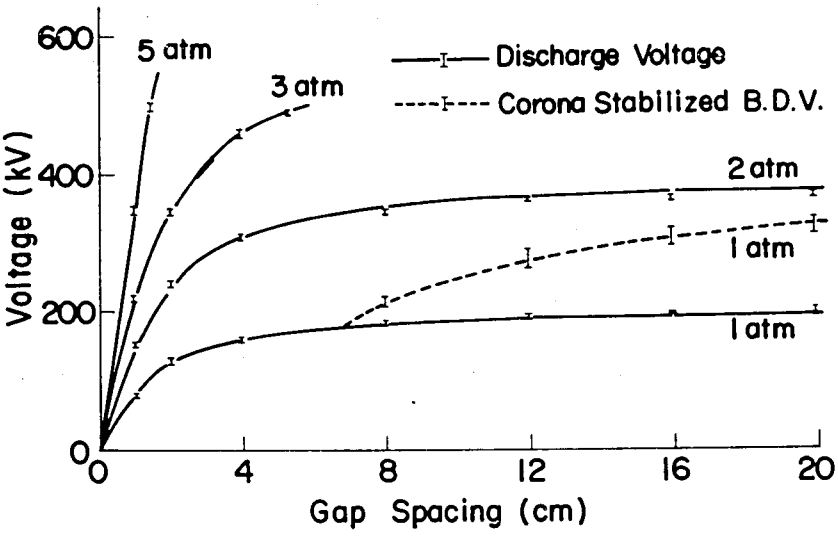


Fig.22(a) Discharge and Corona Stabilized Breakdown Voltages of Gap B for Positive dc Applied Voltage

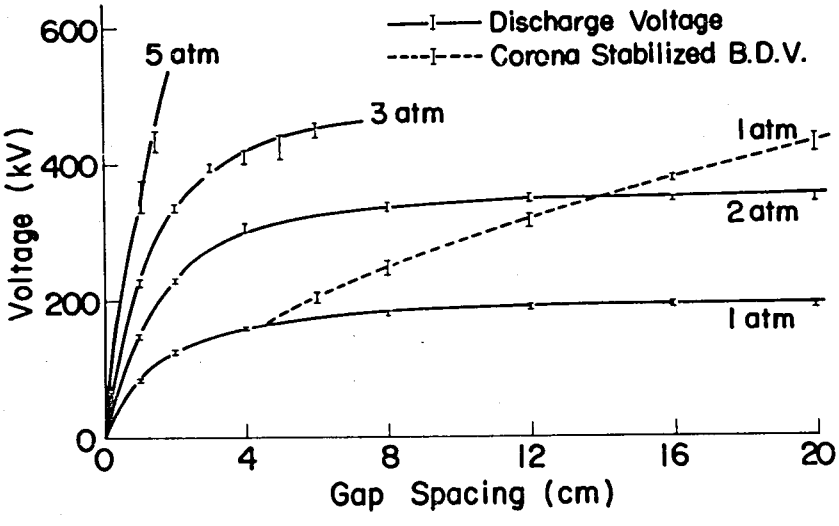


Fig.22(b) Discharge and Corona Stabilized Breakdown Voltages of Gap B for Negative dc Voltage

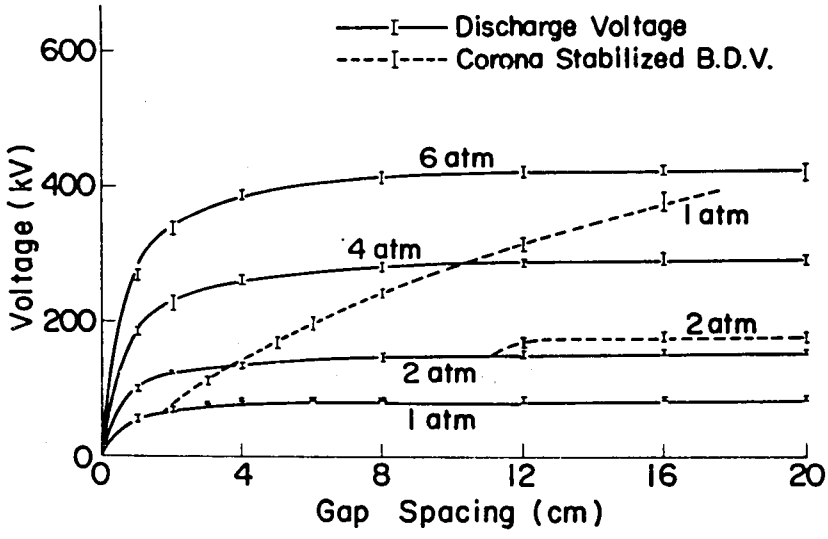


Fig.23(a) Discharge and Corona Stabilized Breakdown Voltages of Gap C for Positive dc Applied Voltage

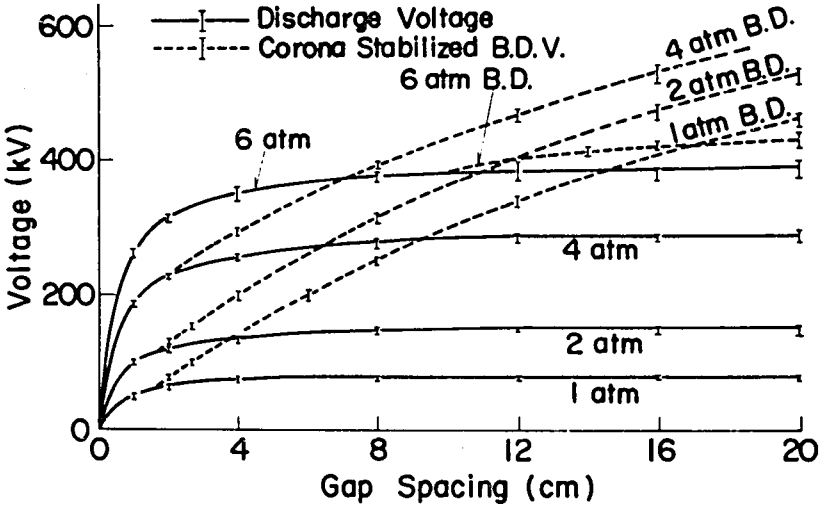


Fig.23(b) Discharge and Corona Stabilized Breakdown Voltages of Gap C for Negative dc Voltage

higher than that for positive polarity. These results show the fact that the corona stabilization is more stable for negative applied voltage.

These dc discharge characteristics should be compared with the results in ac experiments in Fig.14 and 15.

## 5-2. Conditions for Corona Stabilization in $SF_6$ [75]

No quantitative analysis on the conditions of the corona stabilization breakdown in $SF_6$ has been reported so far. As a start of our discussion, we postulate that a steamer, that is initiated at the high field region in the vicinity of the electrode, will cross the gap through the low field region in the gap, when the field at the tip of the streamer is so high that the size of a new avalanche at the head is larger than $N_{crit}$. For simplisity, we simulate the tip of the streamer whose length is x by a conductive sphere of radius r and potential $V_s$ as shown in Fig.24. [72]

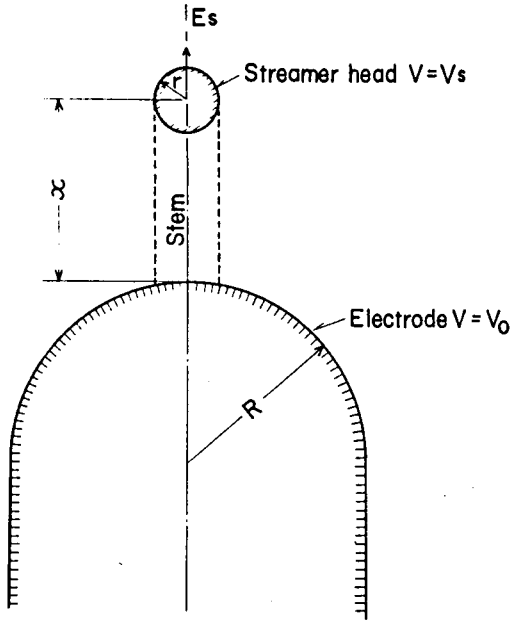


Fig.24 A Model for Streamer Propagation

The value of $V_s$ will be close to that of the electrode $V_o$, when the conductivity of the streamer stem is high. While $V_s$ will coincide to the potential V(x) of the point x before the start of the discharge process, if the conductivity of the stem is sufficiently

low. The actual value of $V_s$ will be in between these two values, depending on gas pressure, field distribution and the polarity of the applied voltage.

$$V(x) < V_s < V_o \tag{29}$$

If we assume the radius of the streamer r is small enough so the applied field strength E(x) is uniform within the range of x ± r, then the field at the tip of the streamer $E_s$ is given by simple electric field theory as;

$$E_s = 3 \cdot E(x) + \frac{V_s - V(x)}{r} \tag{30}$$

As the simplest quantitative analysis, a streamer initiated at the maximum field region under a certain applied voltage is considered to progress across the gap, when the value of $E_s$ in equation 30 at $E(x) = E_{min}$ exceed $E_{max}$. That is;

$$E_{max} \leqslant 3\ E_{min} + \frac{V_s - V(x)}{r}$$

or

$$\left(1 - \frac{3 \cdot E_{min}}{E_{max}}\right) \leqslant \frac{V_s - V(x)}{r \cdot E_{max}} \tag{31}$$

The numerator of the right hand of equation 31 is roughly proportional to the breakdown voltage of the gap. When we consider two similar gaps of different size, breakdown voltages of these gaps at a given pressure are approximately proportional to a characteristic length of the gaps. The radius of the electrode at the point of the maximum field strength will be the best length which represents the geometry of the gap. Since the denominator of the right hand of equation 31 is the function of gas pressure and not too much dependent on the geometry of the gap, the relation is approximately expressed as;

$$\left(1 - \frac{3\ E_{min}}{E_{max}}\right) / R \leqslant F(p) \tag{32}$$

Where, F(p) is a function of gas pressure only.

Equation 32 suggests that the critical condition of the corona stabilized breakdown is expressed as a function of the gas pressure and the parameter $(1 - 3 \cdot E_{min}/E_{max})/R$. To check the validity of the relation, experimental data at the critical point where the breakdown voltage starts to be corona stabilized are plotted on the gas pressure vs $(1 - 3 \cdot E_{min}/E_{max})/R$ plane in Fig.25. There have been reported a number of experimental data on

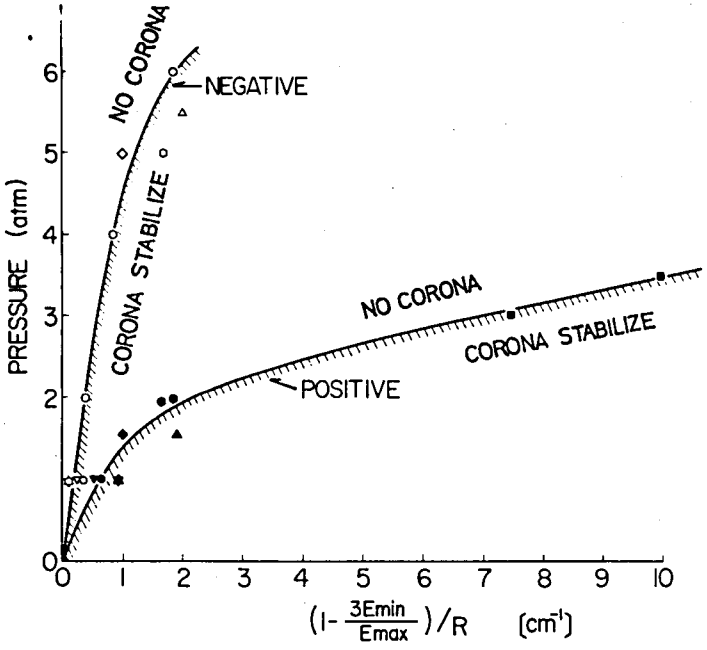


Fig.25 Criterion for Corona Stabilized Breakdown

the corona stabilized breakdown in $SF_6$. Most of these experiments were performed on very divergent field gaps and corona stabilization is observed only for positive polarity within the moderate pressure range of several atms. Some of the reported data in the literature are also plotted in Fig.25. Although the data scatter considerably, the results clearly show the critical condition of the corona stabilized breakdown for positive and negative polarities.

5-3. Corona Stabilization and ac Breakdown

In Section 4 and 5, two very important characteristics of electrical discharge in $SF_6$ were discussed independently.

(1) Discharge voltage of high pressure $SF_6$ gas is lower than the theoretical estimation, and the reduction is caused by the effect of cathode surface. The condition on the surface of anode has little to do with the discharge characteristics of the gap.

(2) Corona stabilization is more likely to occur for negative applied voltage. In the case of Gap C, for example, corona stabilization is observed up to 6 atm for negative polarity, while it is observed only in the pressure range lower than 2 atm for positive polarity.

In comparing Fig.15 and Fig.23, we can see that corona stabilization for ac applied voltage is quite similar to that of positive dc applied voltage. This is quite understandable since positive voltage is lower than the corona stabilized negative breakdown voltage and ac breakdown is determined by the severer half cycle of the applied voltage.

However, the detailed investigation of ac and dc characteristics shows very awkward property of ac discharge voltage at high pressures. As an example, the comparison of ac and dc experimental results of the discharge characteristics on Gap C at 6 atm gas pressure and 20 cm spacing are listed in Table 2 from Fig.15 and 23.

There is no corona observed in this gap condition for ac applied voltage and positive dc case. However, ac breakdown voltage coincides to negative corona inception voltage rather than positive breakdown voltage. On applying ac voltage on the gap, negative corona will onset at 380 kV on negative half cycle. The value is lower than the theoretical estimation which is about 420 kV. The reduction is understood as the effect of the cathode surface. However, the reduction should not cause ac breakdown voltage, due to the high corona stabilized breakdown voltage for negative polarity. But actually ac break-

| | Corona V | B.D.V. |
|---|---|---|
| ac | No Corona | 380 kV |
| Pos. dc | No Corona | 420 kV |
| Neg. dc | 380 kV | 430 kV |

Table 2 Critical Conditions of Corona Stabilized Breakdown for Gap B and C

down occurs when the peak voltage reaches to this negative corona starting voltage.

This relation between ac breakdown voltage and reduced negative corona incpetion voltage is more pronounced for roughned electrode.

Fig.26(a) and (b) are positive and negative dc discharge and corona stabilized breakdown voltages for roughened gap C. If we compare the curves with ac characteristics in Fig.16, again the condition for corona stabilization for ac applied voltage is quite similar to that for positive dc voltage. But ac breakdown voltages without corona coincide to corona inception voltages for negative dc applied voltage.

To understand this awkward property of ac discharge voltage, pre-breakdown current through the grounded electrode has been measured by a parallel detective circuit of 4 KΩ resister and 1000 pF capacitor. Fig.27(a) shows the phase relation of applied voltage and pre-breakdown current. It is clearly seen that the current pulse at the negative peak of the applied voltage triggers the breakdown of the gap at the succeeding positive peak of the applied voltage. This means the ions produced by the negative corona remain in the low field region in the gap or on the electrodes and bring about breakdown in the successive positive half cycle. Fig.27(b) is the detailed wave shape of the negative pre-breakdown current pulse.

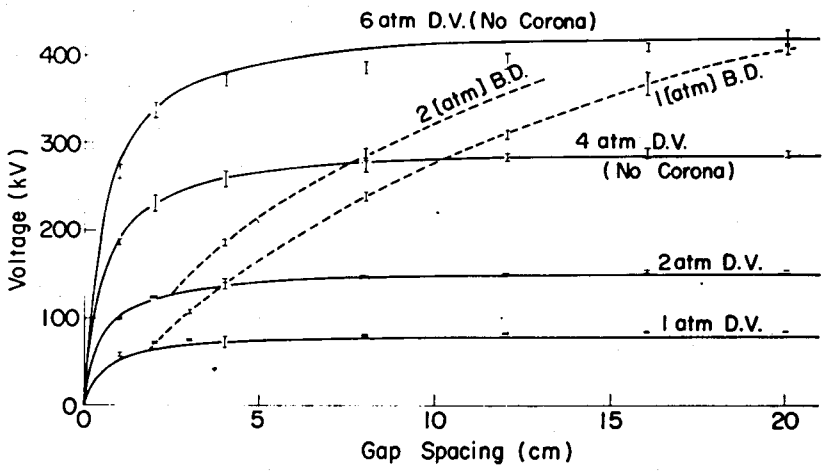


Fig.26(a) Positive Discharge and Corona Stabilized Breakdown Voltages for Roughened Gap C

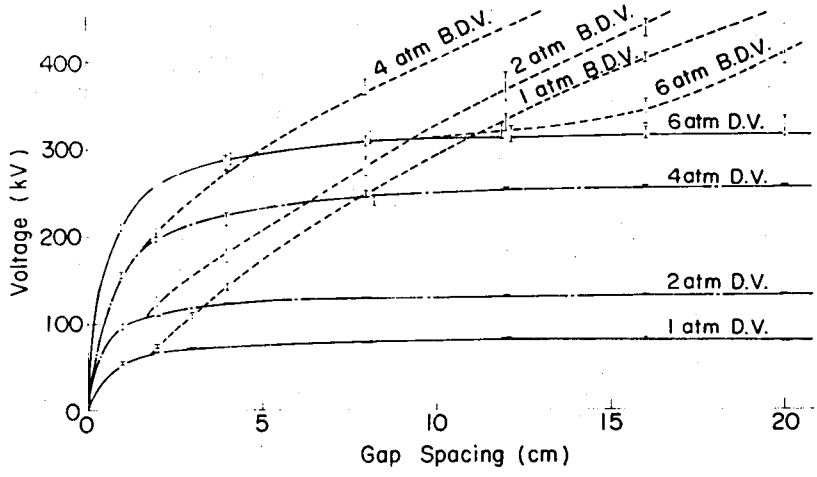


Fig.26(b) Negative Discharge and Corona Stabilized Breakdown Voltages for Roughened Gap C

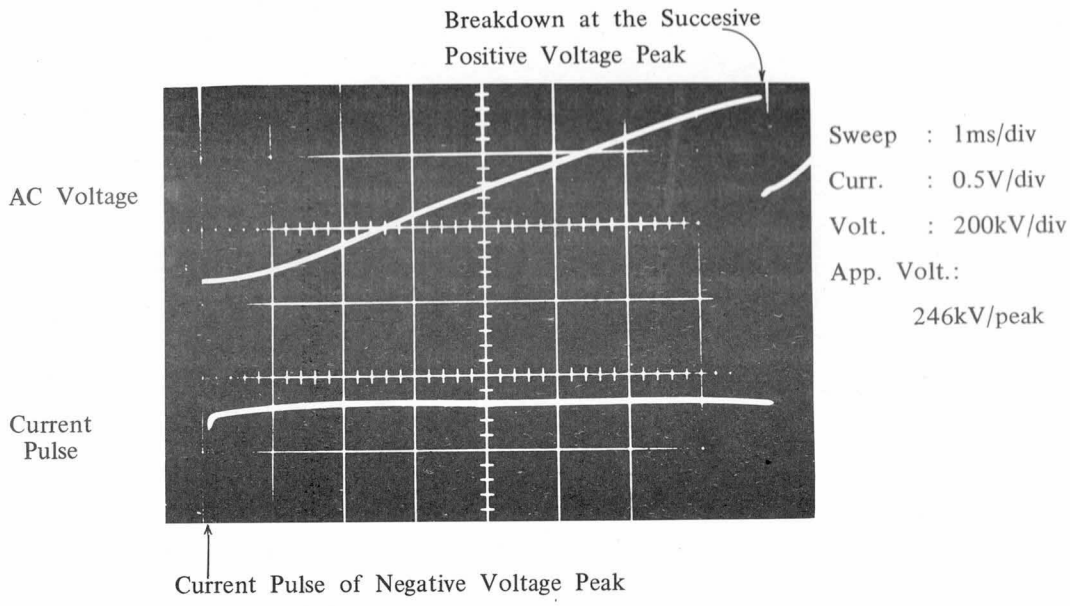


Fig.27(a) Positive Breakdown caused by the Corona Pulse in the foregoing Negative Half Cycle ( Gap C p = 4 atm l = 8cm Rough Surface )

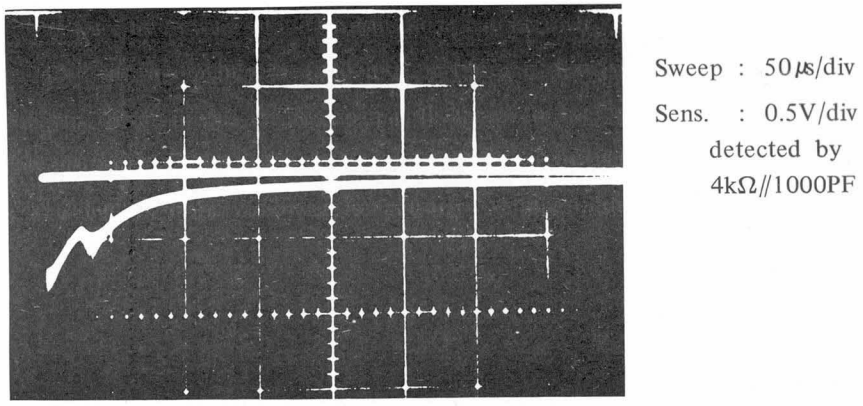


Fig.27(b) Detailed Wave Shape of the Negative Current Pulse

## §6. Conclusion

Breakdown characteristics for ac and dc applied voltages were studied experimentally and the results were compared with the theoretical conclusions discussed in Chapter II.

It is shown that the theory explains the experimental results very well at low gas pressures. At high gas pressures, however, breakdown voltage is found out to be lower than the theoretical estimation due to the effect of negative electrode.

(1) The reduction of the discharge voltage from the theoretical estimation begins at lower pressure and the rate of the reduction increases by the roughening of the electrode.

(2) For carefully polished electrode, the reduction begins when the surface field strength reaches a critical value of about 400 kV/cm independent of the shape of the electrode while it begins at about 150 kV/cm or less for roughened electrode.

(3) According to the results of dc experiment, the reduction is caused by the effect of the negative electrode.

(4) The reduction is the function of the size of the electrode. It is pronounced for larger electrode.

In the case of a very non-uniform field gap in relatively low gas pressure, the discharge started at the highly stressed area in the gap does not develop the breakdown of the total gap. It produces steady corona discharge in the high field region and deconcentrates the electric field to bring about unusually high breakdown voltage. The conditions of this so-called "corona stabilized breakdown" is quantitatively presented as shown in Fig.25.

# IV. EFFECT OF ELECTRODE SURFACE ON THE ELECTRICAL BREAKDOWN OF COMPRESSED $SF_6$ [77]

## §1. Introduction

As a result of experimental studies explained in Chapter III, the effect of electrode surface is found to be playing very important role in the discharge characteristics of $SF_6$. The roughened surface of electrode is effective to reduce the discharge voltage of the gap, particularly at high gas pressures. The following three possible explanations have been proposed for the effect of electrode. [52]

(1) Surface irregularities such as microscopic protrusions on the electrode enhance the electric field strength at the point. Electron multiplication process in this enhanced field is high enough to satisfy the discharge criterion and produce electrical discharge of the gap.

(2) If the applied field strength exceeds a certain critical value, field strength at the tip of an irregularity on the cathode is high enough to cause field emission of electrons. Even if the electron multiplication caused by each field emitted electron is negligible or too low to initiate discharge of the gap, negative space charge field formed by the attachment of these electrons is high enough to produce discharge of the gap.

(3) A charged conducting particle on the electrode is levitated by the effect of applied voltage. Then just before it hits the oppositely charged electrode, it produces micro-discharge which may trigger the breakdown of the gap.

The third mechanism is important when rather large conducting particles of the size of millimeters exist in the gap. The effect has been studied by many people by putting large conducting particles intentively in the gap. [50–55, 57] In the present discussion, we limit our interest in the reduction of discharge voltage of high pressure $SF_6$ with no intentional particles or irregularities. There exist some microscopic irregularities on the electrode, even if the gap is prepared very carefully, and they will work as weak points of the gap to lower the breakdown voltage. These weak points statistically distribute on the electrode at a certain rate depending on the way of the finish of the electrode surface.

In the first part of the present chapter, surface irregularities on the electrode finished in two different grades are studied using electron microscope technique. Then, the field enhancement due to the individual irregularity is discussed, assuming the shape of each protrusion as a hemi-spheroid. The effect of the protrusion on the electrical discharge of $SF_6$ gas is discussed based on the static field distribution in the vicinity of the protrusion.

When the discharge voltage is lower than the theoretical estimation, low dark current of order of $10^{-9}$ to $10^{-5}$ amp is observed depending on the test condition. Results of an experimental study on the dark current are presented and the characteristics are discussed in the last part of the present chapter. The property of the dark current and the succeeding breakdown or discharge inception of the gap have suggested the fact that the discharge at the voltage lower than the theoretical estimation is attributed to the field distortion caused by some kind of charge accumulation in the gap.

## §2. Electrode Surface Condition

It is very difficult to define and control the condition of the electrode surface quantitatively. Even if the surface is finished in the same way, the condition is not exactly reproducible and statistically changes by nature. The surface will also be dependent on the material of the electrode, as the shape and the distribution of the irregularities are different by the kind of materials. The effect of electrode is dependent on the material from this reason as well as the difference in the physical properties of the material such as work function.

Some measurements on the surface irregularities are presented to get an idea of the microscopic properties of electrodes made of stainless steel (SUS 27) and aluminum. Two different grades of surface finish have been tested. Grade A is finished to glassy surface by #2000 emery paper. The surface corresponds to that of carefully treated laboratory electrode. Grade B corresponds to the surface of carefully manufactured gas insulated apparatus and treated by #80 emery paper.

Roughness of these surfaces are measured by a needle type surface roughness meter (Kosaka Laboratory Ltd., Type SE–3C). Examples of the typical roughness curves for grade A and B are shown in Fig.28 and 29, respectively. Roughness of an aluminum electrode is higher than that of a stainless steel electrode about the order of two, even if they are both finished in the same grade.

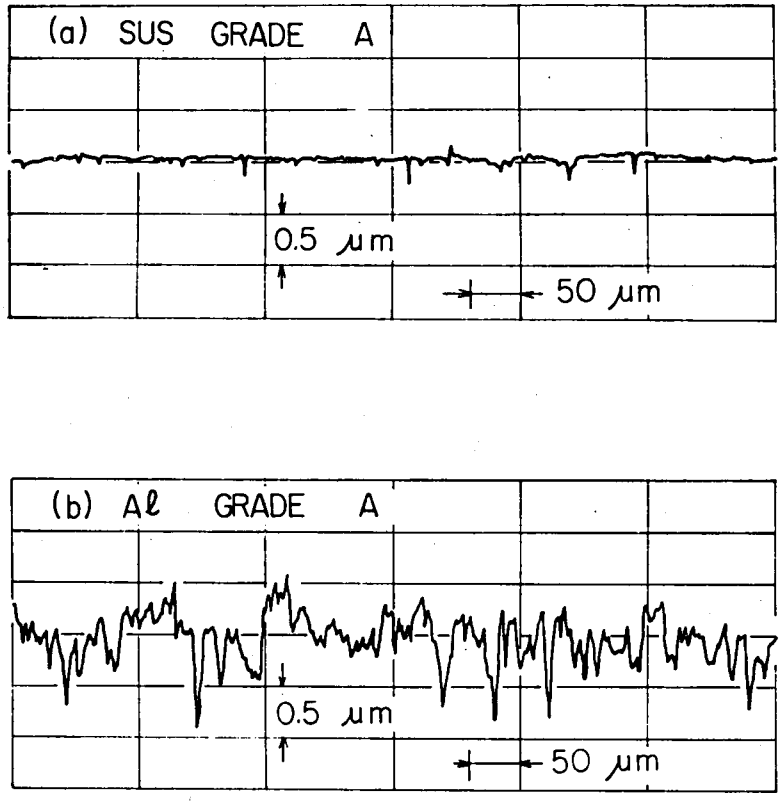


Fig.28 Surface Roughness of Fine Finished Electrodes (Grade A)

If the number of weak points is the origin of the effect of the electrode in $SF_6$ breakdown, equivalent area of an aluminum electrode will be larger than that of stainless steel electrode in the same gap conditions. Most of the irregularities on the electrode are depressions rather than protrusions. Only protrusions will be effective in reducing the breakdown voltage. This means that the number of weak points is not too many as might be felt from the roughness curves in Fig.28 and 29. This is true particularly for a fine finished electrode.

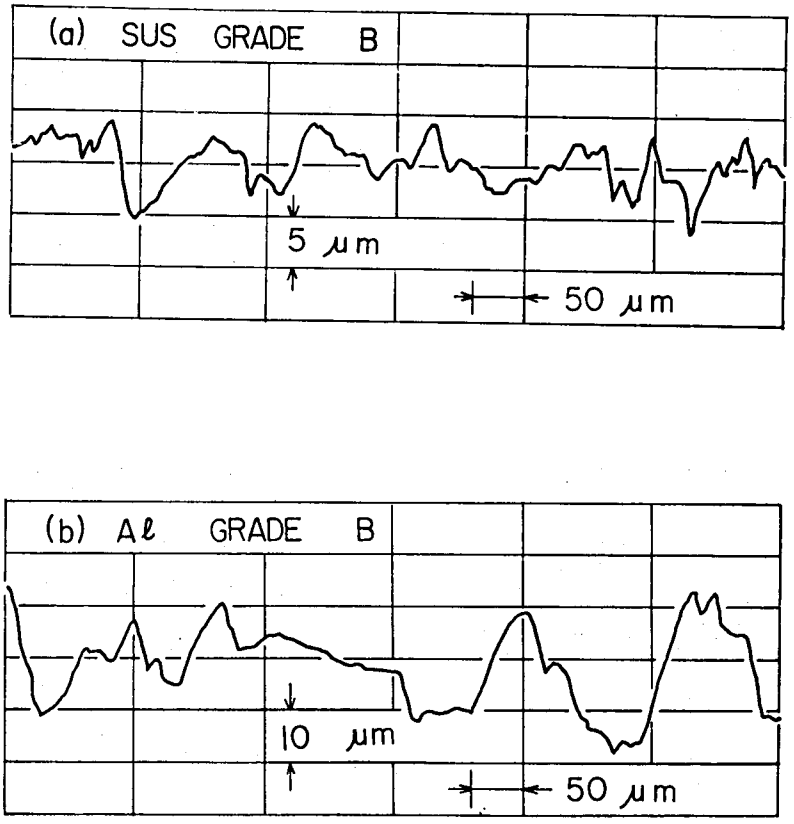


Fig.29 Surface Roughness of Rough Finished Electrodes (Grade B)

The largest protrusion on the electrode finished in Grade A will be of the order of 0.5$\mu$ in its height, while they are of the order of 10 – 20$\mu$ in Grade B. In comparison with this large difference by the way of finish, the difference by the material is only of the order of two as mentioned.

The conditions of the electrode surface are photographed by a scanning electron microscope (S. E. M.). Examples of the S. E. M. photograph are shown in Fig.30 and 31.

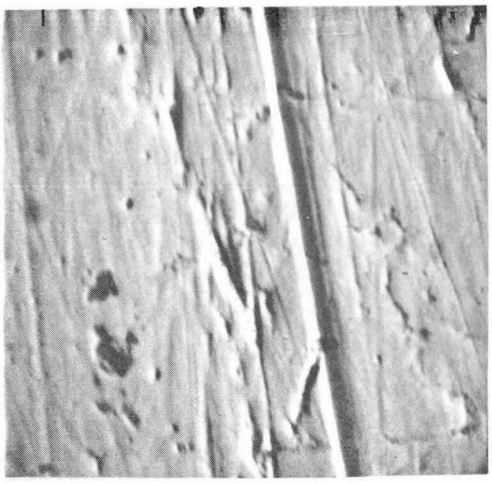

10μm

(a) Stainless Steel, Grade A (X1260)

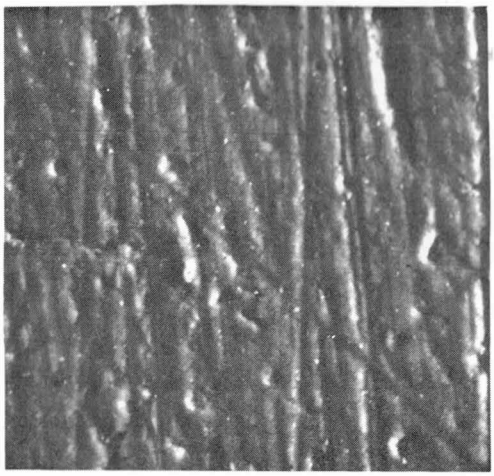

10μm

(b) Aluminum, Grade A (x420)

Fig.30 S.E.M. Photographs of the Surface of Fine Finished Electrodes

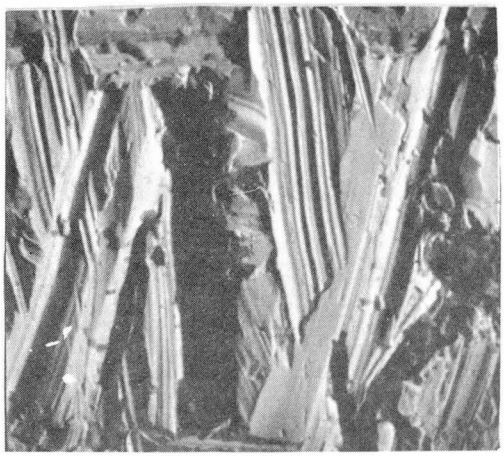

10μm

(a) Stainless Steel, Grade B (x420)

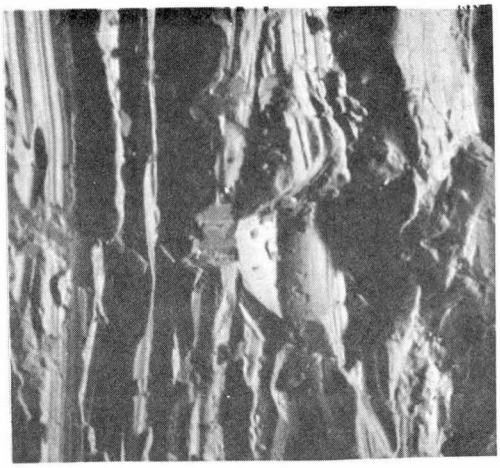

100μm

(b) Aluminum, Grade B (x126)

Fig.31 S.E.M. Photographs of the Surface of Rough Finished Electrodes

The surface has many scratches which will correspond to the depressions observed in the roughness meter experiment. There are also observed some sharp scobs at the edge or the end of the scratches. One of the typical sharp protrusions on the surface of rough finished stainless steel electrode is shown in Fig.32. These sharp protrusions may work as the weak points of the gap which reduce the breakdown voltage of the gap.

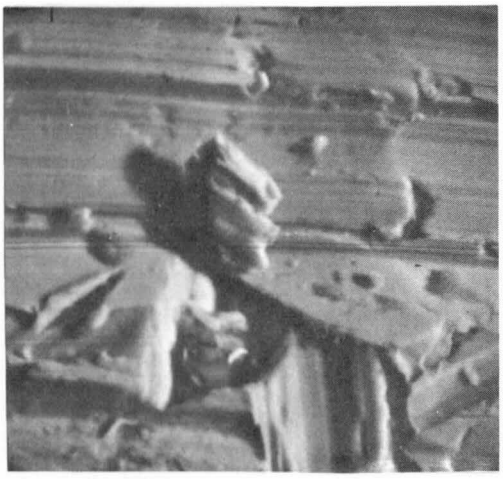


Fig.32 Example of a Sharp Protrusion (SUS, Grade B, x 1260)

## §3. Effect of Microscopic Protrusions on the Electrical Discharge [77]

In the foregoing section, we get an idea of what kind of irregularities are present on the surface of electrode of two different grades of finish. The effect of these surface irregularities on the electrical discharge of uniform field gap in $SF_6$ is discussed in this section from the static field point of view. As the simplest approximation, a protrusion on the surface of electrode is approximated as a hemispheroid as shown in Fig.33. The size of the protrusion is chosen as negligibly small in comparison with the gap spacing.

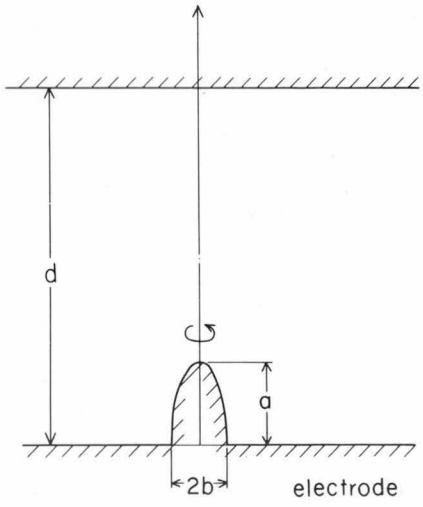


Fig.33 Postulated Hemi-Spheroidal Protrusion

Since the protrusion is very small, not the approximate form of the discharge inception criterion in equation 15 or 16, but equation 10 in Chapter II is applied directly in estimating the discharge voltage under the effect of the protrusion by the aid of an electronic computer. Electrical field distribution along the axis of the hemispheroidal protrusion

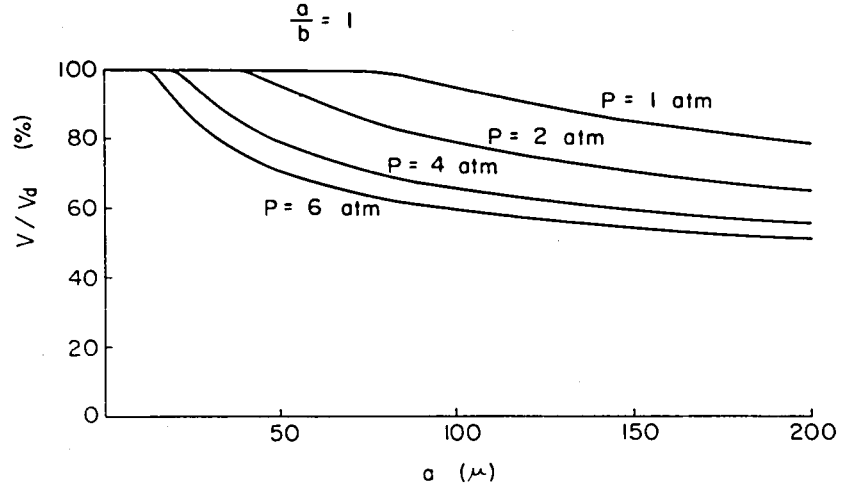


Fig.34(a) Reduction of Discharge Voltage by the Effect of Micro-Protrusion (a/b=1)

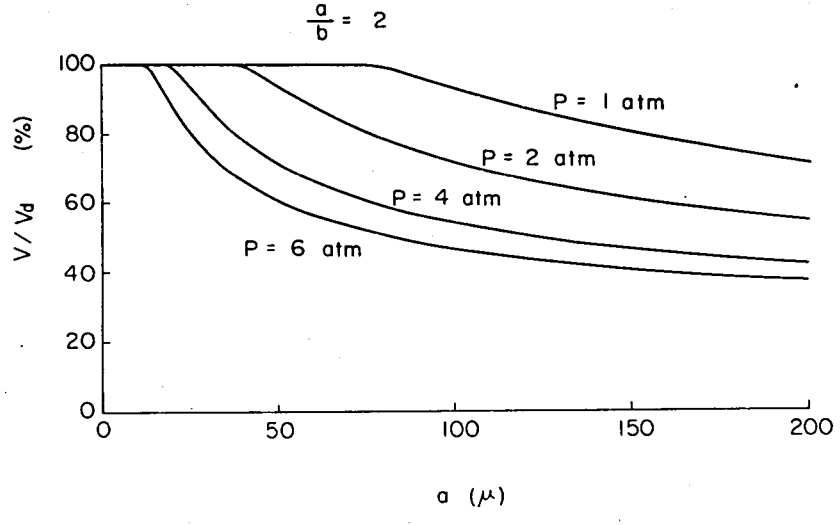


Fig.34(b) Reduction of Discharge Voltage by the Effect of Micro-Protrusion (a/b=2)

is analyzed by a simple approximation as detailed in Appendix II. The approximation is very good when the height of the protrusion is small in comparison with the gap spacing as it is the case in the present application.

It should be noted that, because of the strong dependence of $\alpha - \eta$ of $SF_6$ gas over electric field strength, even a microscopic protrusion on the electrode can be effective to reduce the discharge voltage appreciably. The effect is theoretically estimated for different shape and size of the protrusion.

The calculated reduction of the breakdown voltage of a parallel plane gap with a protrusion is summarized in Fig.34(a), (b) for two different values of a/b, the ratio of vertical and radial radius of the spheroid. Relative value of the breakdown voltage under the effect of the protrusion to that of smooth parallel plane gap is independent of the spacing of the gap, since the height of the protrusion is negligible to the gap spacing. The breakdown voltage of the smooth parallel plane gap $V_d$ is obtained by equation 9 in Chapter II.

The effect of a protrusion is prominent at high gas pressures. A protrusion whose height is more than $10\mu$ is appreciable at 6 atm, while a protrusion smaller than $75\mu$ in height has little effect on the breakdown of $SF_6$ at 1 atm pressure. These values of the critical height where a protrusion becomes effective are almost constant, independent of its shape. The critical height is plotted as a function of gas pressure in Fig.35. For constant height larger than the critical value, sharper protrusion is more

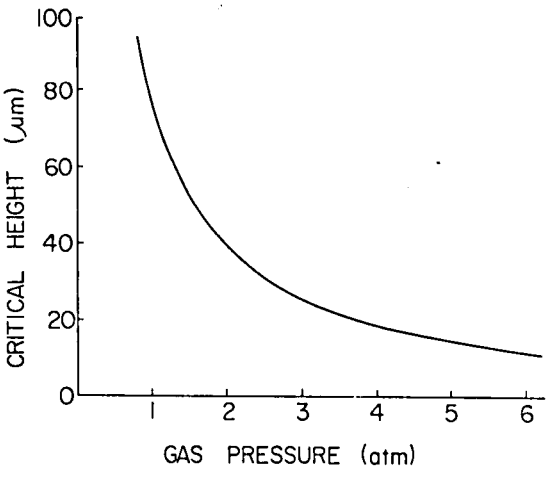


Fig.35 Critical Height of Protrusion as a Function of Gas Pressure

effective in reducing the breakdown voltage of the gap. Any protrusion less than $10\mu$ in height has little effect in deducing the breakdown voltage of the gap as far as the static field concerns.

The experimental results on the reduction of breakdown or discharge inception voltage presented in Chapter III, show that the critical pressures where the reduction becomes appreciable are about 6 and 2 atms for fine and rough electrode surfaces. The expected height of the projections which corresponds to these critical pressures are determined from Fig.35 as $15\mu$ and $40\mu$ for fine and rough electrodes, respectively.

According to the observation on the actual electrode surface in Section 2, a few protrusions of the order of $40\mu$ in height may not be unrealistic for the surface finished in Grade B. However, the protrusions of $15\mu$ in height seems to be too large for the surface of Grade A.

It should be noted that the above calculations are performed based on the breakdown criterion of equation 10, without any farther considerations on the applicability of the criterion. The criterion has the following two problems in applying to these microscopic irregularities.

Firstly, the field strength at the head of the protrusion $E_{max}$ at the calculated breakdown voltage is quite high in comparison with the field strength required for $\alpha = \eta$. Linear relation between $(\alpha - \eta) / p$ and $E/p$ in equation 6 may not hold in this high field region. Neglecting the local field in the vicinity of the protrusion, macroscopic field strength of an uniform field gap at its breakdown is given by equation 8 as;

$$E = \left[ \left( \frac{E}{p} \right)_{crit} \cdot p + \frac{ln\ N_{crit}}{Kd} \right] \frac{V}{V_d}$$

$$\cong \left( \frac{E}{p} \right)_{crit} \cdot p \cdot \frac{V}{V_d}$$

Here, $V/V_d$ is the ratio of the breakdown voltage and its theoretical estimation and the value is the order of 0.4 to 1 in the condition of practical interest.

Field enhancement factor $\beta$ ($= E_{max}/E_{av}$) for hemispheroidal protrusion is calculated as in Fig.36 from Fig.II-3 in Appendix II. The maximum field strength at the head of the protrusion devided by gas pressure p is roughly given as;

$$\frac{E}{p} = \left( \frac{E}{p} \right)_{crit} \frac{V}{V_d} \cdot \beta \qquad (33)$$

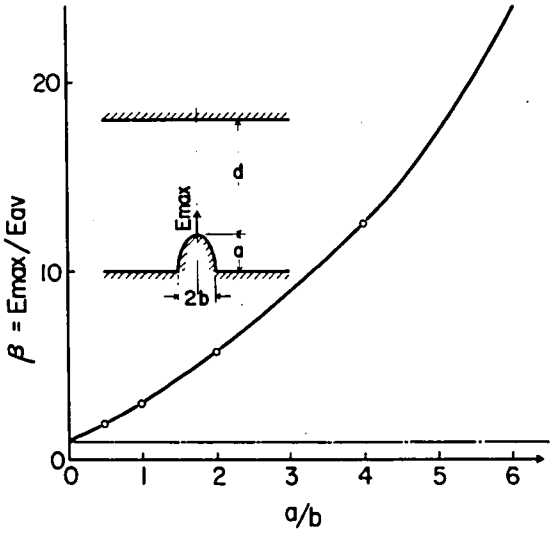


Fig.36 Field Enhancement at the Tip of a Hemi-Spheroidal Protrusion

Equation 33 , together with Fig.36, shows the fact that the calculation may be quite erratic for the protrusion whose a/b value is much larger than unity, since the field strength is too high for proper application of equation 6. For the protrusion of larger a/b, the value of $\alpha - \eta$ will be smaller than the estimated value by equation 6. This means the effect of sharper protrusion will be less than the value estimated by the calculation above.

The second question on the validity of the discharge criterion used is the effect of the field emission of electrons from the tip of the protrusion. The maximum field strength at the tip of a protrusion of a/b = 4 at 6 atm, for example, is about 7 MV/cm. If we consider the uncleanness of the surface, the field strength may be high enough to have an appreciable amount of field emission of electrons from metal surface. The field emitted electrons will produce space charge in the gap and distort the static field.

From these problems on the validity of the discharge criterion, the same type of calculation on the protrusions whose a/b is higher than 4 is meaningless. For these sharper protrusions, effect of field emission will be more important factor in determining the discharge voltage of the gap.

An experimental study of the field emission from the electrode surface will be given in the following section.

## §4. Prebreakdown Dark Current in Compressed $SF_6$

When the discharge voltage of $SF_6$ is lower than the theoretical estimation, there observed very low dark current of the order of $10^{-9} \sim 10^{-5}$ amp., depending on the test condition. [79, 80] This dark current may be a good indication of the importance of the field distortion caused by the space charge due to the field emitted electrons, microparticles in the gap or some other mechanisms alike. [81] The characteristics of the dark current is experimentally studied for various gap conditions. The results of the test are detailed in this section.

### 4-1. Experimental Setup

The dark current is measured by the circuit shown in Fig.37.

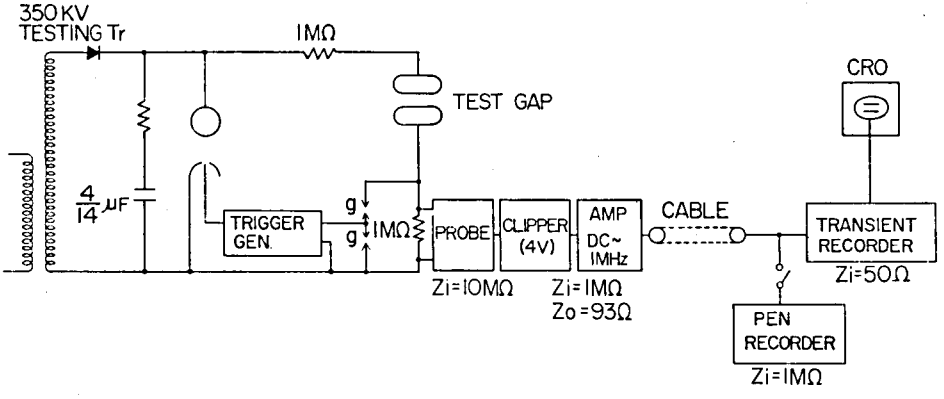


Fig.37 Test Circuit for Dark Current Measurement

Long term variance of the dark current is recorded by a pen recorder. Transient component of the dark current prior to the breakdown is measured by the use of a transient recorder (Biomation, Type 8100) in combination with a synchroscope. The transient recorder has a function to sample the temporal change of the current at a certain interval of time and the data is digitalized and memorized until the memory is replaced by new data after a specified period of time. This temporal memory of data permits to observe the prebreakdown current just prior to the breakdown afterward, using the breakdown itself as a trigger.

The dark current is attributed to the irregularities on the electrode and has statistical property by nature. This means the characteristic is dependent on the surface area of the electrode. The dependence is studied on two gaps, Gap D and E of different electrode surface area shown in Table 3.

| Gap | Shape | Area($cm^2$) | Spacing (cm) | Material |
|---|---|---|---|---|
| D | 2 cm$^{\phi}$ Sp-Pl | ~0.05 | 0.05 ~0.15 | Stainless St. |
| E | 10 cm$^{\phi}$ Pl-Pl | 80 | 0.1 | Stainless St. |

Table 3 Two Gaps used in Dark Current Experiment

Gap D is 2 cm diameter sphere to plane gap. Different from an usual sphere plane gap, a hemi-sphere of 2 cm diameter is placed on the grounded side of a parallel plane gap insulated from the ground, so that the dark current flows into the hemi-sphere is measured separately, the grounded plane as a guard. The dark current is measured by applying positive voltage so the hemi-sphere which gives the maximum field is the negative electrode. Since the spacing of the gap is very small in comparison with the radius of the hemisphere, electric field of the gap is eventually identical to that of a sphere to plane gap. Gap E is 10 cm diameter parallel plane gap whose effective area is three orders of magnitude as large as that of Gap D. The estimation of the effective area of a sphere-plane gap will be discussed more quantitatively in Chapter V and in Appendix IV. The surface of these electrodes are finished in a few different grades including Grade A and B defined in the foregoing sections, to change the dark current flows through the gaps.

These gaps were tested in a small acrylate vessel of 13 cm inner diameter and 60 cm in height shown in Fig.38. The spacing of these gaps are limited to rather small values to limit the applied voltage low enough to be corona free during the measurement of very low dark current and also eliminate the effect of the wall of the vessel. This limitation on gap spacing will be reasonable since we are mostly interested in the effect of electrode surface and gap spacing weight as secondary process. The breakdown voltage characteristics of these gaps will be presented in the following chapter.

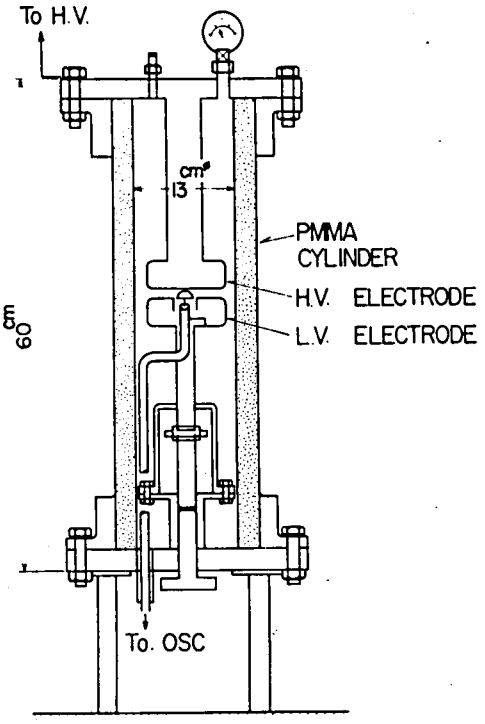


Fig.38 Test Vessel for Dark Current Experiment

4-2. Characteristics of the Dark Current

An example of the slow temporal change of the dark current measured by a pen recorder on Gap D finished in Grade B at p = 6 atm is illustrated in Fig.39. When the applied voltage reaches about 14 kV, or the field strength on the surface of the negative electrode is about 140 kV/cm, very low dark current of the order of $10^{-9}$ amp is observed. It should be noted that the field coincides to the critical field strength for rough finished electrode where the reduction of the breakdown voltage from the theoretical estimation begins. The average current increases with the applied field strength gradually, nevertheless it is not stable and sporadically increases to a very high value of the order of submicro-amperes.

Breakdown of Gap D usually occurs on some point on this sporadic high current, however the breakdown does not necessarily correspond to the highest instantaneous value of the current. To see the characteristics of the dark current in more detail, the current just prior to the breakdown is measured by the transient recorder. Fig.40(a) is the dark current several seconds before the breakdown on the same shot shown in Fig.39.

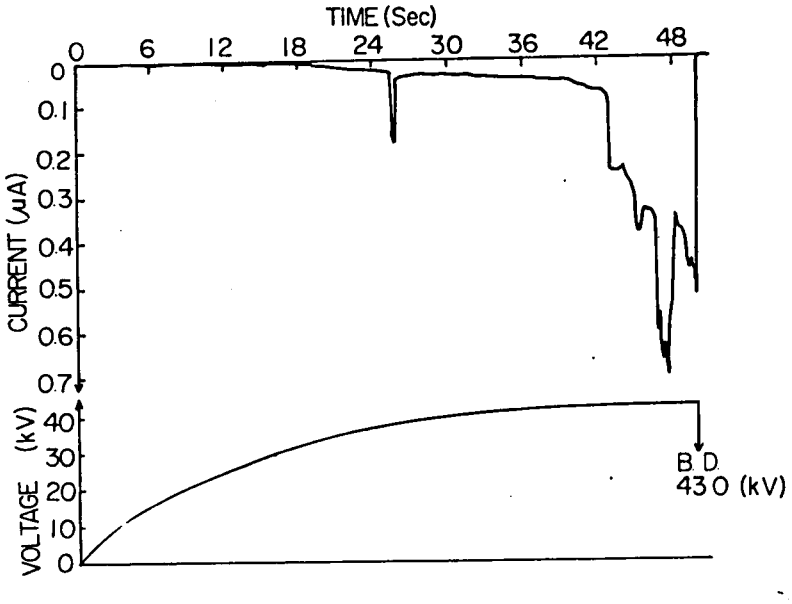


Fig.39 Dark Current Observed under the Effect of Electrode Surface (Gap D, Rough Finished)

Notwithstanding the fact that the dark current of Gap D is not steady as seen in this figure, the temporal change of the dark current is quite slow in comparison with the time required for the breakdown of the gap. If we see a few micro seconds ahead of the breakdown, the dark current is almost constant as shown in Fig.40(b). Continuous dark current of about 0.7 $\mu$A in the oscillogram corresponds to the peak of the fluctuating current in Fig.40 (a). Upper trace of Fig. 40(b) is the oscillogram of the applied voltage which shows the instant of the breakdown.

The sporadic change of the dark current in Fig.40(a) is commonly seen for small area gap D. On the contrary, it is quite stable for Gap E particularly at high pressures. The feature is compared by the oscillograms in Fig.41. Dark current for Gap D at 4 atm is similar to that of the same gap at 6 atm shown in Fig.40(a), while the current for Gap E at 8 atm is quite stable and the value is many times higher than the value for the former case. Average values of the dark current in these two cases are almost proportional to the area of Gap D and E, since the breakdown field of the gaps at the test conditions are at the same level. Note the breakdown field strength decreases with the area of the electrode. If we compare the dark current at the breakdown on these two

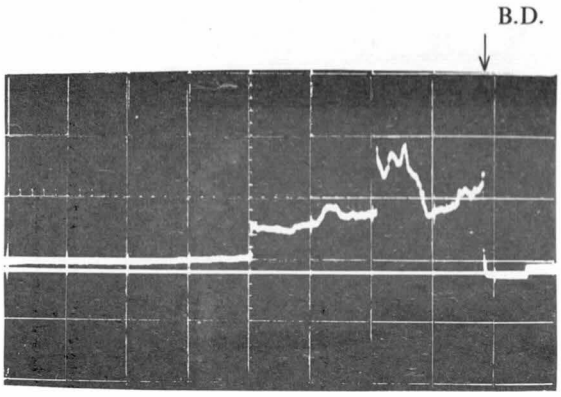


(a) Gap D at p = 6 atm

$V_{app}$ = 43 kV (80.5%)
Sens. : 0.338 μA/div
Sweep : 2 sec/div

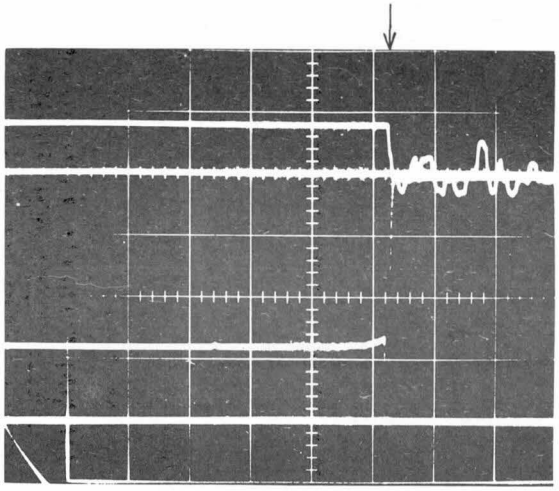

(b) Gap D at p = 6 atm

$V_{app}$ = 41 kV (76.8%)
Sens. Volt. : 51.6 kV/div
Curr. : 0.606 μA/div
Sweep : 2 μs/div

**Fig.40 Examples of the Prebreakdown Dark Current Measured by the Transient Recorder**

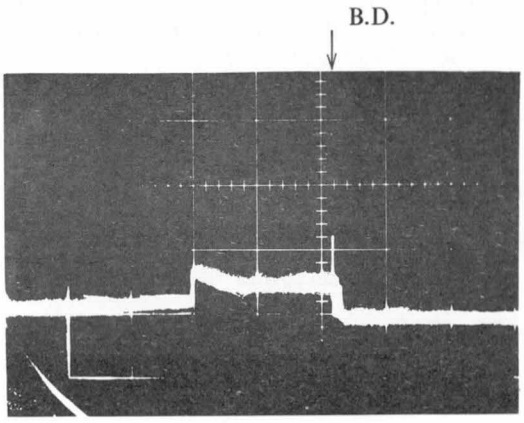


(a) Gap D at p = 4 atm

$V_{app}$ = 33 kV (92.7%)
Sens. : 0.19 μA (92.7%)
Sweep : 1 sec/div

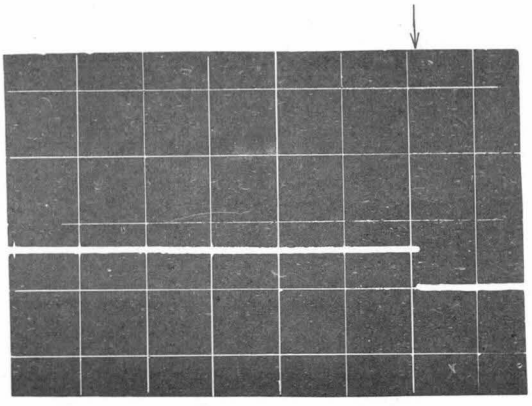

(b) Gap E at p = 8 atm

$V_{app}$ = 35.5 kV (50%)
Sens. : 31.5 μA/div
Sweep : 1 sec/div

Fig.41 Examples of the Dark Current prior to the Breakdown of Rough Finished Gaps D and E

gaps at the same pressure, the amount of the current is by no means proportional to the area of the electrode because of the different breakdown field strength.

A slight increase in the current is observed just prior to the breakdown in the oscillogram in Fig.40(b). If the continuous component of the prebreakdown current comes from more than one site on the electrode, as will be reasonablly expected from the characteristics in Fig.41, while the breakdown occurs only at one point, this transient component of the dark current will be related to the breakdown of the gap.

To know the more detailed characteristics of the transient component just prior to the breakdown, the dark current is measured by cutting off the continuous component by a series capacitor, so that only the transient component can be measured with higher sensitivity.

Examples of the oscillograms of the transient component of the prebreakdown current are shown in Fig.42 to 44. Fig.42 is the comparison of the transient component of Gap D and E at 4 atm. The breakdown voltage of Gap D is pretty close to the theoretical estimation in this example and the amount of the dark current is very low. Percentage in the blacket shown in the figures is the ratio between the breakdown voltage and its theoretical estimation. The dark current is one order of magnitude larger for gap E in this test condition. The breakdown voltage of the gap is 78.6% of the theoretical prediction.

Fig.43 is the same comparison at p = 6 atm. Breakdown voltages of gap D and E are not so different in the examples and the amount of the prebreakdown current is also in the same level. Transient dark currents for Gap D and E at 8 atm are presented in Fig.44. Gap D has higher current than Gap E in the examples, despite of the higher breakdown voltage of Gap D. The amount of the current in both of the examples in the figure is very high in comparison with the cases at lower pressures shown in Fig.42 and 43.

The transient component of the prebreakdown current statistically scatters in wide variety from shot to shot. However, different from the continuous component of the dark current, there is observed no particular difference in the average values of the transient current of these gaps D and E. The fact means that the transient current is originated from one site of the gap, and the site brings about reduced breakdown voltage of the gap. That is, the site works as a "weak point" of the gap. As in the example of Fig.44, higher prebreakdown current does not necessarily mean low breakdown voltage of the gap. But, if we consider the wide variety in the shape and other properties of the weak

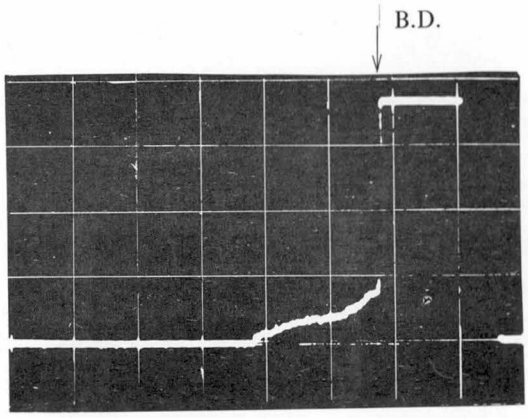


(a) Gap D

$V_{app}$ = 35 kV (98.4%)
Sens. : 0.0135 μA/div
Sweep : 2 μs/div

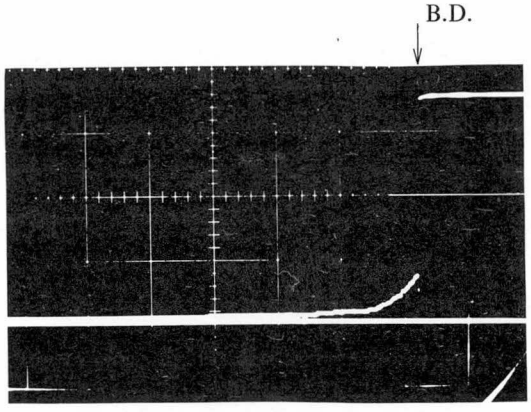


(b) Gap E

$V_{app}$ = 28 kV (78.6%)
Sens. : 0.357 μA/div
Sweep : 2 μs/div

Fig.42 Transient Component of the Prebreakdown Dark Current of Gap D and E at p = 4 atm

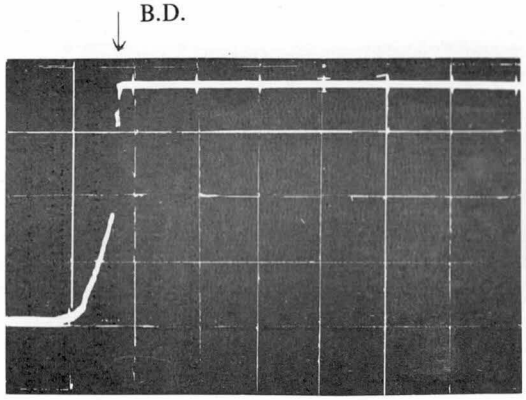


(a) Gap D

$V_{app}$ = 39.5 kV (74.2%)
Sens. : 0.27 μA/div
Sweep : 2 μs/div

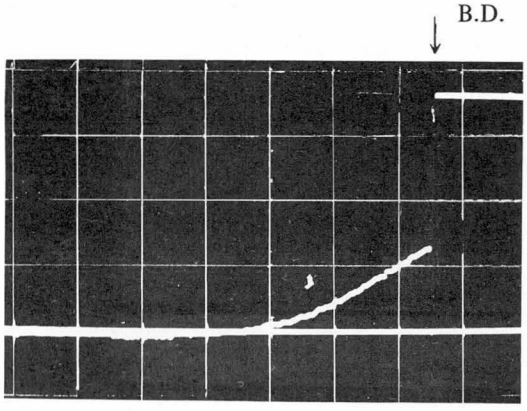


$V_{app}$ = 37.0 kV (69.3%)
Sens. : 0.281 μA/div
Sweep : 2 μs/div

Fig.43 Transient Component of the Prebreakdown Dark Current of Gap D and E at p = 6 atm

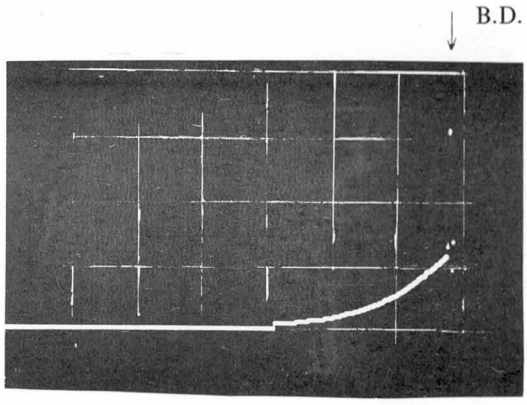


(a) Gap D

$V_{app}$ = 44 kV (61.8%)
Sens. : 3.57 μA/div
Sweep : 2 μs/div

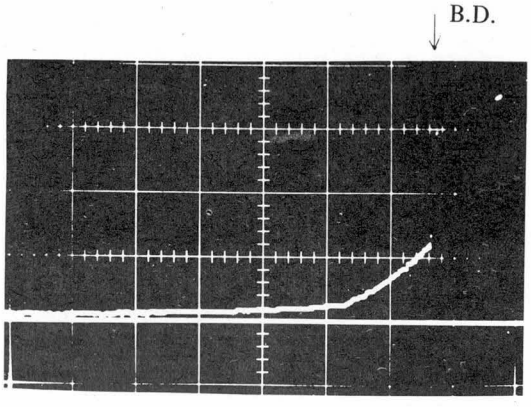


(b) Gap E

$V_{app}$ = 42 kV (59.0%)
Sens. : 0.725 μA/div
Sweep : 2 μs/div

Fig.44 Transient Component of the Prebreakdown Dark Current of Gap D and E at p = 8 atm

points on the electrode, the statistical scattering of the prebreakdown current will be quite understandable.

## 4-3. Prebreakdown Current and Breakdown Voltage of a Gap

In spite of the variety of the transient component of the prebreakdown current, there seems to be some correlation between the amount of the current and the reduction of the breakdown voltage from the theoretical estimation. The relation is testified in this section.

The correlation is more apparent in a series of succesive tests. Fig.45 shows examples of the transient component of the prebreakdown current of fine finished Gap D at 6 atm taken in series. We can see the corelation very clearly. In the case of Fig.45(c), the breakdown voltage is very close to the theoretical estimation and the breakdown is built up very abruptly with small prebreakdown current. Wiggles on the zero line of this oscillogram is the noise in the measuring circuit. They are stepwise because of the digitalization of the noise in the transient recorder.

The correlation between the amount of the prebreakdown current and the reduction of the breakdown voltage is not always in order as in the examples in Fig.45. Despite of the scattering, there observed some statistical correlation between these two phenomena. The reduction of the breakdown voltage from the theoretical estimation is plotted as a function of the peak of the transient component of the prebreakdown current from a number of oscillograms in Fig.46. The figure shows clear correlation and the plots falls on a single curve independent of gas pressure and the type of gaps. The fact shows that the breakdown is caused by the single weakest point on the electrode. Temporal build up of the transient component of the prebreakdown dark current in Fig.42 to 45 may suggest that the phenomena involves some kind of discharge caused by the weakest point on the electrode. More detailed study is necessary to clarify the relation between the prebreakdown current and the breakdown of the gap.

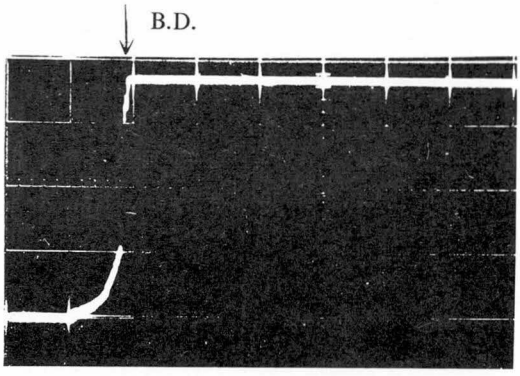


(a) $V_{app}$ = 43.2 kV (80.9%)
Sens. : 0.27 μA/div
Sweep : 2 μs/div

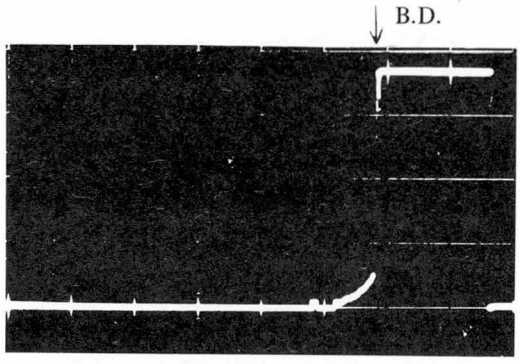


(b) $V_{app}$ = 44.5 kV (83.3%)
Sens. : 0.27 μA/div
Sweep : 2 μs/div

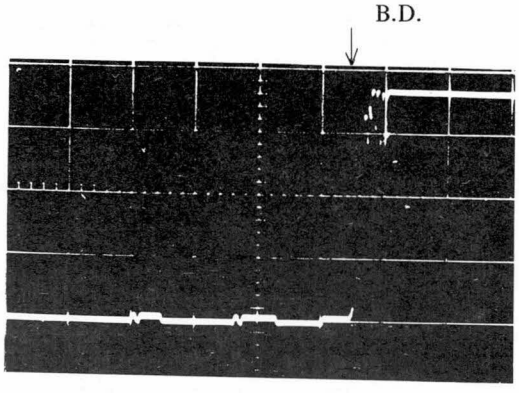


(c) $V_{app}$ = 52.0 kV (97.4%)
Sens. : 0.27 μA/div
Sweep : 2 μs/div

Fig.45 Transient Component of the Prebreakdown Dark Current and the Reduction of the Breakdown Voltage (Gap D, Fine Finish, p = 6 atm)

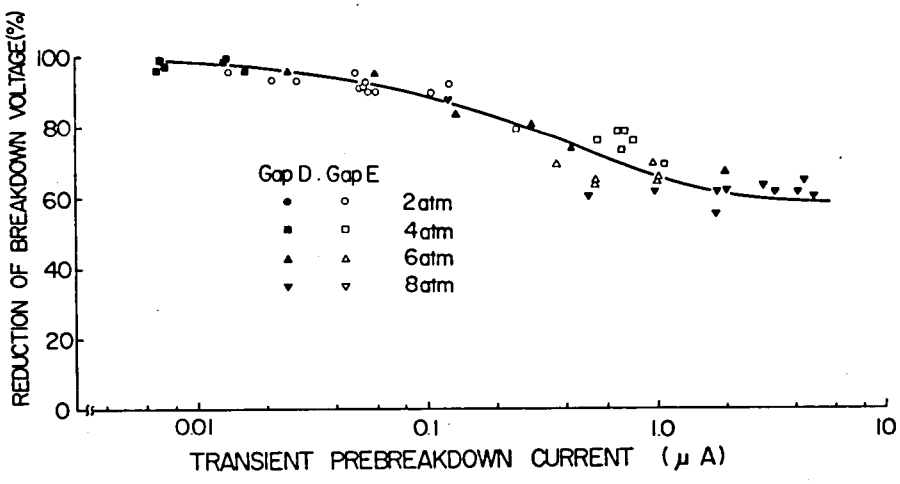


Fig.46 Transient Component of Dark Current and the Reduction of Breakdown Voltage

## §5. Conclusion

Microscopic irregularities or protrusions on the surface of electrode and their effects on electrical breakdown of $SF_6$ gas were studied.

(1) A glassy surface of laboratory electrode has the irregularities of the order of 0.5μ, while the surface of the electrode of a typical gas insulated equipment will have those of the order of a few tens of microns in height.

(2) The roughness of an aluminum electrode is higher than that of a stainless steel electrode about the order of two, even if they are finished in the same way.

(3) If we consider that the electron multiplication process in the vicinity of a protrusion is the cause of the reduction of the breakdown voltage, the effect of the protrusion will be very small, unless the height of the protrusion is higher than the critical values shown in Fig.35. However, the protrusion may be effective to reduce the breakdown voltage by the field emission of electons from its sharp tip and it works as a weak point of the electrical insulation of the gap.

(4) When the breakdown voltage is lower than the theoretical estimation, dark current of the order of $10^{-9}$ to $10^{-5}$ amp flows, depending on the test condition. The correlation between the transient component of the dark current just prior to the breakdown and the reduction of the breakdown voltage from the theoretical estimation is observed. The relation is independent of gas pressure and the area of electrode. The fact suggests that the reduction of the breakdown voltage is caused by the single weakest point on the electrode. The shape of the transient dark current prior to the breakdown also suggests some kind of electrical discharge caused by the weakest point.

# V. EFFECT OF ELECTRODE AREA ON THE ELECTRICAL BREAKDOWN IN $SF_6$

## §1. Introduction

Breakdown field strength of $SF_6$ gas is theoretically formulated in Chapter II as a function of gas pressure and the shape of electrode. The formulation explains experimental results very well for highly polished small electrode in relatively low pressure $SF_6$. The relation does not hold, however, when the field strength on the negative electrode exceeds a certain critical value determined by the finish of the electrode surface and gas pressure. Experimental discharge voltage is lower than the theoretical estimation in this condition.

The critical field strength and the discrepancy between the theoretical estimation and the experimental discharge inception field strength depend very much on the area and the surface conditions of electrode as discussed in the previous chapters. Fig.47 shows the examples of the experimental evidence of the electrode area effect reported by Bornik and Cooke [82] and Morii et al [18] plotted on the same figure. Remarkable reduction of the breakdown field strength can be seen by the increase of electrode area.

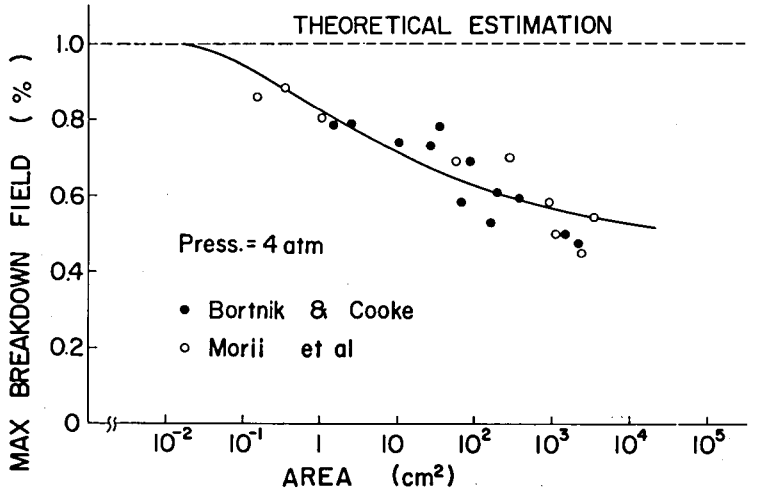


Fig.47 Electrode Area Effect of Breakdown Field in $SF_6$

It is concluded in Chapter IV that the discharge voltage at high pressure is governed by the weak points on the electrode which have statistical property by nature. If the weak points statistically distribute evenly on the surface of the electrode and the breakdown of the gap is determined by the weakest point in the gap, statistical property of a gap whose area is S is identical to that of a parallel connection of S gaps of unit area. Because of this property of the weak points, stressed area of the electrode becomes one of the most important factors in determining the breakdown field of compressed $SF_6$ gas.

In this chapter the results of experimental study on the statistical distribution of the breakdown voltages, electrode area effect and the conditioning effect of the electrical breakdown of the gas for various gap conditions will be discussed. [83, 84] Then, the reduction of the breakdown voltage from the theoretical estimation under the effect of the electrode is quantitatively analyzed by the light of Weibull statistics. [85]

## §2. Experimental Setup

The effect of electrode area on breakdown characteristics of $SF_6$ is tested using five gaps with different surface area listed in Table 4. The gap of the smallest area is 2 cm diameter sphere to plane Gap D, the same gap used in the dark current experiment. The effective area of the sphere electrode of Gap D is about 0.05 $cm^2$. (See Appendix IV)

| gap | dimension | area ($cm^2$) | relative area | spacing (cm) | material |
|---|---|---|---|---|---|
| D | 2cm$^\phi$ sphere - plane | ~0.05 | ~ 1/1600 | 0.1 | stainless steel |
| E | 10cm$^\phi$ plane - plane | 80 | 1.0 | 0.5 | stainless steel |
| F | 13.2cm$^\phi$ - 15.2cm$^\phi$ x 11.6 cm coaxial - cylinder | 480 | 6.0 | 1.0 | stainless steel aluminium |
| G | 23.75cm$^\phi$ 25.75cm$^\phi$ x 40.2cm coaxial - cylinder | 3000 | 37.5 | 1.0 | aluminium |
| H | 3cm$^\phi$ rod - plane | ~0.40 | ~ 1/200 | 0.5 | stainless steel |

Table 4 Five Electrodes used in the Area Effect Experiment

Gap E is 10 cm diameter parallel planes also used in the dark current experiment, the area of which is about 80 $cm^2$. Most of the tests on this gap are performed at 0.5 cm spacing to assure highly uniform electric field.

Gap F and G are coaxial cylinders. The inner and outer diameters and the length of Gap F are 13.2 cm, 15.2 cm and 11.6 cm, respectively. Those dimensions of Gap G are 23.75 cm, 25.75 cm and 40.2 cm. The effective area of the internal electrode of Gap F and G are about 480 $cm^2$ and 3,000 $cm^2$, respectively. The spacing of Gap F and G is 1.0 cm. This value is chosen in considering manufacturing tolerance of gap setting.

Gap D and E are tested in the acrylate vessel in Fig.38. The metal tank in Fig.11 is used for the large coaxial cylinder gaps F and G.

Gap H is particularly used in the study of the effect of ultra violet light irradiation on the breakdown voltage distribution in the metal tank. U.V. light is irradiated through a qualtz window provided on the wall of the tank.

Asymmetric field distribution of the gap except that of Gap E permits to study the effect of positive and negative electrodes of the gap separately.

The precision of the gap setting of all of these gaps is within 1%. Preliminary test has been performed on Gap E on the effect of the gap spacing, considering the variety of the gap spacing used in the experiment. According to the result of the test, gap spacing between 0.1 to 1.0 cm tested has little effect on the statistical properties of breakdown of $SF_6$ as far as breakdown field strength concerns.

Surface of these five electrodes is finished in two different grades A and B discussed in section 2 in Chapter IV.

Tests are performed applying 60 Hz ac and in some cases, positive and negative dc voltages by the same circuit as in Fig.12. Breakdown characteristics for ac and negative dc voltage are scarcely different for nearly uniform field gaps like those used in the present experiment. Direct current voltage is used only in testing the effect of the polarity of applied voltage.

Applied voltage is raised to about 50% of the expected breakdown voltage of the gap in 20 sec, then slowly to the breakdown voltage by the rate of about 1% of the expected breakdown voltage per second. Two hundred breakdowns are obtained in each case with time interval of about 2 min without refinishing the electrode.

Damage of the electrode by the breakdown is minimized, using the high speed diverter technique presented in Chapter III. Voltage source is short circuited by a series of trigger

gaps about 1 μs after the breakdown of the gap under test. If the diverter missed to work, the damage of the electrode caused by the breakdown was heavy enough to lower the succeeding breakdown voltage considerably. In this case, the surface of electrode had to be refinished and the test was run from the beginning.

Surface of the test electrodes is refinished after 200 shots of breakdown in each test case.

## §3. Types of the Breakdown Characteristics

Fig.48 to 51 show the historical sequences of ac breakdown voltages of the four fine finished gaps D to G shown in Table 4. The pressures denoted are absolute values at 20°C. The theoretical estimations of the breakdown voltage by equation 18 are shown by dotted lines in the figures.

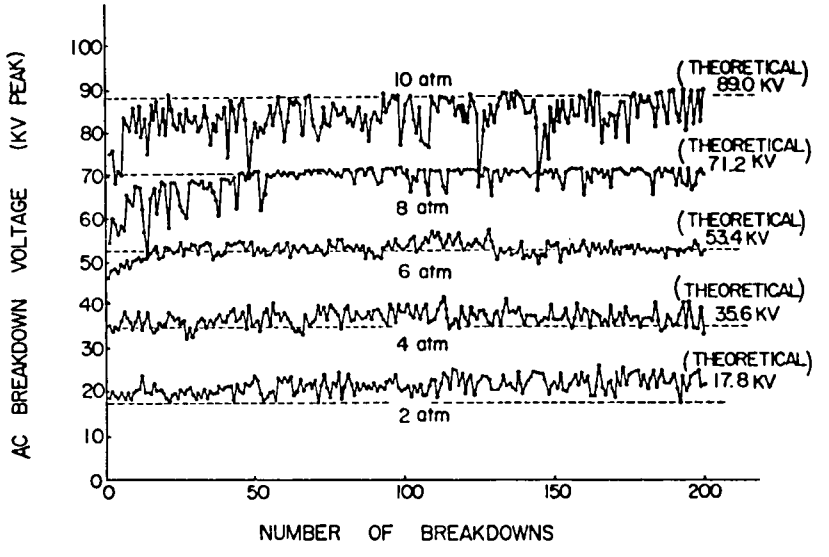


Fig.48 Sequence of the Breakdown Voltages for Fine Finished Gap D

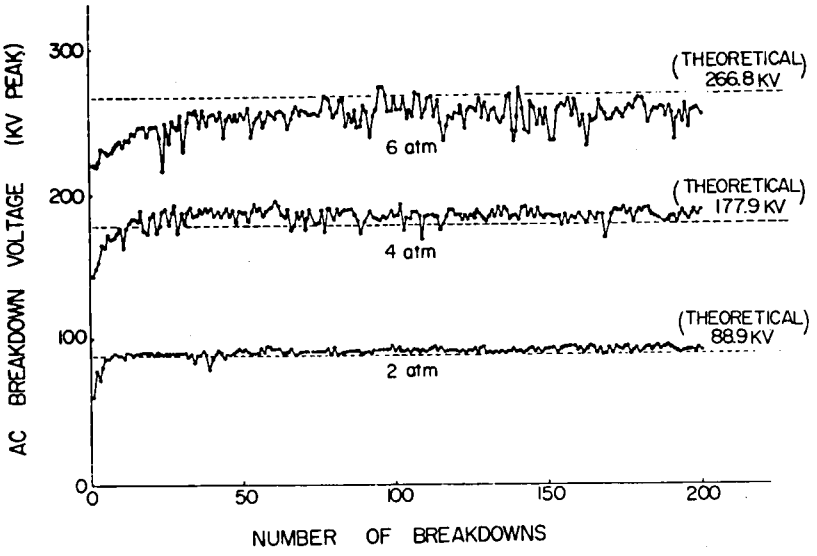


Fig.49 Sequence of Breakdown Voltages for Fine Finished Gap E

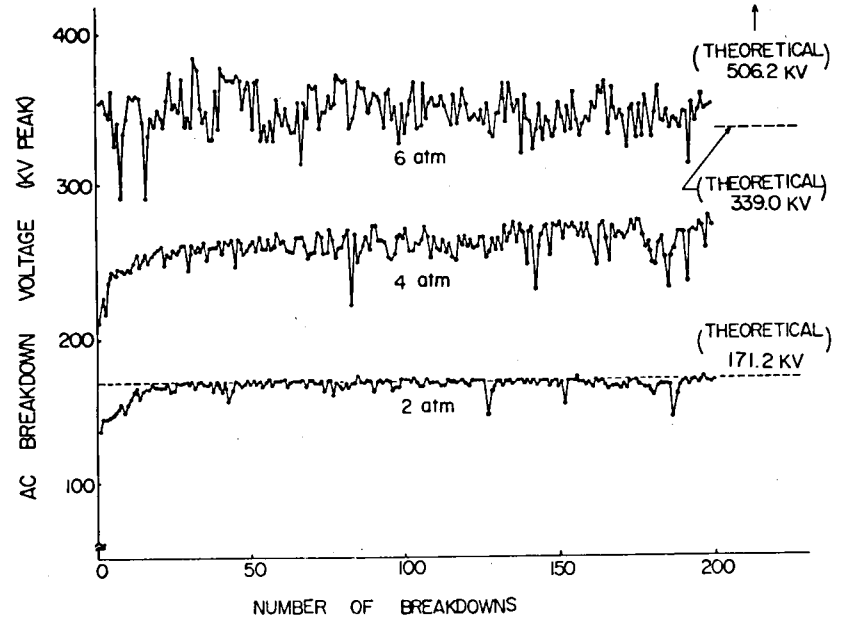


Fig.50 Sequence of Breakdown Voltages for Fine Finished Gap F

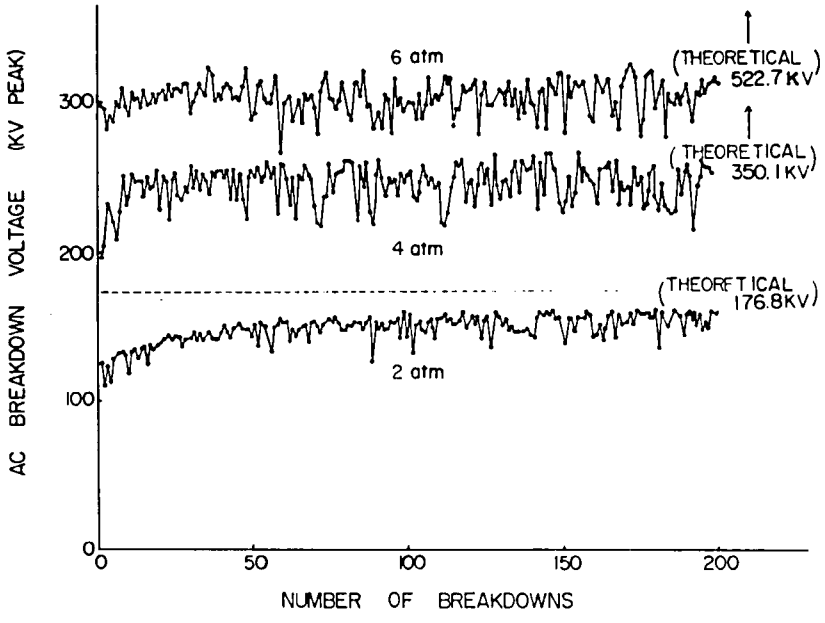


Fig.51 Sequence of Breakdown Voltages for Fine Finished Gap G

Careful investigation of Fig.48–51 suggests the fact that these historical sequences of ac breakdown voltage can be classified into four types, depending on the test condition of electrode area and gas pressure.

Type I: Breakdown voltages are always higher than the theoretical estimation shown by the dotted lines. The lowest value in the distribution is close to the theoretical estimation. (Example, Gap D at p = 2 atm) This type of breakdown characteristic is observed only for the gaps with smaller electrode area at low gas pressures. This type of the breakdown voltage represents the characteristic of $SF_6$ gas and no electrode effect is involved.

Type II: Several breakdowns in the beginning of a test occur at low voltage in comparison with the theoretical estimation. However, after a certain number of breakdowns, the characteristic is quite similar to that of Type I. (Example, Gap E at p = 2 atm)
Low breakdown voltages in the beginning will show the existence of appreciable weak points on the electrode and the destruction of them by breakdown sparks. The increase of the breakdown voltage with the number of sparks is called as "spark conditioning effect". [81, 86]

Type Ⅲ: In this type of breakdown characteristic, the low breakdown voltages never reach to the theoretical estimation even after the gap is fully conditioned. In some cases, sporadic low breakdown voltages are observed after the gap is conditioned. (Example, Gap D at p = 8 atm) The sporadic low breakdown voltages will probably be attributed to the production of new intensive weak points by the effect of the foregoing breakdown. The frequency of the low breakdown voltage increases with the area of electrode and also with gas pressure, because the energy of the breakdown discharge increases with the capcitance of the gap and the breakdown voltage. Even if the voltage source is diverted within a very short period of time, the energy stored in the stray capacitance of the gap is beyond the reach of the diverter technique. For larger electrode area and/or higher gas pressures, every breakdown occurs at the voltage lower than the theoretical estimation (Examples, Gap G at p = 2 atm, Gap F at p = 4 atm) This type of breakdown characteristics will show the existance of a large number of small weak points but limited number of intensive weak points on the electrode.

Type Ⅳ: Breakdown voltages are very low in comparison with the theoretical estimation. No conditioning effect is observed in the historical sequence of the breakdown voltages. (Examples, Gap F and G at p = 6 atm) This type of breakdown characteristic will show the existence of many intensive weak points so that the destruction of weak points by breakdown does not change the statistical distribution of the rest of the weak points.

The breakdown characteristic of a given gap is in one of these four types depending on the properties of the weak points on the electrode. There is a possibility of the fifth type of breakdown characteristic whose breakdown voltage is lowered by deconditioning effect of sparks for large electrode in very high pressure $SF_6$.

For a specified finish of the electrode surface, the number of weak points will be proportional to the area of the electrode. If there exists a certain irregularity on the electrode, the effect as a weak point is dependent on the gas pressure. A given irregularity will be more effective at high gas pressure.

All the experimental results on fine finished gap in Fig.48 to 51 are classified into these four types and plotted in the electrode area vs gas pressure plane in Fig.52, specifying the type of the breakdown characteristics by different marks. For example, the characteristic for Gap D whose effective electrode area is 0.05 $cm^2$ at p = 2 atm is Type I and marked by a solid circle to the bottom left in Fig.52. A few point on 3 cm diameter

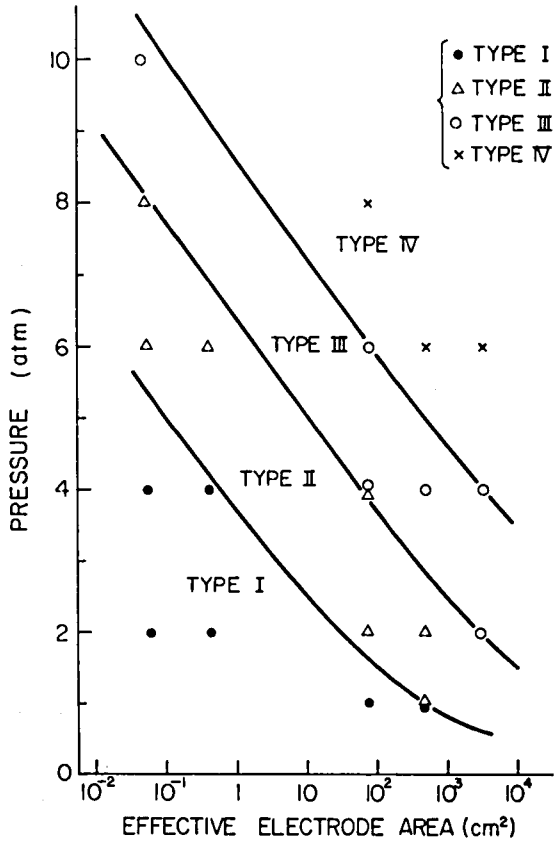


Fig.52 Criterion of Electrode Area and Gas Pressue for Four Types of Breakdown Characteristics of Fine Finished Gaps

rod gap (Gap H) and others not shown in Fig.48 to 51 are added in the figure. Solid lines show the rough estimate of the boundaries of the regions of the electrode area and the gas pressure for the above four types of the breakdown characteristic.

It is interesting to note that the boundary between Type I and II and the boundary between Type III and IV disappear after the gaps are fully conditioned. In this case, the whole range of the electrode area and the gas pressure is divided into two regions for Type I and IV and the boundary is that between Type II and III in Figure 52.

On the other hand, the difference between Type II, III and IV has no meaning for unconditioned electrode. The characteristic for an unconditioned electrode is of practical interest, since most of gas insulated apparatus are not conditioned before they are energized and the first breakdown voltage is the failure voltage of the apparatus. The breakdown

characteristic of an unconditioned gap in Type II and III with conditioning effect have to be obtained as the characteristic of the first breakdown voltage of a number of new gaps. If it is done so, the characteristic in the regions for Type II, III and IV will eventually have no difference. In this case, the breakdown characteristic will be classified into two types and the boundary between these two types of breakdown characteristic is the boundary between Type I and II in Fig.52.

The scattering of the breakdown voltage decreases with the area of electrode and the scattering seems to be due to the lack of initiation electrons in the region of Type I breakdown characteristic. This is quite understandable since we can expect more initiation electrons on larger electrode area. If this is the case, the scattering will deminish by ultra violet light irradiation. On the contrary, the scattering in the regions where the breakdown voltage is lower than the theoretical estimation is supposed to be caused by the statistical nature of the weak points on the surface of the electrode. As we discussed in the previous chapter, when the weak point is effective, there observed small dark current prior to the breakdown of the gap. The fact will show the existence of plenty of initiation electrons in the gap under the effect of the weak point. From this reason, the scattering in the regions should not be influenced by ultra-violet light irradiation.

These features of ultra-violet light irradiation are clearly shown by an experimental results on Gap H shown in Fig.53. Without irradiation, breakdown voltages at 2 atm

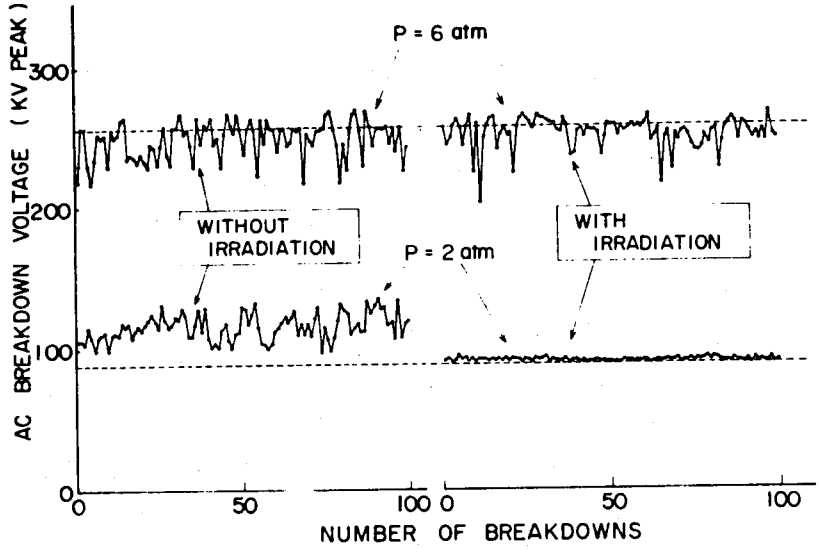


Fig.53 Effect of UV Irradiation on Sequence of ac Breakdown Voltages (Gap H, d=0.5cm, Grade A)

which is in Type I scatter widely, but the scattering decreases drastically by ultra-violet light irradiation and the modal breakdown voltage is lowered from 101 kV to 80 kV. In comparison to this characteristic at low pressure, ultra-violet irradiation has no appreciable effect on the breakdown voltage at 6 atm which is in Type III.

## §4. Statistical Properties of the Breakdown Field Strength

Statistical distribution of the breakdown voltage is one of the explicit indications of the mechanism of the breakdown. Since the breakdown is principally determined by the maximum field strength, statistical distribution of the maximum field strength at the breakdown is discussed in the following.

### 4-1. Transition of the Statistical Distribution

When the statistical distribution is discussed, conditioning effect has to be taken into account to garrantee the identity of the sample population of the data. However, to get a rough idea on the type of the statistical distribution, examples of cumulative probability distribution of the breakdown field strength of fine finished Gap D at various pressure in Fig.48 are plotted in Figure 54 on normal probability paper, neglecting the effect of conditioning.

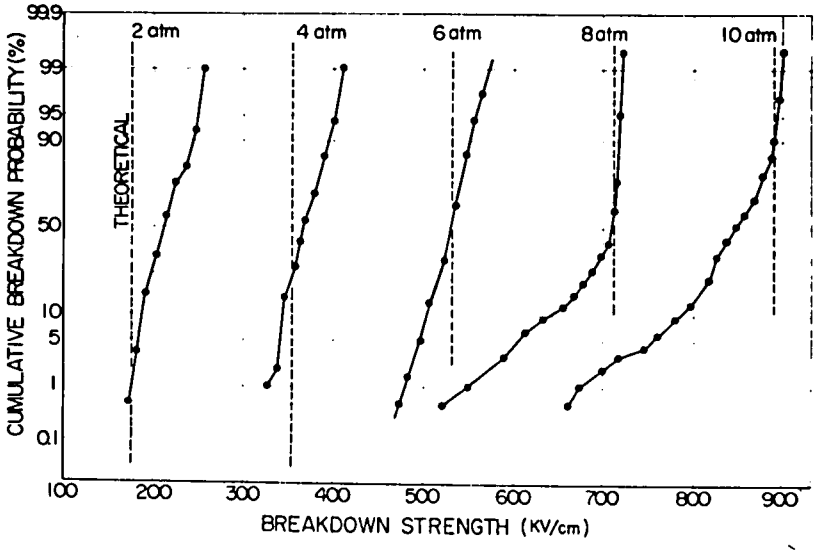


Fig.54
Normal Probability Distributions of Breakdown Field Strength for Fine Finished Gap D

The plots in Figure 54 show that the distributions are normal at low pressures. The slope of the plots is getting steeper with pressure, because high field strength at high gas pressure is effective in the provision of initiation electrons. The distribution departs from the normal at high pressures, where the breakdown strength is appreciably lower than the theoretical estimation. We can notice the transition of the type of the distribution occurs at the boundaries of the regions of area and gas pressure for Type I and II discussed in the foregoing section. The same type of transition of statistical distribution is observed when the area of electrode is increased. These evidences show that the breakdown voltages at high pressure is caused by the irregularities on the surface of electrode. Hence, the statistical properties of the breakdown voltages should be dependent on those of the irregularities. Statistical properties of these irregularities or weak points on the surface of the electrode and their relation to the statistical distribution of the breakdown field strength will be discussed in the followings.

## 4-2. Properties of Weak Points

The weak points may be destroyed or intensified by the energy of the breakdown. In the theoretical discussions, statistical characteristic of the weak points is assumed to be unchanged by the successive breakdown of the gap. This means that the statistical characteristic of the successive breakdown voltages obtained on a given gap is identical to the characteristic of the first breakdown voltages obtained on a number of new gaps.

If a breakdown voltage in successive breakdown experiment is lower than the foregoing value due to the intensification of the weak point, the breakdown will occur at the same site or near-by site to that of the foregoing breakdown. On the other hand, the location of higher voltage breakdown will be transfered to a new site, when the weakest point is destroyed by the foregoing breakdown. From this point of view, the above assumption means the existence of many weak points on the electrode whose intensity is close to that of the weakest point. The experimental observation showed that the breakdown spots usually distributed all over the stressed part of the electrode. This fact will support the plausibility of the assumption on the property of the weak points.

If the number of these intensive weak points is small in comparison with the number of the breakdowns, the average value of the breakdown voltages will increase with the number of breakdowns. This phenomena corresponds to the conditioning effect of the gap. The phenomena is observed experimentally on the gaps of small electrode area in low gas pressure whose number of weak points are limited. The characteristic will be

discussed in the last part of this section.

## 4-3. Weibull Statistics of the Breakdown Field Strength

It is known that the distribution of the breakdown strength which is governed by the weakest point obeys in Weibull distribution or more generally in extreme-value distribution. [87] Weibull distribution is first applied to the problem of high voltage breakdown by Weber and Endicott for the statistical properties of breakdown voltages of transformer oil. [88] The principle can be extended to explain the area effect of compressed gas insulation. [81, 83, 89] Theoretical basis of the statistics of weak points which explain Weibull distribution of the breakdown field strength is presented in the following. [85]

Grade of Weak Point:

The grade of a weak point is expressed quantitatively as the rate of the reduction of the breakdown field strength or more strictly as the ratio of the breakdown field strength E and its theoretical estimation $E_d$. By this difinition small value of $E/E_d$ corresponds to more intensive weak points.

Density of Weak Points:

For an electrode of specified grade of surface finish, number density of weak points whose grade is between $E/E_d$ and $(E+dE)/E_d$ per unit field strength per unit area of electrode, $n(E/E_d)$, will be given as a function of $E/E_d$ something like in Fig.55 for a given gas pressure. The value of $E_o/E_d$ is the grade of the largest possible weak point corresponding to the surface finish in question. The density of the intensive weak point whose grade is $E_o/E_d$ will be very low, but it increases with the value of $E/E_d$. The weak points whose grade $E/E_d$ is larger than unity has little meaning, since they have no effect in reducing the breakdown voltage of the gap.

As a simple approximation, following equation is assumed for the mathematical expression of $n(E/E_d)$.

$$n(E/E_d) = n_o \cdot \left( \frac{E-E_o}{E_d} \right)^{m-1} \quad (cm^{-1} \cdot kV^{-1}) \tag{34}$$

where $n_o$ and m are constants at given surface finish and gas pressure.

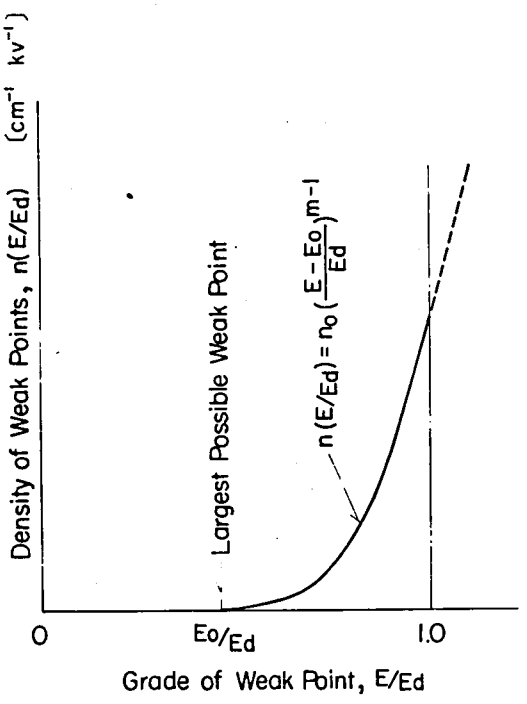


Fig.55 Average Number of Weak Points as the Function of the Grade $E/E_d$

Cumulative number density N(E) of weak points whose breakdown field strength is lower than E is obtained by integrating $n(E/E_d)dE$ from $E_o$ to E as;

$$N(E) = n_o \frac{E_d}{m} \left( \frac{E-E_o}{E_d} \right)^m = \lambda_o \left( \frac{E-E_o}{E_d} \right)^m \qquad (35)$$

where

$$\lambda_o = \frac{n_o}{m} E_d \qquad (36)$$

In this expression, the value of $n_o$ will be given as a function of the density of the irregularities exist "*a priori*" on the electrode, while constant m will be determined by the effect of these irregularities in reducing the breakdown voltage of the gap.

Statistical Distribution of Breakdown Field Strength

For a given electrode area S, probability F(S, E) of having at least one weak point

whose breakdown field strength is less than E, hence the cumulative probability of the breakdown field strength of the gap, is obtained as follows.

The probability of having a weak point whose breakdown field is lower than E on infinitesimally small electrode area dS is N(E)·dS. Then;

$$F(S, E) + \left\{ 1-F(S, E) \right\} \cdot N(E) \cdot dS = F(S + dS, E) \tag{37}$$

The first term of left hand side of the equation and right hand side of the equation are the probabilities of having a weak point whose breakdown field is lower than E on the electrode whose area are S and S+dS, respectively. The second term of the left side of the equation is the same probability on the electrode area dS, providing none of them is on area S. Equation 37 is transformed in a differential equation as;

$$\left\{ 1 - F(S, E) \right\} \cdot N(E) = \frac{dF(S, E)}{dS} \tag{38}$$

The integration of equation 38 gives the expression of F(S, E) as;

$$F(S, E) = 1 - exp \left\{ -N(E) \cdot S \right\} \tag{39}$$

Substituting equation 35,

$$F(S, E) = 1 - exp \left\{ -\lambda_o S \left( \frac{E-E_o}{E_d} \right)^m \right\} \tag{40}$$

or

$$ln\ ln \frac{1}{1 - F(S, E)} = m \cdot ln \left( \frac{E-E_o}{E_d} \right) + ln\ \lambda_o S \tag{41}$$

Equation 40 or 41 of the cumulative probability of the breakdown field strength is Weibull distributuion. [87]

These discussions lead us to the conclusion that when the density of weak points is expressed by equation 34 as a function of $E/E_d$, cumulative probability of the breakdown field strength of the gap obeys Weibull distributuion expressed in equation 41 or *vice-versa.*

In analyzing experimental results by Weibull probability curve, the relation between

$ln\ ln \dfrac{1}{1-F(S,E)}$ and $ln\ (E-E_o)$ may be plotted instead of $ln\ (\dfrac{E-E_o}{E_d})$. Then the relation is;

$$ln\ ln \frac{1}{1-F(S,E)} = m \cdot ln\ (E-E_o) + ln\ \lambda \cdot S \tag{42}$$

where

$$\lambda = \lambda_o / E_d^m \tag{43}$$

And Weibull probability curve is simply shifted downward by $m \cdot ln\ E_d$. More detailed discussion on the properties of Weibull distribution is given in Appendix III.

4-4. Weibull Distribution of Experimental Breakdown Field Strength

The value of $E_o$ at a given pressure will be determined as an asymptotic value of the minimum breakdown field strength when the area of electrode is increased, as it is understood from equation III-3 in Appendix III. Figure 56 shows 0.5% breakdown field strength at various pressure estimated from the experimental data in Fig.48-51 plotted as a function of electrode area. The same plots are also given in the figure for rough finished

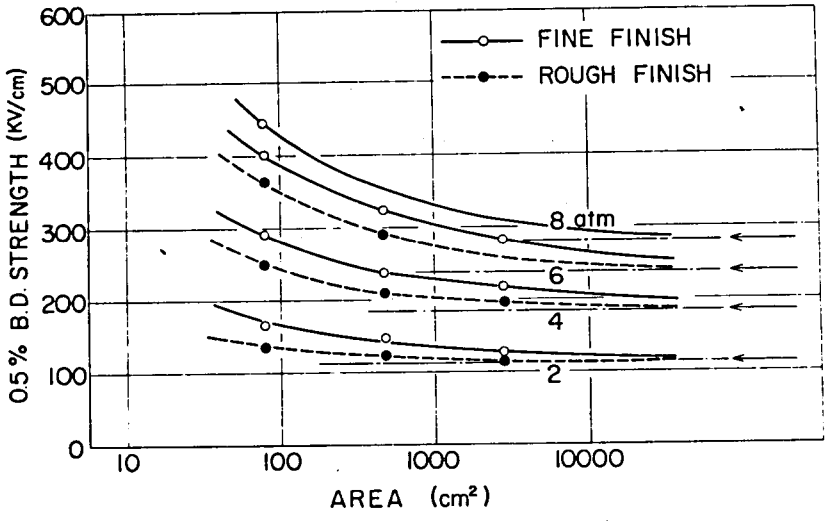


Fig.56 Minimum Breakdown Field Strength as a Function of Electrode Area

electrodes whose characteristics will be discussed later in section 6. The field strength converges to $E_o$ with the area of electrode, and the asymptotic value at each pressure is almost independent of the roughness of electrode. The values of $E_o$ are plotted as a function of gas pressure in Figure 57. The value of $E_o$ obtained experimentally in this fashion may be slightly higher than the actual value of $E_o$.

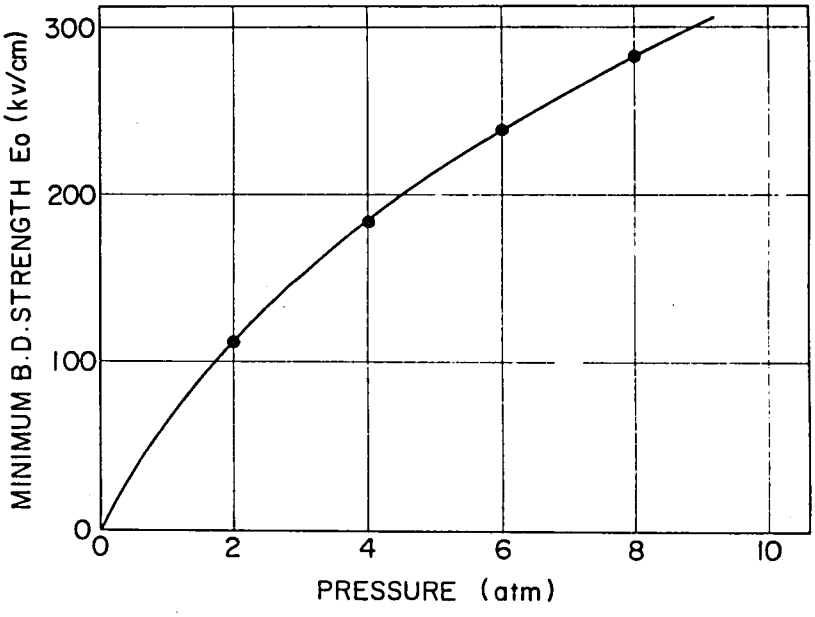


Fig.57 Minimum Breakdown Field Strength of Very Large Electrode, $E_o$

The value of $E_o$ is interpreted as the breakdown field strength of infinitely large electrode at the pressure. The probability of having such a low breakdown field strength will be eventually zero for the gap with small electrode area whose breakdown characteristic is in Type I.

The ratio of $E_o$ and $E_d$ is plotted in Fig.58. Solid line in the figure is an empirical expression of the relation given by;

$$\frac{E_o}{E_d} = \frac{1}{1 + 0.355 \cdot p^{0.7}} \tag{44}$$

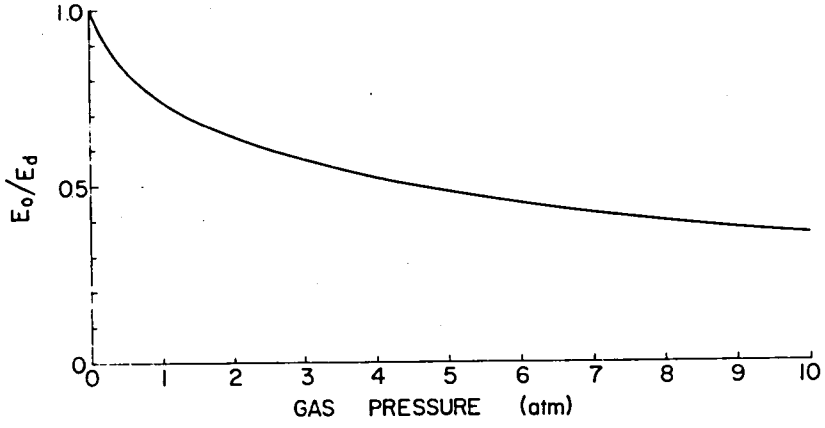


Fig.58 Pressure Dependence of $E_o/E_d$

The relation fit with sufficient accuracy within the pressure range of practical interest.

The relations between $ln\ ln\ 1/\{1 - F(E, S)\}$ and $ln\ (E - E_o)$ plotted on Weibull probability paper using the value of $E_o$ in Fig.57 show good linearity for entire range of electrode area and gas pressure where the breakdown strength is lower than the theoretical estimation (Type III and IV). Fig.59 is the examples of Weibull plots of three high pressure cases in Fig.54. Contrary to the normal probability plots in Fig.54, linearity of the

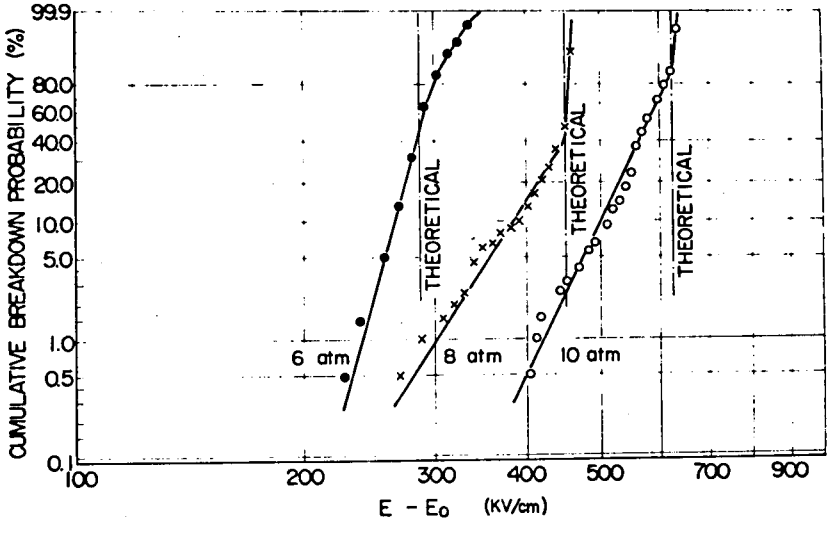


Fig.59 Weibull Probability Distributuions of Fine Finished Gap D

plots at high pressures where the breakdown field strength is lower than the theoretical estimation is very good.

4-5. Conditioning Effect

Conditioning effect of breakdown voltages is notable except in Type I and IV. Type I is free from the conditioning effect since the gap is only governed by the characteristics of $SF_6$ gas and initiation electrons, and the electrode or weak point has little to do with the breakdown characteristic. On the other hand, breakdown characteristic in Type IV is free from the conditioning effect because electrode has plenty of radical weak points in comparison with the number of breakdowns in a test. Damage of electrode by the foregoing sparks is also the factor to be taken into account in this type of breakdown characteristics. It should be noted that the energy stored in the gap is several orders of magnitude higher in the region of Type IV breakdown characteristic in comparison with that in Type I.

For Type II and III, spark conditioning effect is dependent on the characteristics of the weak points, hence, the area of electrode, electrode roughness and gas pressure. Breakdown characteristics of the gaps in these types will be different from those shown in Fig.48 to 51, if two hundred new gaps prepared in the same way are tested or the electrode surface is refinished after each breakdown.

Fig.60 is Weibull distribution plots of the breakdown field strength of fine finished

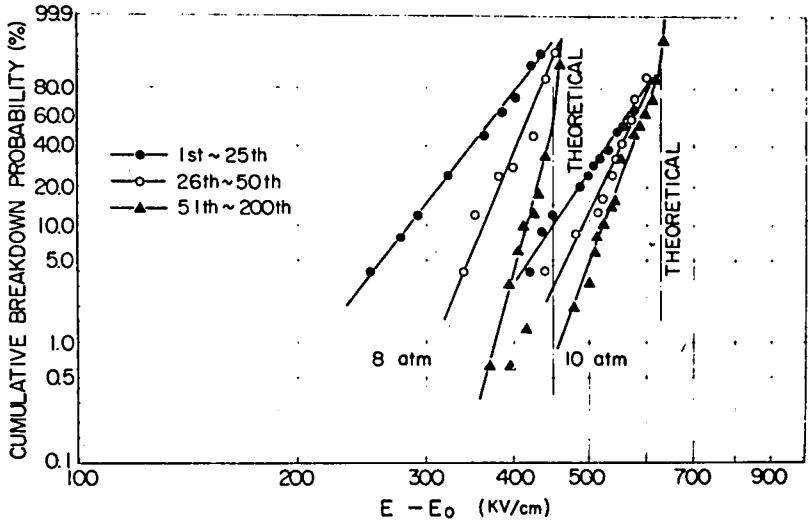


Fig.60 Change of Weibull Probability Distributions by Spark Conditioning Effect

Gap D at 8 and 10 atm pressures. The data of the first 25, succeeding 25 and the rest of all breakdowns are plotted separately. The curves clearly show how the distribution of the breakdown field strength changes by spark conditioning effect. The number of breakdowns required for conditioning increases when the area and gas pressure move from the region in Type II to Type III.

In many cases shown in Fig. 48 to 51 particularly in Type II, spark conditioning progresses so rapid that only the information on the distribution of the breakdown field strength of unconditioned electrode is the fact that the first few breakdown voltages only show the approximate modal value of the distribution. Statistical property of this type of gap can only be obtained by the first few breakdown voltages of many new gaps.

## §5. Area Effect of Electrode on the Breakdown Voltage

Breakdown field strength of a gap in Type IV and also in Type II and III in unconditioned state obeys Weibull distribution as mentioned. The evidence allows theoretical discussion of electrode area effect as follows.

According to the property of Weibull distribution, cumulative breakdown probability of a gap of electrode area $S_1$ plotted on Weibull probability paper should be parallel to that of a gap of area $S_2$ and the vertical distance between the two curves is $ln\ S_2/S_1$. (See Appendix III) Figure 61 is the examples of Weibull probability plots for fine finish-

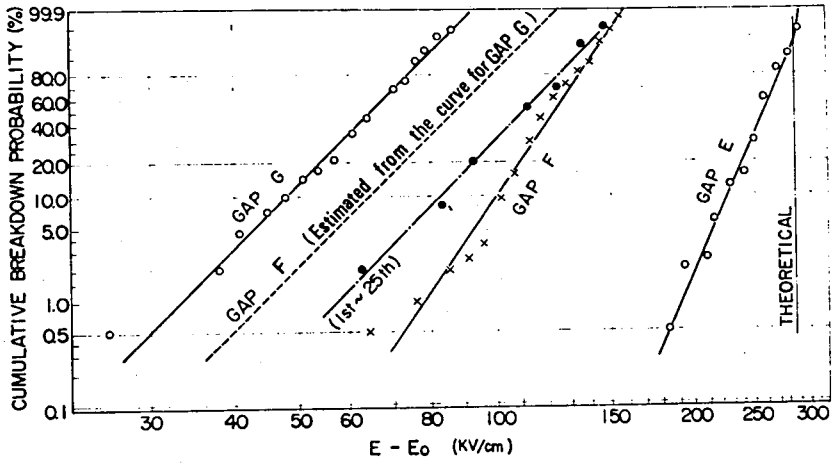


Fig.61 Effect of Electrode Area of Fine Finished Gaps at 6 atm Pressure

ed Gap E, F and G at 6 atm pressure. Three probability plots are not parallel to each other because of the different conditioning effect of these gaps. But the distribution of the first 25 breakdowns for Gap F plotted by dots is parallel to that of Gap G as expected. As it is seen here, cumulative probability of Gap G is the most reliable representative of the statistical property at the pressure, because large electrode area is equivalent to large number of small gaps connected in parallel. This means large sample size in statistics.

As we can see in Fig.51, breakdown characteristic of Gap E at p=6 atm has little conditioning effect. So, Weibull distribution of the breakdown field strength at the pressure shown in Fig.61 will be a good representative of the characteristic of unconditioned electrode. We can calculate the parameters of Weibull distribution, $\lambda$, m, by fitting the curve to the expression in equation 42. The parameters calculated in the manner are substituted in equation 42 to estimate the cumulative probability of other gaps of arbitrary electrode area. Dashed line in Fig.61 is an example of estimated curve for Gap F.

There are considerable difference between the estimation and the experimental data on Gap F even for the first 25 breakdowns. Possible reason for the difference is one or both of the followings. The first 25 breakdowns on Gap F still have some influence of conditioning effect. Secondly, though both electrodes are finished in the same manner as far as possible, surface condition of smaller electrode may be slightly better than that of larger electrode.

The difference between the estimation and the test data are not so great as will be impressed at the first sight. The relation between *ln* S and the breakdown field E is quite weak since we are dealing with $E-E_o$ rather than E and a slight difference in E may cause very large difference in $E-E_o$. However, the first few breakdown voltages show at least the approximate modal value of the distibution. Lower tail of the experimental distribution of $E-E_o$ for Gap F is pretty close to the modal value of the estimated distribution shown by dashed line. From this reason, the calculated probability distribution shown by dashed lines in Fig.61 will be a good estimation of Weibull distribution for unconditioned Gap F at the pressure.

At low gas pressures, breakdown characteristics have considerable conditioning effect even for the largest Gap G. However, in realizing the fact that the gap is made of aluminum whose surface is rougher in comparison with stainless steel electrode and also fine finish of large electrode area is not as good as that of small electrode, a rough estimation of the parameters of the Weibull distribution for fine finished electrode will be given as

the parameters for Gap G after the gap is conditioned.

Weibull distribution of Gap G at the pressures 2, 4 and 6 atm are parallel to each other, after the gap is conditioned as shown in Fig.62. The fact shows that the parameter m is constant independent of gas pressure. The value of m is estimated from the slope of the curves in the figure as;

$$m \cong 7.4 \tag{45}$$

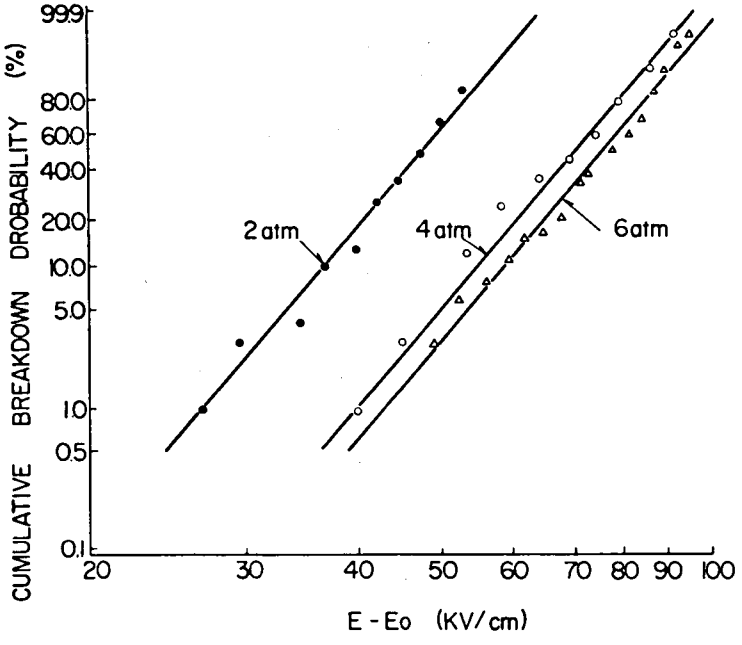


Fig.62 Weibull Distribution of Fine Finished Gap G after the Gap is Fully Conditioned

Values of $\lambda_o$ are obtained from equation 43 by fitting these curves to equation 42. The parameters used in the calculation and the calculated values of $\lambda_o$ are given in Table 5. The values of $\lambda_o$ are plotted in Fig.63 as a function of gas pressure. Empirical expression of the relation is given as;

$$\lambda_o = 0.40 \cdot exp \left\{ 1.15p \right\} \tag{46}$$

Equation 46 is the estimated empirical expression of $\lambda_o$ for fine finished electrode. The values are different by the finish of the electrode as will be discussed later.

| | 2 atm | 4 atm | 6 atm |
|---|---|---|---|
| $E_d$ (kV/cm) | 178 | 356 | 534 |
| $E_o$ (kV/cm) | 113 | 184 | 238 |
| $E_m$ (kV/cm) | 162 | 257 | 317 |
| m | 7.4 | 7.4 | 7.4 |
| $\lambda_o$ | 4.03 | 36.1 | 406 |

$$\lambda_o = \lambda E_d^{\,m}$$

Table 5 Parameters of Weibull Distribution

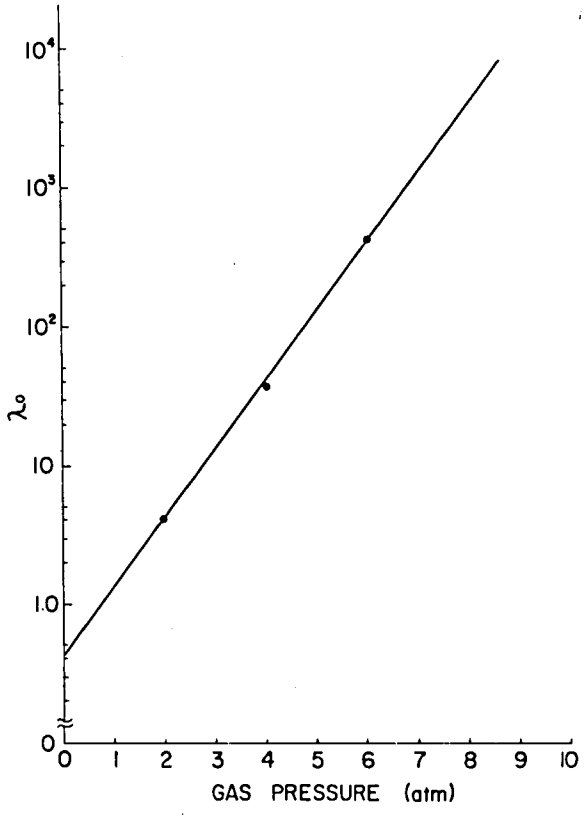


Fig.63 Estimated Values of $\lambda_o$ as a Function of Gas Pressure

Since we have all the parameters of Weibull distribution of fine finished electrode, statistical distribution of the breakdown field strength of a given gap can be evaluated quantitatively by equation 40 or 42. Solid lines in Fig. 64 are the examples of the calculated modal values of the breakdown voltages of fine finished electrode by equation III–2 in Appendix III. The results show prominent area effect of the breakdown voltage of compressed $SF_6$.

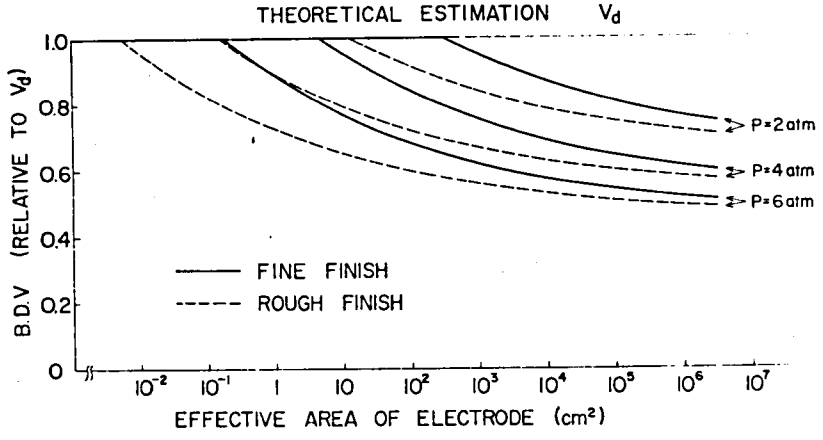


Fig.64 Calculated Modal Values of the Breakdown Voltages for Fine and Rough Finished Electrodes

## §6. Effect of Electrode Roughness [83]

Fig.65 and 66 show the examples of the sequence of breakdown voltages of Gap D and G finished rough in Grade B.

As we can see in Fig.65, the breakdown characteristic in Type II is not observed in the cases experimented. The result shows that Type II exists in a very limited range of area and gas pressure, if any. Breakdown voltages of roughened electrode are much lower than those of fine finished electrode in Type III, since there exist considerable number of radical weak points, even in small electrode area. As it is shown in Fig.56, the strongest possible weak point or the minimum possible breakdown field strength $E_o$ is almost constant independent of the finish of the electrode tested, while the number of weak points of a certain intensity on rough finished electrode is many times that of fine finished

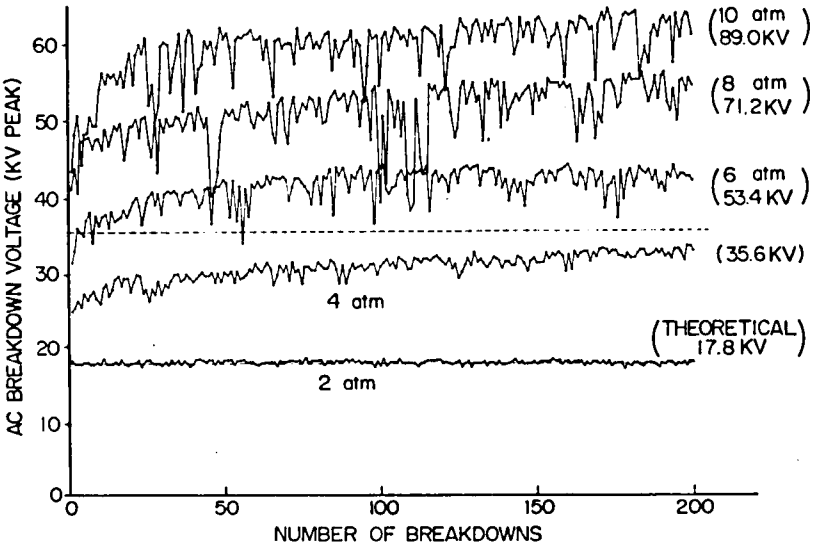


Fig.65 Sequence of Breakdown Voltages for Rough Finished Gap D

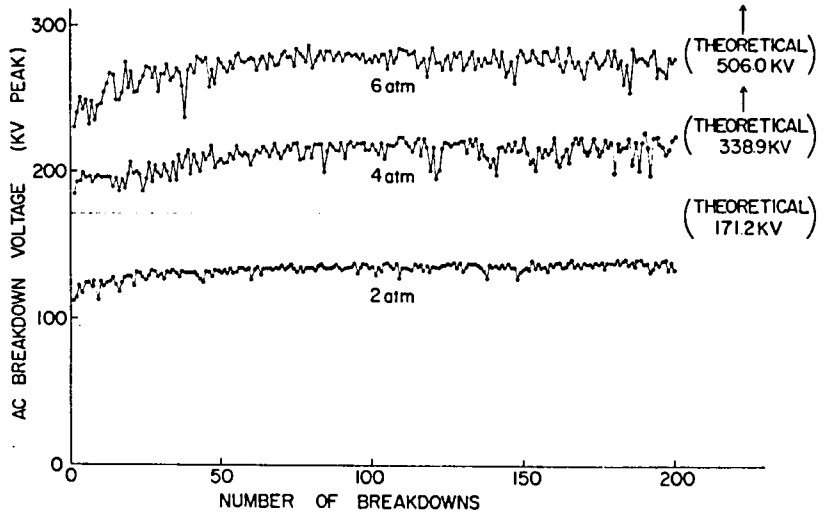


Fig.66 Sequence of Breakdown Voltage for Rough Finished Gap G

electrode. From this point of view, breakdown characteristic of a rough finished electrode is quite similar to that of fine finished electrode of larger area. It is worth noticing that the characteristic in Fig.65 is similar to that of fine finished Gap E or F (Fig.49 or 50) rather than the characteristic of the corresponding fine finished Gap D. (Fig.48) Number of sparks required for conditioning for roughened electrode is also many times larger than that of fine finished electrode of the same area.

Electrode area and gas pressure diagram which shows the boundary between Type I and III breakdown characteristic is shown by solid line in Fig.67 for roughened electrode. The same curve for fine finished electrode is replotted by dashed line from Fig.52 for comparison. These curves are of practical importance, since they show the critical condition of having the reduced breakdown voltage under the effect of electrode for the respective grade of the electrode surface.

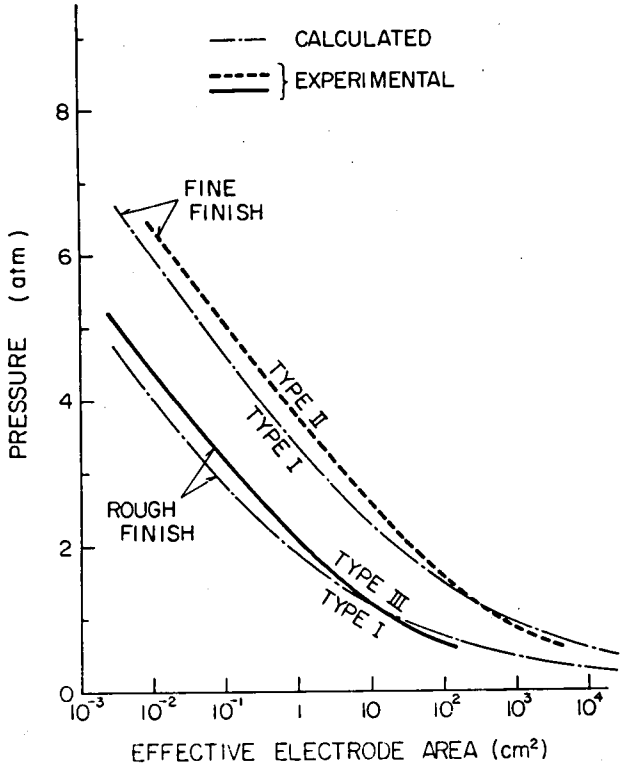


Fig.67 Boundaries of Electrode Area and Gas Pressure where the Effect of Electrode becomes Evident for Fine and Rough Finished Gaps

These two curves in Fig.67 for fine and rough finished electrodes have similar shape and if we shift one curve horizontally about one and half decade, they fit very well to each other. This means that a rough finished electrode has quite similar breakdown characteristic of a fine finished gap whose electrode area is about 30 times as large as the area of the gap. The evidence is understood as that the value of $\lambda_o$ for rough finished electrode is about 30 times as large as the value in equation 46.

The boundaries in Fig.67 are estimable theoretically as follows. Under the effect of electrode, breakdown field strength of a gap whose effective electrode area is S scatters statistically between $E_o$ and $E_d$ obeying Weibull distribution in equation 40. When the applied field exceeds $E_d$, needless to say, the gap breaks down without any effect of weak points. The probability that a breakdown occurs at the field lower than the theoretical breakdown field strength $E_d$ is given by equation 40 as;

$$F(E_d, S) = 1 - exp \left\{ -\lambda_o \cdot S \left( \frac{E_d - E_o}{E_d} \right)^m \right\} \qquad (47)$$

If we set F ($E_d$, S) to a certain low critical value, equation 47 is the criterion whether the gap is under the influence of the electrode or not. Since $E_o/E_d$ and $\lambda_o$ are expressed as a function of gas pressure as in equation 44 and 46, the criterion is given as a relation between the effective area of the gap S and gas pressure p.

If we set F ($E_d$, S) = 0.05, that means the probability that the breakdown voltage of a given gap is lower than the theoretical estimation under the influence of electrode is less than 5%, the estimated boundaries are obtained from equation 47 as the dot-dash lines in Fig.67 for fine and rough finished electrode. In the calculation, the value of $\lambda_o$ for rough finished electrode is set 30 times to that given in equation 46.

The comparison in Fig.67 shows that the experimental curves are in very good coincidence to the theoretical estimation. The modal values of the breakdown voltages for rough finished electrode are calculated by equation III–2 in Appendix III and plotted by dashed lines in Fig.64. The experimental results of the area effect in published papers shown in Fig.47 is explained quantitatively by the curve for rough finished electrode at p=4 atm, although no quantitative data on the finish of the electrode are presented in the original papers.

## §7. Effective Area of Electrode and Polarity Effect [75, 85]

The importance of the stressed area of negative electrode on the breakdown characteristics of compressed $SF_6$ is explained in the foregoing sections. In some gaps such as parallel plane and coaxial cylinder gaps, a finite area of negative electrode is stressed at its maximum and the area can be considered as the effective area of the electrode. However, the maximum field strength on negative electrode appears only at one point in many gap configurations. For example, the maximum field of a sphere plane gap exist at the tip of the sphere facing to the plane electrode. Field strength decreases gradually with the distance from the point of the maximum field strength. It is quite understandable that the area of the sphere electrode far from the tip of the sphere has little to do with the electrical discharge phenomena. Then a question arises what part of the electrode is "effective" to the breakdown of the gap.

Electrode area effect in oil insulation has been discussed, taking the effective area of a gap as the area or volume whose electric field is more than 90% of the maximum field. [88, 90, 91] There is no rational reasoning for the critical value of 90%. Even if the value is reasonable for oil insulation, it is dubious if the same 90% is applicable to the breakdown in compressed $SF_6$.

A more reasonable way to define the effective area of a given gap in $SF_6$ is discussed based on Weibull statistics of breakdown field strength.

Effective area of a gap $S_{eff}$ is defined as the area of an uniform field gap stressed at $E_{max}$ of the original gap, and the statistical property of weak points of the gap is equivalent to that of the original gap. Since the number of potent weak points on the negative electrode increases with E as in equation 34, the area of each part on the negative electrode has to be weighted by the field strength at the point.

First, the area on the negative electrode whose field strength is higher than E is defined as S(E). Then the area stressed at the field between E and E + dE is $-\frac{dS(E)}{dE}\,dE$. The negative sign is attached, since S(E) is a decreasing function of E. If the average number density of the weak points which can produce breakdown at the field strength lower than E is expressed as a function of E as N(E) in equation 35, the effective area of a gap $S_{eff}$ is given by the above definition as;

$$N(E_{max}) \cdot S_{eff} = - \int_0^{E_{max}} N(E) \cdot \frac{dS(E)}{dE} \, dE \qquad (48)$$

The left hand side of the equation is the number of the weak points on an uniform field gap of area $S_{eff}$ which can produce breakdown at the field stress lower than $E_{max}$ of the original gap. The right hand side of the equation is the number of the weak points which can produce breakdown of the original gap when the maximum field strength of the gap is equal to $E_{max}$. Since N(E) is zero for $E<E_o$, lower range of the integral in equation 48 can be set as $E_o$ instead of zero.

The negative electrode is less stressed for positive polarity in comparison with the case for negative polarity. The difference in the number of the weak points by the polarity of the applied voltage is evaluated by taking the value of $- \frac{dS(E)}{dE} dE$ as the area only on the negative electrode, while $E_{max}$ is the maximum field in the gap either on positive or negative electrode.

By this definition, the polarity effect on the breakdown field strength is interpreted as the difference in the effective area $S_{eff}$. If we put the maximum field strength on the negative electrode as $E^-_{max}$, the effective area of the gap is;

$$S_{eff} = - \frac{1}{N(E_{max})} \cdot \int_{E_o}^{E^-_{max}} N(E) \cdot \frac{dS(E)}{dE} \, dE \qquad (49)$$

Here, $E^-_{max}$ is given by the polarity of the applied voltage as;

$$\begin{aligned} E^-_{max} &= E_{op} \quad : \text{for positive polarity} \\ &\quad\ E_{max} \quad : \text{for negative polarity} \end{aligned} \qquad (50)$$

where, $E_{op}$ is the maximum field strength on the electrode opposite to the one that gives the maximum field of the gap. Substituting equation 49, the effective area for positive and negative polarity $S^+_{eff}$, $S^-_{eff}$ are given as;

$$\begin{aligned} S^+_{eff} &= - \int_{E_0}^{E_{op}} \left( \frac{E - E_0}{E_{max} - E_0} \right)^m \cdot \frac{dS^+(E)}{dE} \, dE \\ S^-_{eff} &= - \int_{E_0}^{E_{max}} \left( \frac{E - E_0}{E_{max} - E_o} \right)^m \cdot \frac{dS^-(E)}{dE} \, dE \end{aligned} \qquad (51)$$

Here, $S^-(E)$ is the area defined above on the maximum field electrode, and $S^+(E)$ is the same area on the opposite electrode.

The ratio $\delta = E_{op}/E_{max}$ and functions $\frac{dS^-(E)}{dE}$ and $\frac{dS^+(E)}{dE}$ are determined by the static field distribution of the gap. But, the effective area in equation 51 is a function of the maximum field $E_{max}$ and $E_o$ which is a function of gas pressure as in Fig.57. The dependence on $E_{max}$ means different effective area at different levels of the applied field strength. This is not realistic, since the breakdown field scatters statistically from shot to shot. The most reasonable representative of $E_{max}$ of a given gap will be the modal value of the breakdown field strength obtained in equation III–2 in Appendix III.

$$E_{max} = E_o + \left( \frac{m-1}{S_{eff} \cdot \lambda_o \cdot m} \right)^{\frac{1}{m}} \cdot Ed \qquad (52)$$

or, from equation 44,

$$\frac{E_o}{E_{max}} = 1/\left\{ 1 + (1+0.355 \cdot p^{0.7}) \left( \frac{m-1}{S_{eff} \cdot \lambda_o \cdot m} \right)^{\frac{1}{m}} \right\} \qquad (53)$$

We can calculate the value of $S_{eff}$ as a function of gas pressure by solving equation 53 with equation 51, simultaneously. The equations can not be solved analytically for general gap configuration, but can readily be solved numerically by the aid of an electronic computer. Some numerical examples of the effective area for the gaps used in the present work are given in Appendix IV.

(1) By the above definition of effective area, the effect of weak points on negative electrode of a given gap can be evaluated quantitatively as the value of $S_{eff}$.

(2) Statistical properties of a given non-uniform field gap is equivalent to an uniform field gap whose area is $S_{eff}$.

(3) $S^-_{eff}$ has finite value as far as $E_{max}$ is larger than $E_o$, while $S^+_{eff}$ has positive value only when $E_{max} > E_o/\delta$, ($\delta<1$). This is why the effect of electrode is observed in more extensive test conditions for negative polarity.

(4) Since the ratio $E_{op}/E_{max}$ is less than unity, $S^+_{eff}$ is always smaller than $S^-_{eff}$. Polarity effect of the breakdown field strength shown in Fig.17 to 19 can be

explained by the difference in $S^{+}_{eff}$ and $S^{-}_{eff}$.

Examples of the quantitative discussion on the effective area will be given in Chapter VI for switching surge breakdown.

## §8. Conclusion

Electrode area effect is studied as a consequence of the effect of weak points for breakdown of the gap which statistically distribute on the surface of electrode.

(1) The criterion whether the breakdown characteristics of a given gap is under the effect of electrode surface or not is expressed as a function of gas pressure p and the effective area of the gap $S_{eff}$ as in Fig.52 and 67.

(2) In small p·S region, no effect of electrode is observed, while the electrode plays prominent role in reducing the breakdown voltage at large p·S region. In the intermediate region of p·S, breakdown voltage has spark conditioning effect in the begining of the breakdown experiment. The number of the breakdowns required for the conditioning increases with p and S.

(3) In high p·S region, distribution of cummulative probability of the maximum breakdown field strength obeys in Weibull distribution rather than normal distribution and expressed mathematically by equation 41 or 42. Constants m in the expression is approximately 7.4, independent of electrode and gas pressure. The value of $\lambda_o$ for fine finished stainless steel electrode is given as in equation 46. For rough finished electrode, the value of $\lambda_o$ is about 30 times as large as the value for fine finished electrode. The value of $E_o$ experimentally given as in equation 44 as a funciton of gas pressure.

(4) The statistical properties of the breakdown field strength of a given gap can be evaluated by equation 41 or 42, using these constants. The effect of the electrode area observed in the experiment is quantitatively explained by the evaluation.

(5) Effective electrode area of an asymmetric field gap is given by solving equation 51 and 53 simultaneously. The value is always larger for negative polarity in comparison

with the value for positive polarity. This difference in the effective electrode area explains polarity effect of the breakdown field strength.

# VI. VOLTAGE-TIME CHARACTERISTIC OF THE ELECTRICAL BREAKDOWN IN $SF_6$ [75]

## §1. Introduction

The characteristics of ac and dc breakdown in $SF_6$ have been discussed in the previous chapters. In all the discussions, temporal change of applied voltage is assumed to be so slow that the voltage can be looked upon as constant while any discharge phenomena is taken place in the gap.

The assumption is not valid when the voltage-time characteristic of electrical breakdown for impulse and switching surge applied voltage (V-t characteristic) is considered. The effect of the electrode surface discussed in Chapter V, for example, is in its full force for dc applied voltage. The effect will be relatively inefficient for impulse applied voltage. The characteristic of corona stabilization breakdown is another factor which is strongly influenced by the temporal change of the applied voltage.

Voltage-time characteristic of the electrical breakdown of compressed $SF_6$ is of practical importance in designing protection and insulation coordination of gas insulated substation and other power equipments. Since the systems are completely enclosed in grounded metal vessel, abnormal voltages which they encounter in the field are different from those in conventional systems. [92] Beside the difference, V-t characteristics of the systems are quite different from those of conventional systems insulated in air.

V-t characteristics of $SF_6$ have been studied by many people on various gap conditions. The results have shown that the characteristic is different in wide variety depending on the conditions of the gap and gas pressure. V-t curves of relatively uniform field gap in low gas pressures at around 1 atm (absolute) are reported to be quite flat and impulse ratio is limited within the range from unity to 1.2 depending on the test conditions. [38, 40, 72, 92–94] At elevated pressures, the impulse ratio increases with gas pressure and also with the geometrical size of electrode. A value of as high as 1.8 is reported for 20 cm diameter sphere to plane electrode in 4 atm $SF_6$ gas. [40] Polarity effect is one of the most confusing matters in the breakdown characteristics for surge applied voltage. In some test conditions, positive breakdown voltage is higher than the negative, [38, 40, 72, 92–94] while it is opposite in other test conditions. [35, 76, 95] In some cases,

there observed little difference in the positive and negative breakdown voltages. [38, 72] There is no generalized theory or experimental formula to understand these varieties of V-t characteristics in connection with the test conditions.

In the present chapter, V-t characteristics of $SF_6$ gas are studied in wide time range from steep front impulse to switching surge under various gap conditions and gas pressures. V-t characteristics are categolized into three patterns and formulated in a generalized expression by which the characteristic of an arbitrary gap can be evaluated quantitatively. The test conditions in which each of these three patterns is observed are also discussed in the light of the results of dc and ac experiments discussed in the foregoing chapters.

## §2. Experimentals

### 2-1. Test Setup

Three gaps, A, B and C in Table 1 used in ac and dc experiments in Chapter III were used again in the present experiment. The surface of these stainless steel electrodes were finished by #80 emery paper. The finish corresponds to the rough surface which was defined as Grade B in Chapter IV. The electrodes are finished only in rough surface because of the technical difficulty of keeping the surface fine in the course of impulse test.

One of the three gaps is set in a large metal tank in Fig.11 and prepared for test in the same manner as in ac and dc experiments. In most cases, ultra violet light irradiation is utilized through a qualtz window provided on the wall of the tank. Gas pressure and gap spacing are set within the range of 1 to 6 atm and 1 to 16 cm, respectively.

Fig.68 show the schematic diagram of the test circuit. Impulse voltage is produced putting the switches in "a" position, while they are put in "b" position for switching surge voltage.

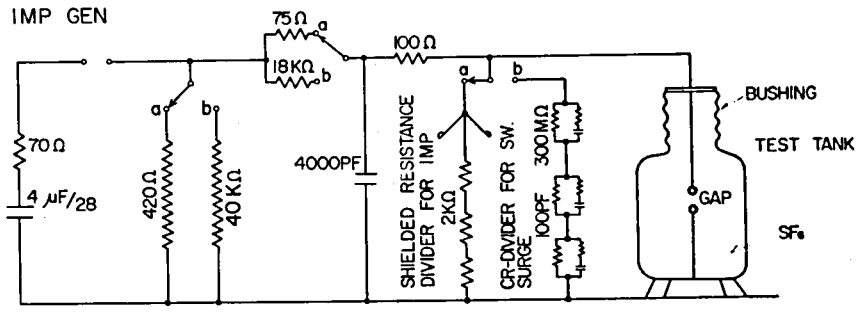


Fig.68 Test Circuit for Impulse and Switching Surge Experiment

Impulse voltages of 1.7 x 40 μs and switching surge voltages of 170 x 3,000 μs are used to obtain V-t characteristics of these gaps by increasing the applied voltage stepwise and applying about 5 shots at each voltage level. The increment of the voltage level is about 5% of the minimum breakdown voltage of the gap. Time interval between the succesive voltage applications is at least 30 seconds which is required for the charging of the impulse generator.

Impulse voltage is measured by a resistance divider which is specially designed for steep impulse measurement. [96] The response time of the total measuring circuit is about 0.1 μs. Since the time is not low enough for the measurement of steep front impulse voltage whose time to breakdown is less than 1 μs, measured values for steep impulse are corrected by the rate of rise of voltage and the response time $\tau_o$ by the following relation. [97]

$$V_{correct} = (1 + \tau_o \cdot \frac{d}{dt}) \cdot V_{measure} \qquad (54)$$

Switching surge voltage is measured by a capacitance-resistance divider whose response time is about 1 μs. This value is low enough for the switching surge measurement. Examples of the oscillogram of the impulse and switching surge applied voltages are illustrated in Fig.69.

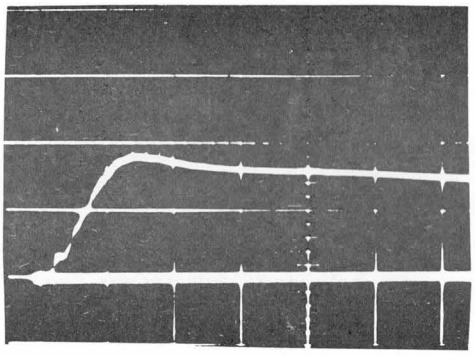

(a) Impulse Voltage
W/O B.D.
Sens. : 262 kV/div
Sweep : 2 μs/div

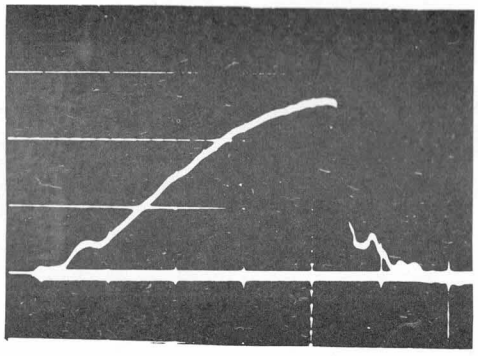

(b) Impulse Voltage
W/ B.D.
Sens. : 262 kV/div
Sweep : 0.5 μs/div

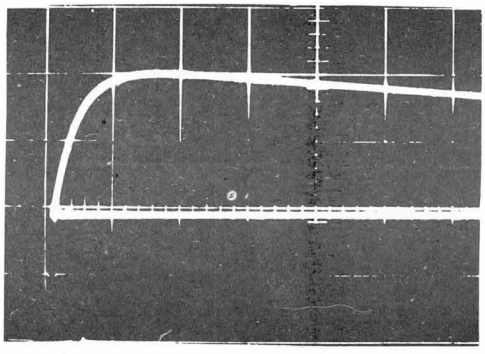

(c) Switching Surge Voltage
W/O B.D.
Sens. : 103 kV/div
Sweep : 200 μs/div

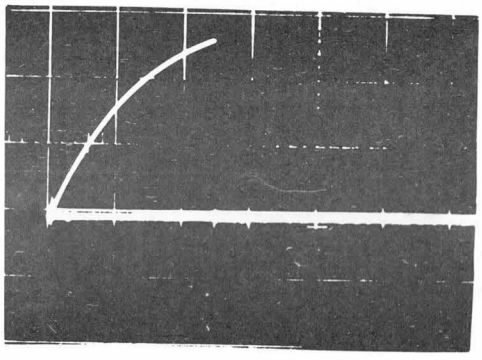

(d) Switching Surge Voltage
W/ B.D.
Sens. : 103 kV/div
Sweep : 50 μs/div

Fig.69 Wave Shape of Impulse and Switching Surge Applied Voltages

## 2-2. Test Results

Examples of V-t characteristic of Gap A are shown in Fig.70 and 71. Theoretical estimations of the breakdown voltage based on single avalanche theory by equation 18 are

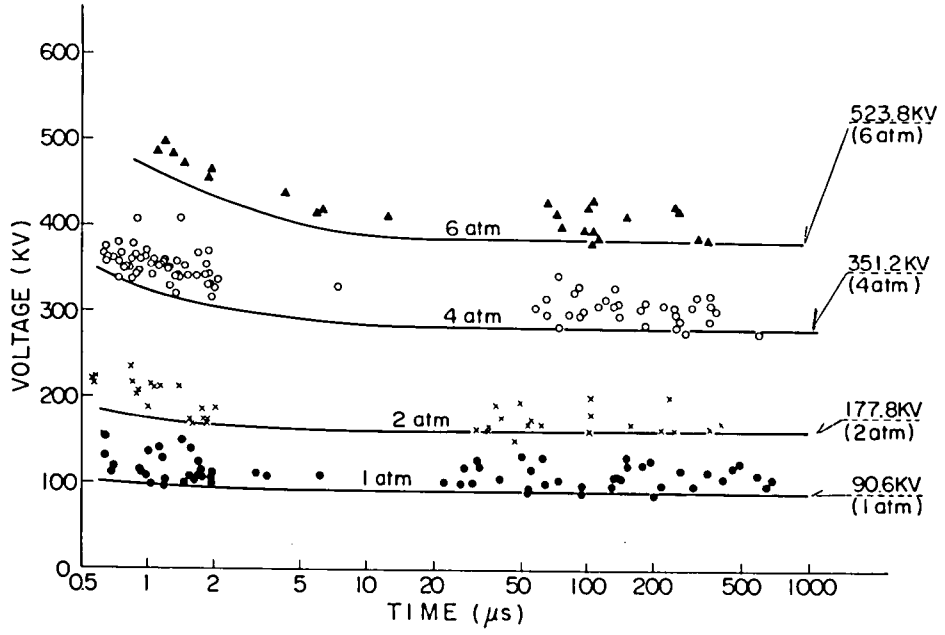


Fig.70(a) V-t Characteristics of Gap A (d=1cm, u=0.956, Positive)

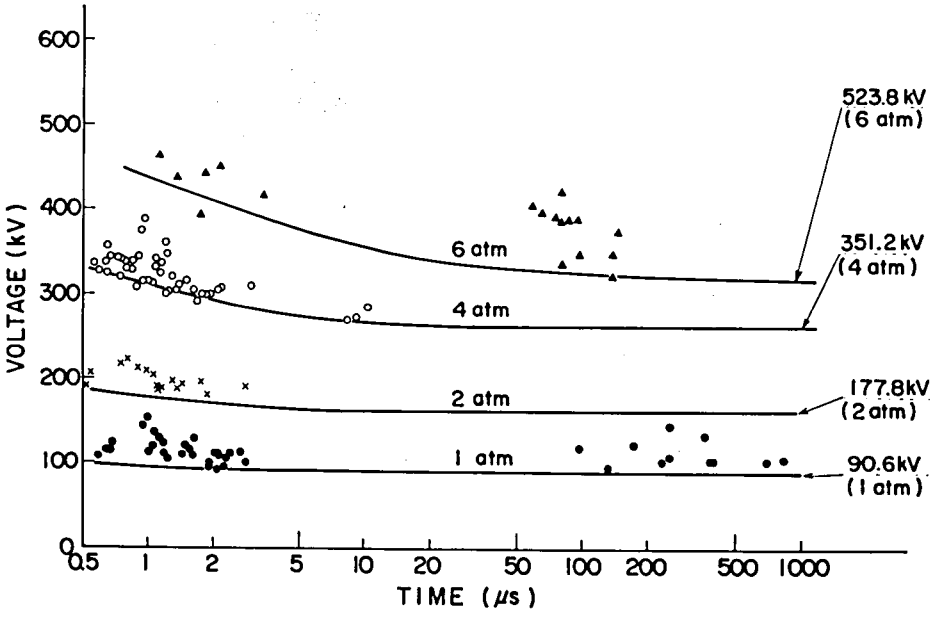


Fig.70(b) V-t Characteristics of Gap A (d=1cm, u=0.956, Negative)

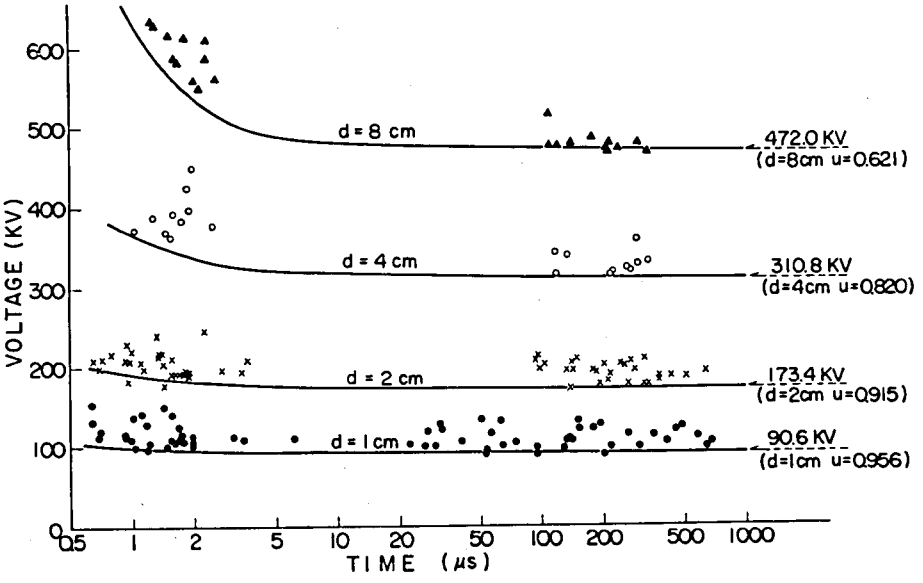


Fig.71(a) V-t Characteristics of Gap A (p=1atm, Positive)

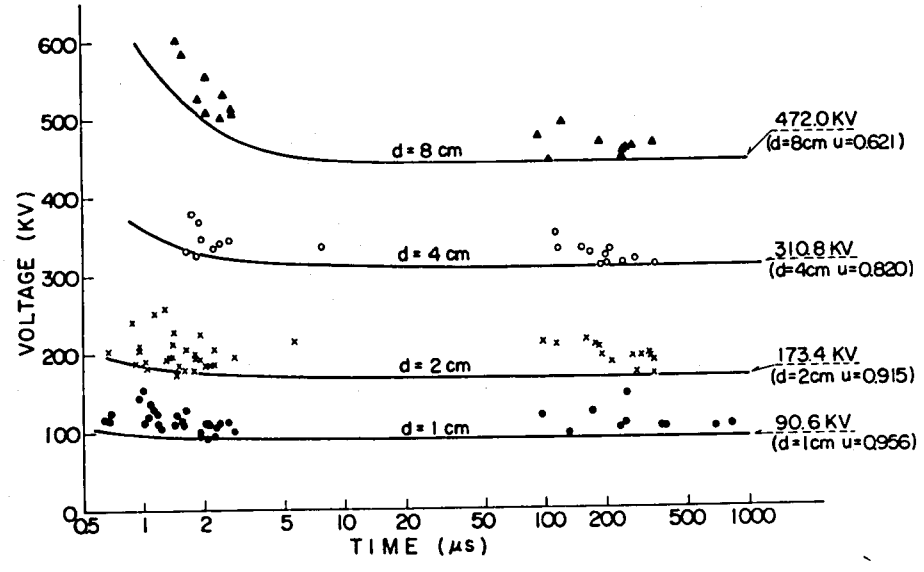


Fig.71(b) V-t Characteristics of Gap A (p=1atm, Negative)

shown at the right hand side of the figures. As seen in Fig.70, breakdown voltage for switching surge never goes below the theoretical estimation at 1 atm and the minimum breakdown voltage coincides with the theoretical value, while the reduction of the breakdown voltage from the theoretical value is remarkable at high gas pressures under the effect of the electrode as it is for ac and dc breakdown.

It should be noted that the polarity effect is negligible as far as the effect of the electrode is not involved and the minimum switching surge breakdown voltage coincides with the theoretical estimation. The minimum switching surge breakdown voltages at high pressures are almost identical to those for dc breakdown discussed as the effect of the irregularities on negative electrode in Chapters IV and V. Since the reduction of the breakdown voltage from the theoretical estimation is dependent only on the negative electrode, or the effective electrode area is larger for negative polarity as discussed in Chapter V, negative breakdown voltage is lower than the positive for asymmetric field gaps.

Dependence of the breakdown characteristics on gap spacing at 1 atm pressure are shown in Fig.71. The minimum breakdown voltage coincides with the theoretical estimation up to 4 cm spacing both positive and negative polarities. The reduction of the breakdown voltage is observed only for negative polarity at d=8 cm spacing. Since the asymmetry of the electric field of the gap is very small in the range of the gap spacing tested, the effect of the polarity of the breakdown voltage is very limited in this test condition.

Fig.72 to 74 are the examples of V-t characteristics of Gap B. Breakdown voltages at 1 and 2 cm spacing are higher than the theoretical estimation up to 4 atm for positive polarity and up to 2 atm for negative polarity because of the moderate asymmetry of the field. In the experiment at atmospheric pressure for different gap spacing in Fig.74, the characteristics for positive applied voltage are similar to these up to 16 cm spacing. For negative polarity, however, the characteristics are quite different from those for positive polarity at the gap spacing larger than 4 cm. Breakdown voltages are unusually high in comparison with the positive case. In this condition, the breakdown voltage seems to be high due to the coroan stabilization discussed in Chapter III.

Positive breakdown voltage of this gap at 2 and 4 atm in Fig.73(a) is slightly higher than the negative value or the theoretical estimation. The same slightly higher positive breakdown voltage is observed in many other cases at low gas pressures where the reduc-

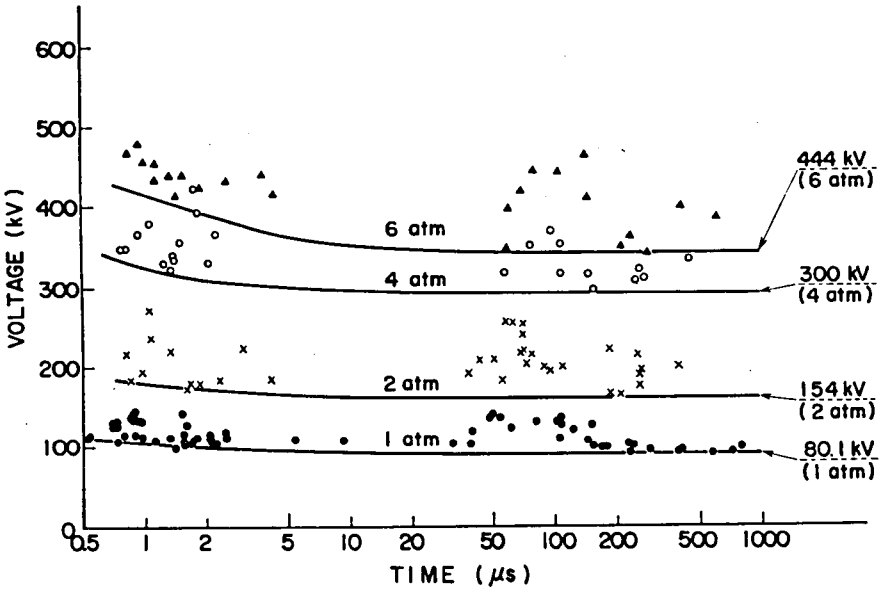


Fig.72(a) V-t Characteristics of Gap B (d-1cm, u=0.787, Positive)

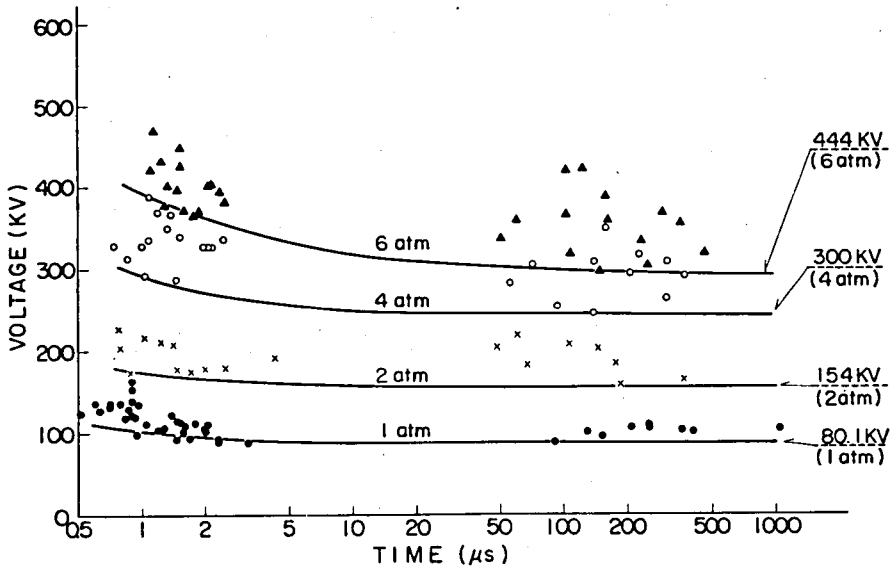


Fig.72(b) V-t Characteristics of Gap B (d=1cm, u=0.787, Negative)

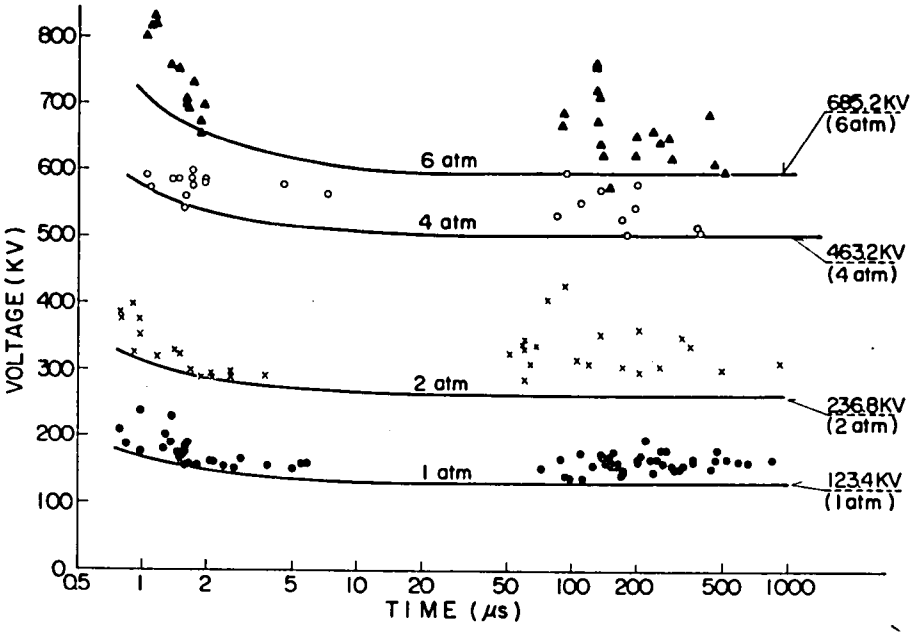


Fig.73(a) V-t Characteristics of Gap B (d=2cm, u=0.606, Positive)

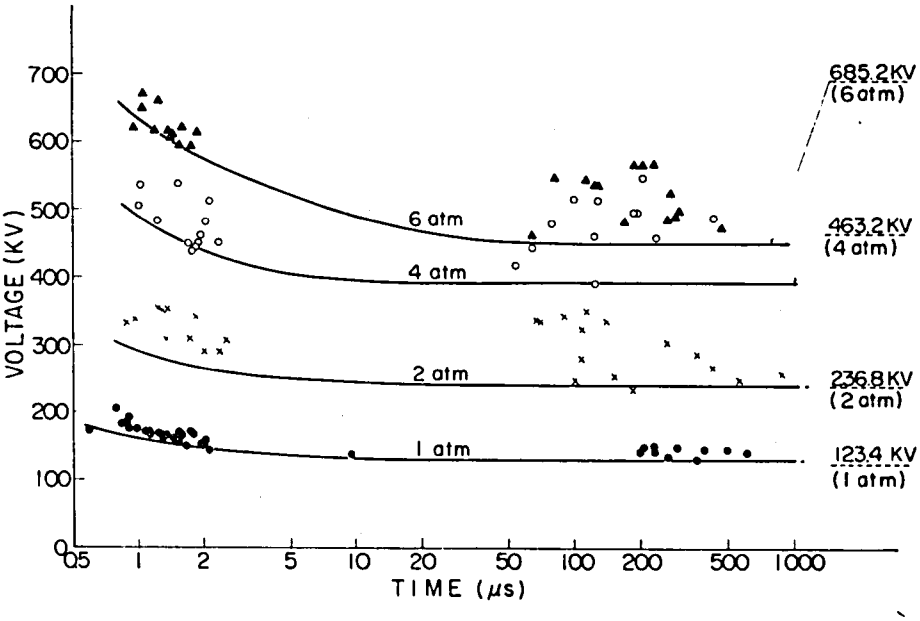


Fig.73(b) V-t Characteristics of Gap B (d=2cm, u=0.606, Negative)

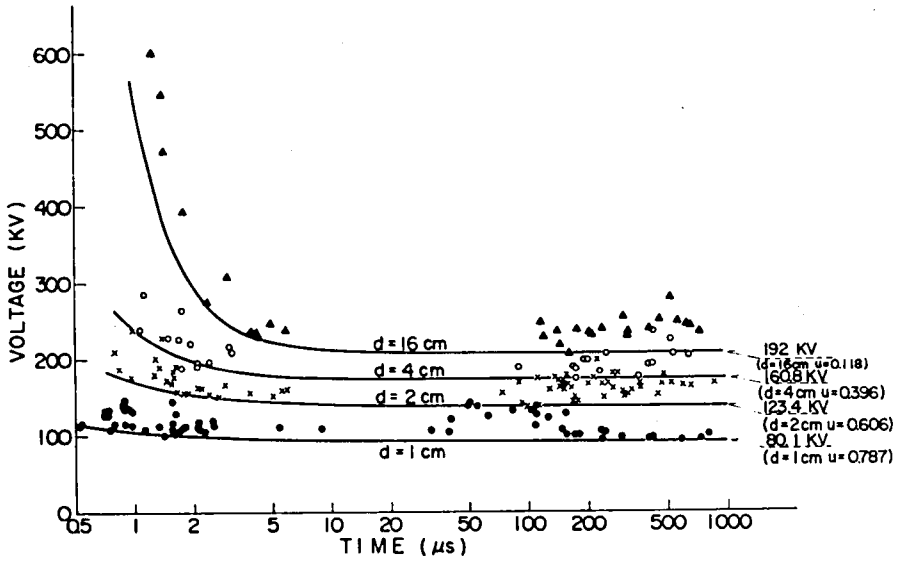


Fig.74(a) V-t Characteristics of Gap B (p=1atm, Positive)

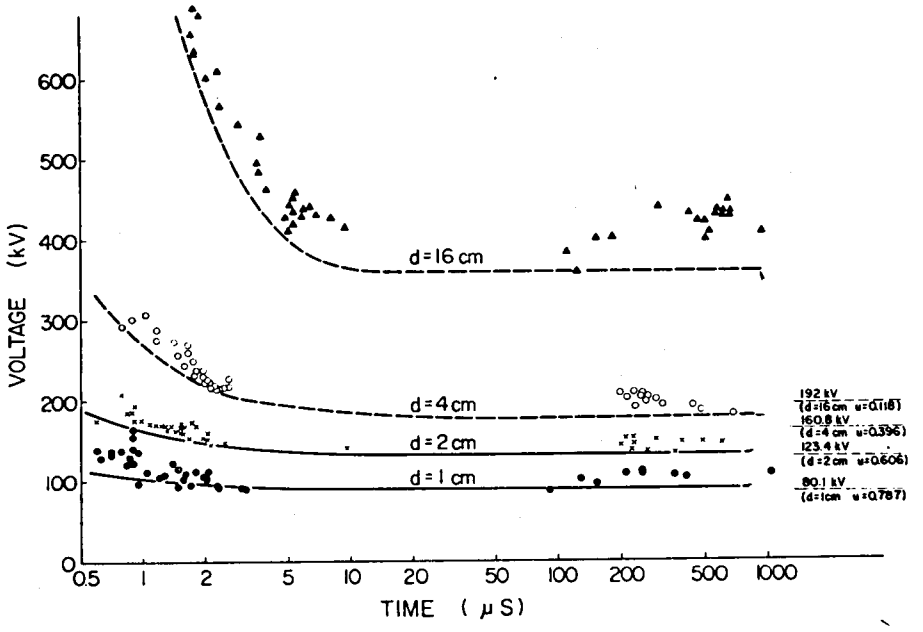


Fig.74(b) V-t Characteristics of Gap B (p=1atm, Negative)

tion of breakdown voltage by weak points is not appreciable. This property is not appreciable for Gap A of large electrode area but more pronounced for smaller electrode Gap C as will be seen in the following. This slightly higher positive breakdown voltage is probably caused by the statistical scattering due to the lack of the initiation electrons in the stressed part of the gap. They will be more efficiently supplied from the surface of electrode for negative polarity, while they have to be provided at high stressed region in the mid gap for positive polarity.

Similar V-t characteristics of Gap C are shown in Fig.75 to 77. At the gap spacing of 1 cm, the reduction of the breakdown voltage from the theoretical estimation occurs in between 4 and 6 atm for positive polarity and 2 and 4 atm for negative polarity. At larger gap spacings, the increse of the breakdown voltage due to corona stabilization observed both in positive and negative polarities. But it is more likely to occur for negative polarity as expected from the data on dc experiment in Fig.25. Since the corona stabilization is likely to occur in the divergent field gap, the characteristic is observed in wider range of gas pressure, gap spacing and the polarity of the applied voltage in this gap.

## §3. Three Patterns in V-t Characteristic

The results of these experiments suggest the fact that all of the V-t curves of Fig.70 to 77 are categolized into three patterns. The patterns are distinctive by the following features.

Pattern I: The minimum value of switching surge breakdown voltage coincides with the theoretical prediction by single avalanche theory. The rise of V-t curve is moderate as typically shown in Fig.78. The effect of the polarity of applied voltage is negligible in the pattern. (Example, Gap A, p = 1 atm, d = 1 cm, Positive and Negative)

Pattern II: The minimum value of switching surge breakdown voltage is lower than the theoretical estimation under the effect of negative electrode. V-t curve rises more rapidly than that in Pattern I in the time range of order of microsecond as typically shown in Fig.78. Since only the negative electrode rules the breakdown, appreciable polarity effect is observed for asymmetric field gaps. (Example, Gap A, p = 6atm, d = 1cm, Positive and Negative)

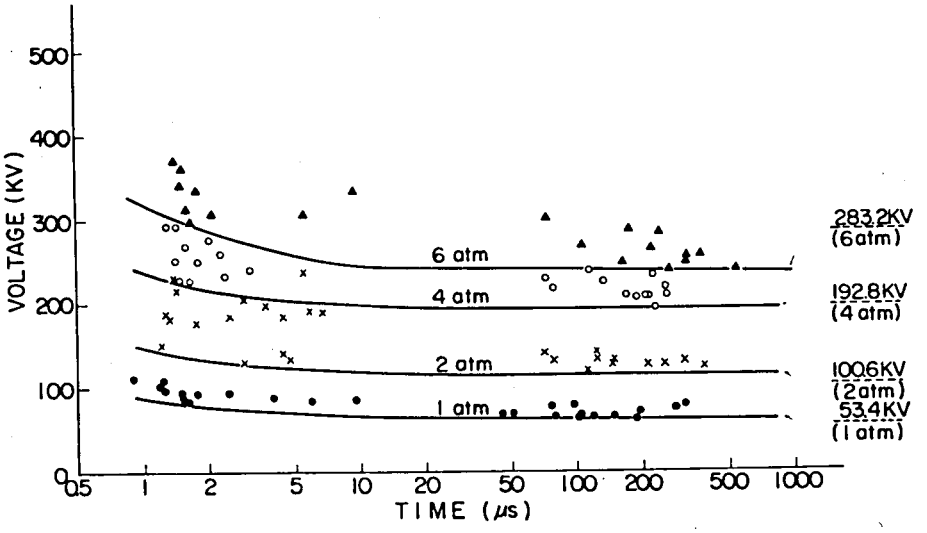


Fig.75(a) V-t Characteristics of Gap C (d=1cm, u=0.481, Positive)

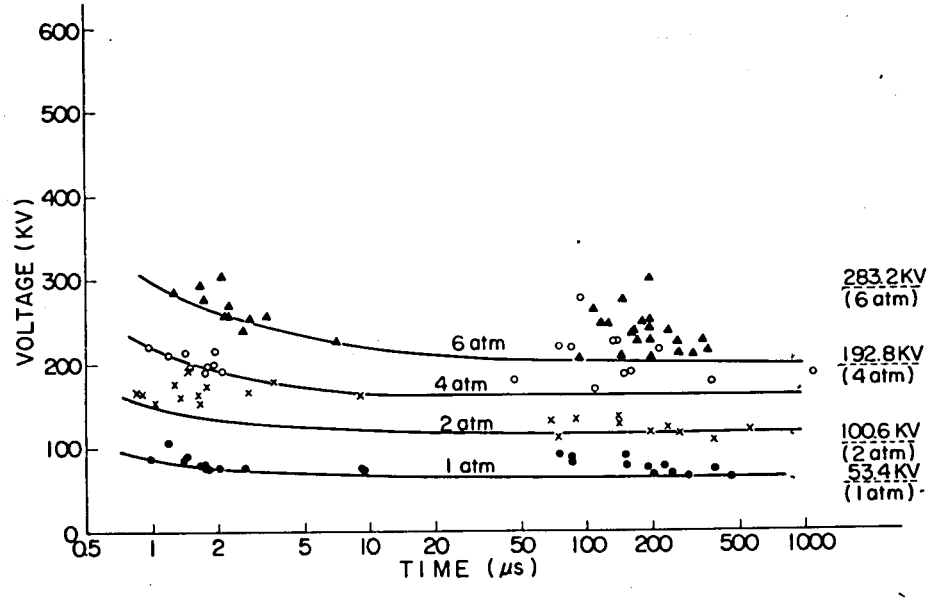


Fig.75(b) V-t Characteristics of Gap C (d=1cm, u=0.481, Negative)

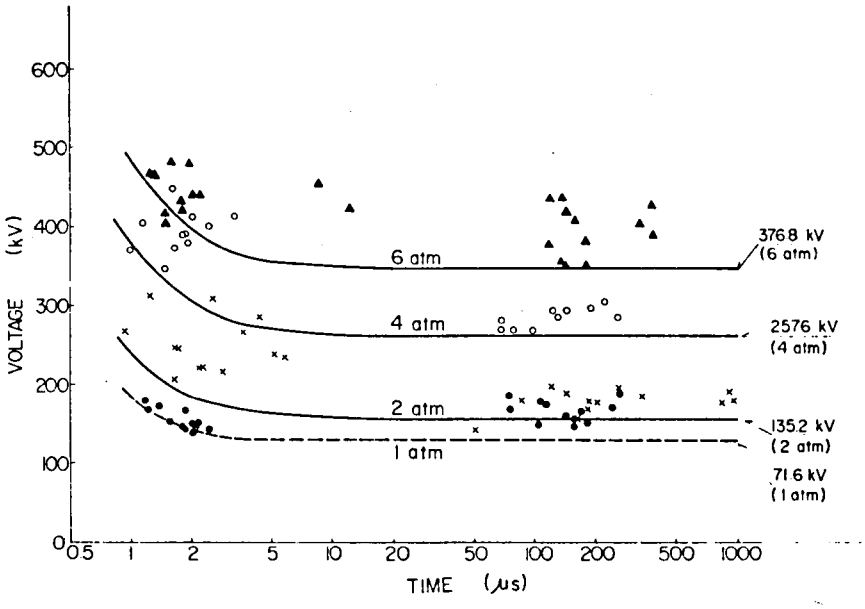


Fig.76(a) V-t Characteristics of Gap C (d=4cm, u=0.161, Positive)

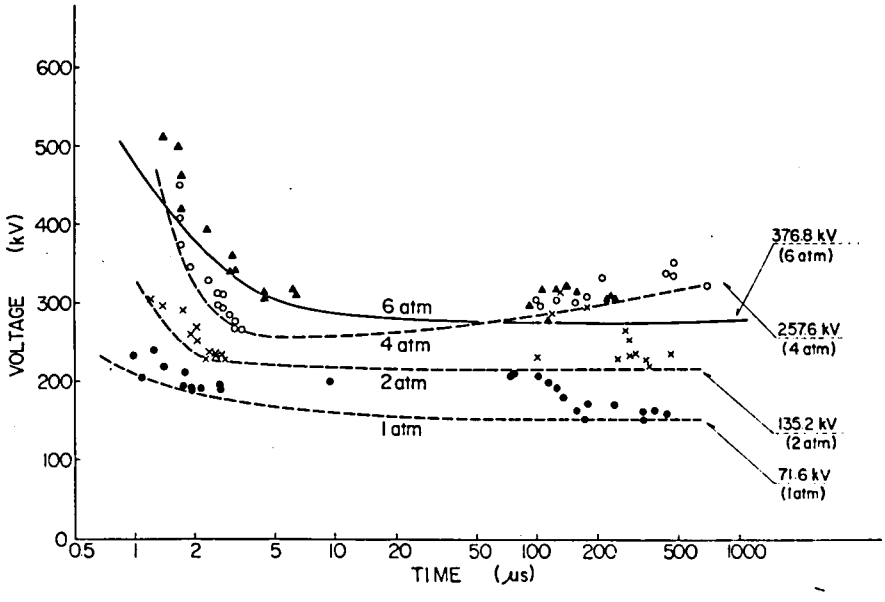


Fig.76(b) V-t Characteristics of Gap C (d=4cm, u=0.161, Negative)

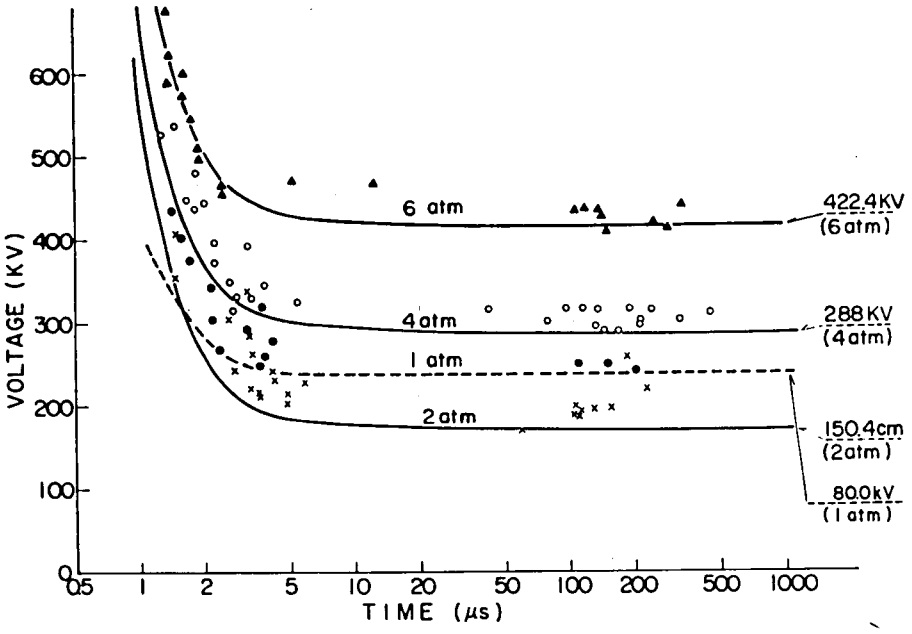


Fig.77(a) V-t Characteristics of Gap C (d=16cm, u=0.045, Positive)

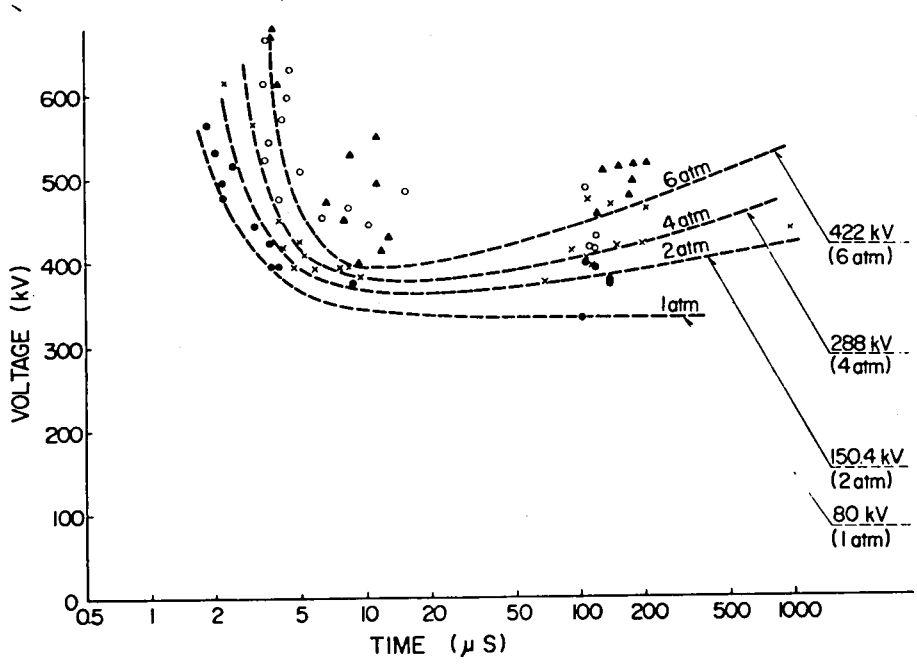


Fig.77(b) V-t Characteristics of Gap C (d=16cm, u=0.045, Negative)

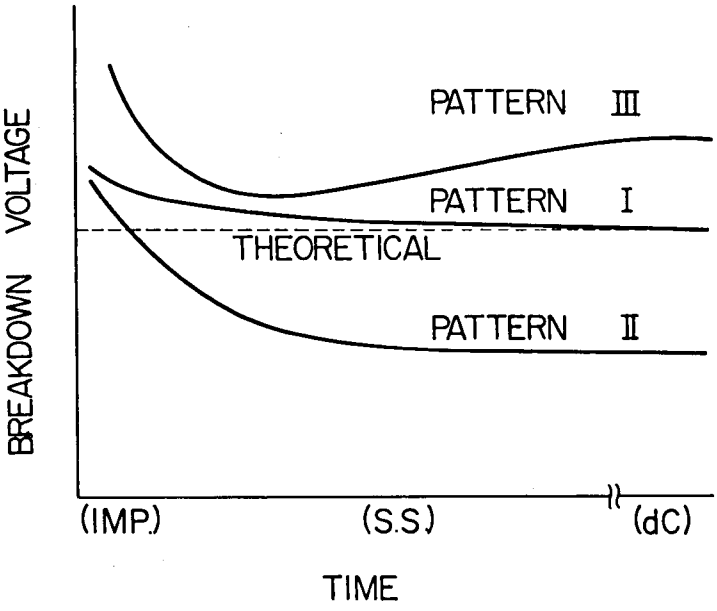


Fig.78 Three Patterns of V-t Characteristics

Pattern III: The minimum value of switching surge breakdown voltage is abnormally higher than the theoretical estimation due to the corona stabilization. V-t curve has its minimum in the time range of order of 10 $\mu$s as typically shown in Fig.78, although the minimum may not be appreciable in some cases at low pressures. Negative breakdown voltage is higher than the positive, which is opposite to the characteristic in other patterns. (Example, Gap C, p = 1, d = 16, Positive and Negative)

For a given test condition, which of these V-t characteristics occurs is dependent on the gap configuration and gas pressure. All the gap conditions experimented and the patterns of their V-t curves are listed in Table 6.

| Gap \ Press ure (atm) | | Positive | | | | | Negative | | | | |
|---|---|---|---|---|---|---|---|---|---|---|---|
| | | Gap spacing (cm) | | | | | | | | | |
| | | 1 | 2 | 4 | 8 | 16 | 1 | 2 | 4 | 8 | 16 |
| Gap A | 1 | I | I | I | I | | I | I | I | II | |
| | 2 | II | II | | | | II | II | | | |
| | 4 | II | II | | | | II | II | | | |
| | 6 | II | II | | | | II | II | | | |
| Gap B | 1 | I | I | I | | I | I | I | III | | III |
| | 2 | I | I | | | | I | I | | | |
| | 4 | II | I | | | | II | II | | | |
| | 6 | II | II | | | | II | II | | | |
| Gap C | 1 | I | | III | | III | I | | III | | III |
| | 2 | I | | I | | I | I | | III | | III |
| | 4 | I | | I | | I | II | | III | | III |
| | 6 | II | | II | | I | II | | II | | III |

Table 6 List of Test Conditions and the Patterns of V-t Characteristic

The critical condition between Patterns I and II coincides with the condition that dc breakdown voltage of a gap is influenced by the surface irregularities on the negative electrode in Fig.67. The cases in Pattern I and II are plotted on gas pressure and the effective area coordinates, specifying their patterns as in Fig.79 and compared with the curve for rough electrode in Fig.67, since the experiment in the present chapter is performed on rough finished electrode. The effective area in these test conditions are estimated as a function of gap spacing and gas pressure in Appendix IV. For example, the values of $S_{eff}$ of Gap A for negative polarity at the spacing of 4 and 8 cm at atmospheric pressure are read from Fig.IV−1(b) as 6.9 and 23 $cm^2$, respectively. V-t characteristic of the gap at 1 atm is in Pattern I at 4 cm spacing, while it is in Pattern II at 8 cm spacing. These data are plotted as the two plots at the lower right in the figure.

These plots clearly show that the criterion between Pattern I and II is expressed as a function of $S_{eff}$ and gas pressure. The criterion coincides with that of the reduction of

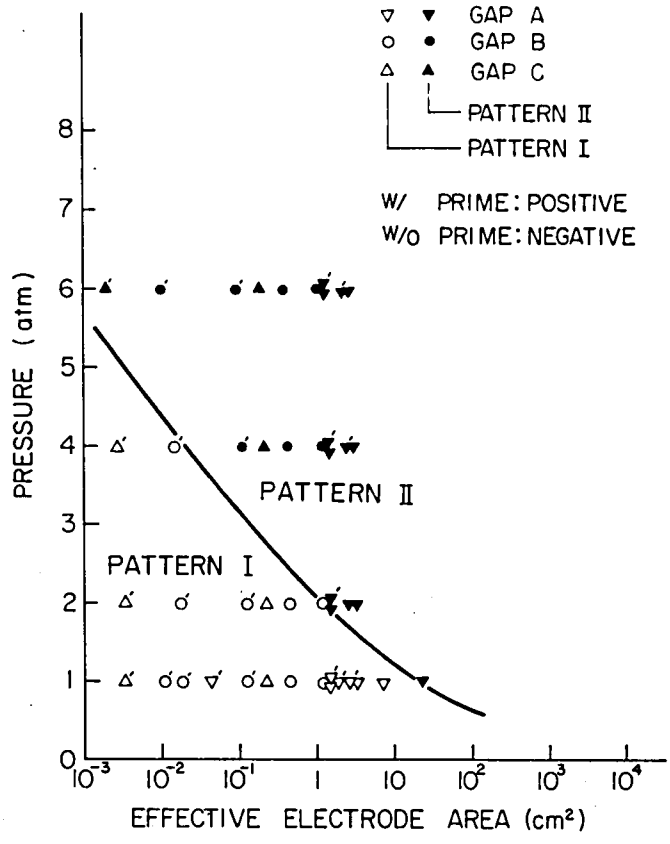


Fig.79 Regions of Pattern I and II on Pressure vs Electrode Area Diagram.

ac and dc breakdown voltages presented in Fig.67 and replotted by solid curve in Fig.79.

V-t characteristic in Pattern III is observed only for very nonuniform field gaps. The criterion is determined by the condition if a discharge initiated at the highly stressed area can produce the breakdown of the gap or cease at the low field region in the mid gap. The condition coincides to the criterion for corona stabilization in dc breakdown presented in Fig.25.

## §4. Shape of V-t Characteristic

The shapes of the V-t characteristics in the three patterns are studied. Those in Pattern I and II are generalized as a semi-empirical formula which will be useful in the quantitative discussion of insulation coordination of gas insulated equipments.

### 4-1. Shape of V-t Characteristic in Pattern I

The envelopes of the minimum breakdown voltage for both positive and negative polarities in Pattern I are expressed mathematically as;

$$\frac{V_1(t) - V_d}{V_d} = \kappa_1 \cdot t^{-n_1} \tag{55}$$

Where, $V_1(t)$ is the minimum breakdown voltage at time t ($\mu$s) in Pattern I, $V_d$ is the theoretical breakdown voltage of the gap, $\kappa_1$ and $n_1$ are constants determined by the test conditions.

The value of $\kappa_1$ is the rate of the increase of breakdown voltage $\left\{ V_1(t) - V_d \right\} / V_d$ at t = 1 $\mu$s, and the value will be expressed as a function of the time which is required for the development of the breakdown to cross the gap. From the experimental results in Fig.70 to 77, the value of $\kappa_1$ is dependent on gap configuration and gas pressure, and expressed as a function of d/pu as shown in Fig.80. Here, u is field utilization factor, the ratio of the average and the maximum field of the gap.

The dependence on d/pu will be understood as follows. Field utilization factor u is usually introduced to show the breakdown voltage of a non-uniform field gap is equivalent to the breakdown voltage of an uniform field gap of spacing u·d. However, for the development of breakdown across the gap at constant pressure, equivalent spacing of the gap should be larger than d. We consider the gap is equivalent to an uniform field gap whose spacing is d/u and stressed at the maximum field strength of the original gap. By this interpretation, a non-uniform field gap is equivalent to an uniform gap which has longer spacing and stressed at the maximum field of the original gap. At different pressures, breakdown field strength is roughly proportional to gas pressure. Since the velocity of the development of the breakdown is suspected to be proportional to the field strength, the time required for the development of the breakdown, hence the value of $\kappa_1$ is expressed as a function of d/pu.

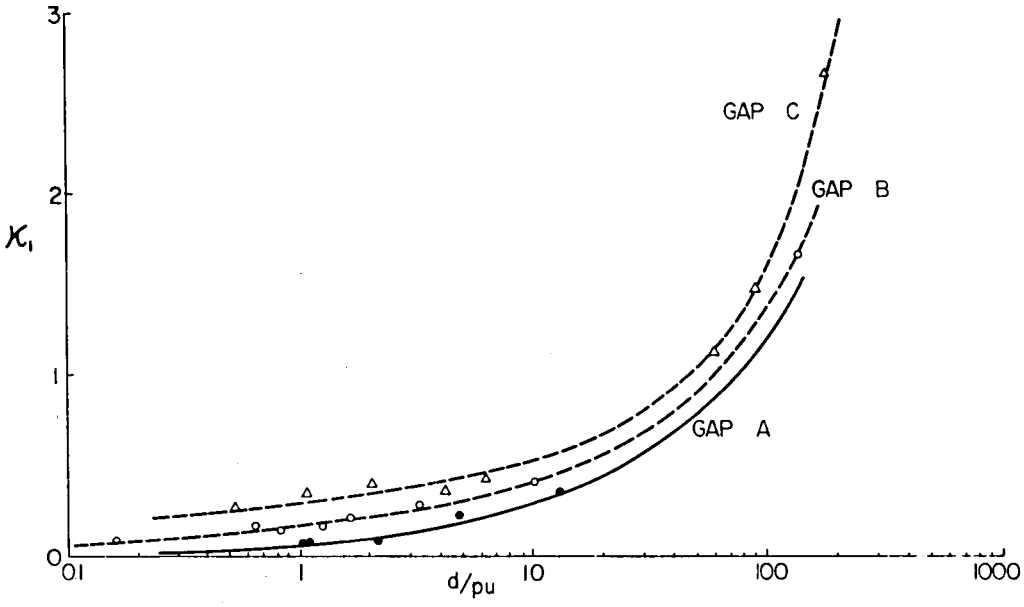


Fig.80 Parameter $\kappa_1$ of V-t Curve in Pattern I

The values of $\kappa_1$ fall on almost one curve within the accuracy of the data as in Fig.80, although the values for smaller electrode are slightly higher than those for larger electrodes. This slight difference by the size of electrode is probably attributed to larger statistical scattering of impulse breakdown voltages due to the lack of initiation electrons as pointed out before. If this is the case, the value for the largest Gap A is most reliable. The values of $\kappa_1$ for Gap A are given by the following expression as shown by the solid curve in Fig.80.

$$\kappa_1 = 0.06 \left(\frac{d}{up}\right)^{0.66} \tag{56}$$

While $\kappa_1$ determines the value of the breakdown voltage at 1 $\mu$s, $n_1$ in equation 55 determines the rate of rise of V-t curve in Pattern I. The value of $n_1$ will be expected to be given as a function of the equivalent gap spacing d/u. Since the value is only related to the relative value of $V_1(t) - V_d$ at different time t, it will be independent of the velocity of the development of the breakdown or gas pressure. Fig.81 is the values of $n_1$ obtained by the data in Fig.70 to 77 plotted against d/u for the three gaps used in the test. All the plots fit very well on a single curve expressed as;

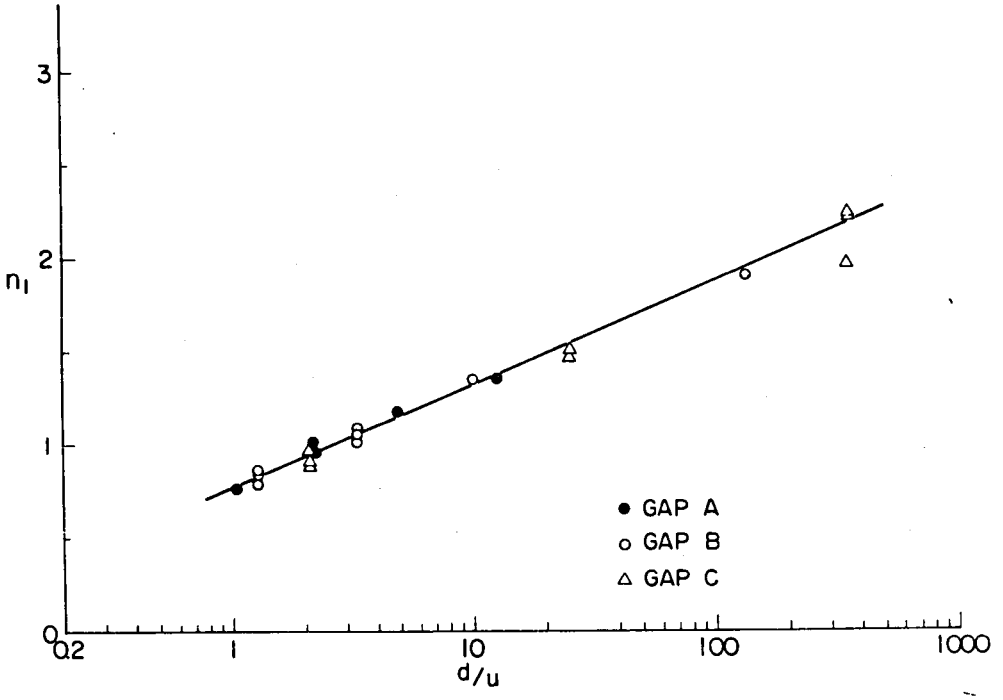


Fig.81 Parameter $n_1$ of V-t Curve in Pattern I

$$n_1 = 0.24 \ln \left( \frac{d}{u} \right) + 0.77 \qquad (57)$$

From these values of $\kappa_1$ and $n_1$, V-t characteristic of a given gap in Pattern I can be calculated. This characteristic is understood as the basic V-t curve of the minimum breakdown voltages of $SF_6$ gas with negligible effect of electrode.

## 4-2 Shape of V-t Characteristic in Pattern II

At high gas pressures, breakdown characteristic is in Pattern II, and switching surge breakdown voltage is lower than the theoretical estimation under the effect of electrode. The reduction of breakdown votlage is more pronounced for slow applied voltage. In this case, the time dependence involved in Pattern I is mixed up with that of the effect of electrode.

The time dependence of the effect of electrode is obtained separately as the V-t

characteristic of a gap whose d/pu is very small. In this case, the value of $\kappa_1$ is very small as seen in Fig.80 and V-t curve of the gap in Pattern I is essentially flat. Any rise in the V-t curve will be attributed to the effect of electrode. Fig.82 is the examples of V-t characteristic of an uniform field gap of d=1 cm, whose d/pu is very small. [38]

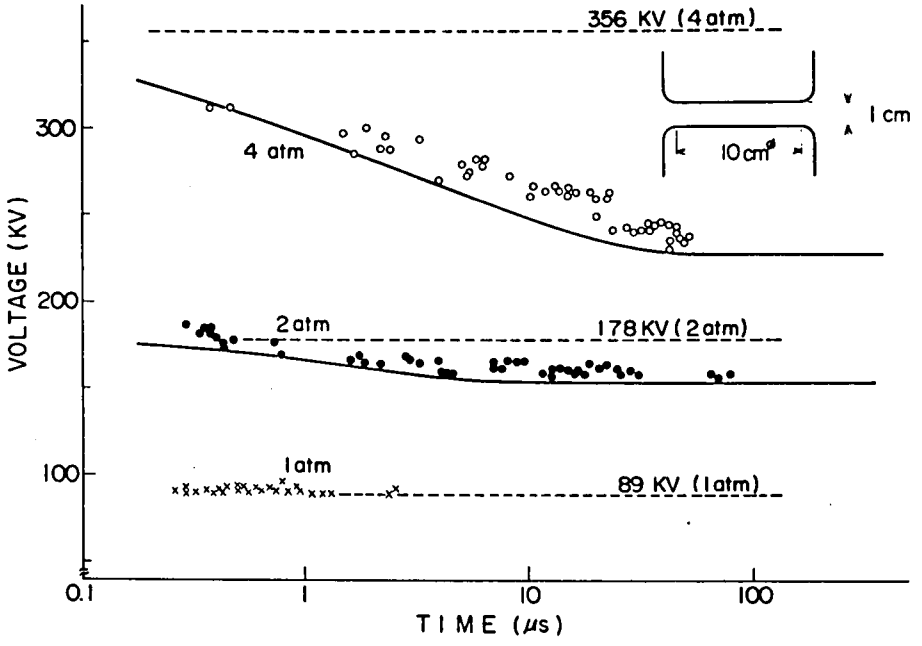


Fig.82 V-t Characteristics of Gap E (d=1 cm u=1)

Theoretical breakdown voltages are shown by dotted lines in the figure. The characteristic is in Pattern I at p=1 atm, and it is quite flat as expected. The rise of the V-t curves under the effect of electrode at p=2 and 4 atm are expressed mathematically as;

$$V_2(t) = V_0 + (V_d - V_0) \cdot exp\ (-\kappa_2 \cdot t^{n2}) \qquad (58)$$

Where, $V_2(t)$ is the breakdown voltage at time t under the effect of electrode, $V_o$ the minimum breakdown voltage for long switching surge. $V_2(t)$ converges to $V_d$ when time t tends to zero, while it converges to $V_o$ with the increase of t.

Equation 58 will be applied to more general gap configuration as in the following fashion. V-t curve $V_1(t)$ in Fig.83 is an imaginary characteristic obtained by equation 55, postulating the gap is in Pattern I. Since the minimum value of switching surge breakdown voltage $V_o$ is lower than $V_d$, V-t curve in Pattern II will be approximated as

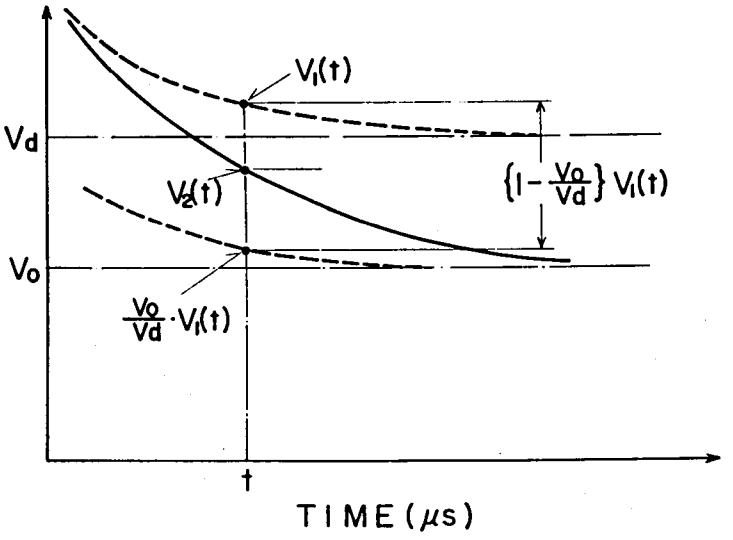


Fig.83 Estimation of the V-t Characteristic in Pattern II

$\frac{V_o}{V_d} \cdot V_1(t)$, provided the effect of electrode is not dependent on the steepness of the applied voltage. In reality, as the effect of electrode is less effective for steep applied voltage as in equation 58, actual V-t curve will be close to $V_1(t)$ for small values of t, while it approaches to $\frac{V_o}{V_d} \cdot V_1(t)$ and then to $V_o$ with time t. As an expression of this relation, V-t characteristic in Pattern II is expressed as;

$$V_2(t) = V_1(t) \cdot \frac{V_o}{V_d} + (1 - \frac{V_o}{V_d}) \cdot V_1(t) \cdot exp\ (-\kappa_2 \cdot t^{n_2}) \qquad (59)$$

If we put $V_o = V_d$ as it is in Pattern I, the expression coincides to equation 55. This means that equation 59 is a general expression of V-t curve of $SF_6$ in Pattern I and II.

The value of constant $\kappa_2$ is independent of the gap conditioins tested in the present experiment and the value is;

$$\kappa_2 = 0.615 \qquad (60)$$

The value of $n_2$ is determined by the rate of the reduction of breakdown voltage from the theoretical estimation $(1-V_o/V_d)$ as shown in Fig.84. The relation is expressed as;

$$n_2 = \frac{1}{4.5\ (1-\frac{V_o}{V_d}) + 0.5} \tag{61}$$

From these values of $\kappa_1$, $n_1$, $\kappa_2$ and $n_2$, V-t characteristic of $SF_6$ of a given gap in Pattern I and II is expressed with sufficient accuracy. V-t curves calculated by equation 59 are shown by solid lines in Fig.70 to 77. They fit very well for all of the experimental results in Pattern I and II. In the calculation, the minimum breakdown voltage for switching surge is used as $V_o$. However, even if we do not have any experimental data for the value, it will readily be estimated by $E_{5\%}$ in equation III–3 in Appendix III as will be shown in Section 5.

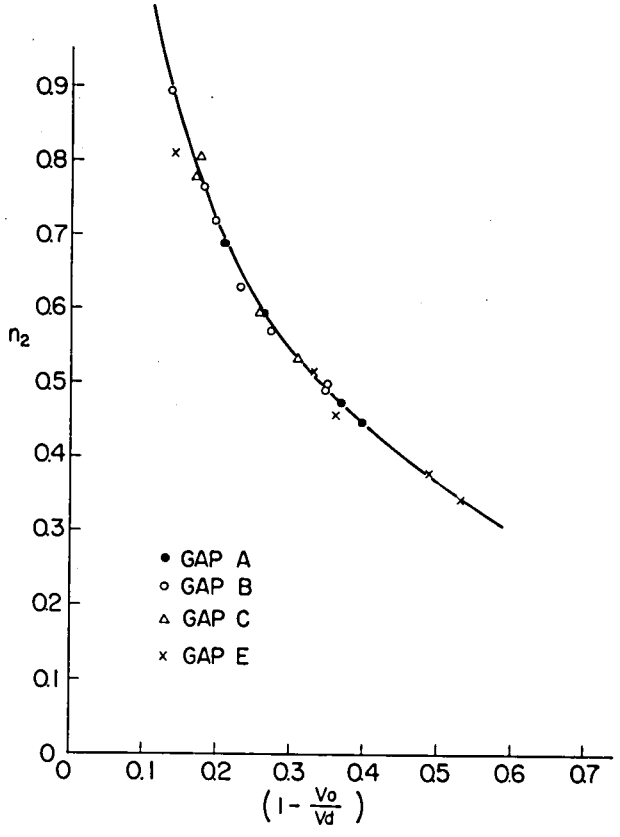


Fig.84 Parameter $n_2$ of V-t Curves in Pattern II

## 4-3. V-t Characteristic in Pattern III

Breakdown characteristic of $SF_6$ in Pattern III is not very much important practically, since $SF_6$ gas insulated apparatus are usually designed to have nearly uniform field distribution in every part of the insulation. Steady corona discharge precedes to the breakdown in Pattern III and the decomposition products of $SF_6$ due to the corona may deteriorate the insulation in its life. This is the reason why a gap in Pattern III is not utilized in practical applications.

However, the breakdown characteristic in Pattern III is important as we encounter this pattern quite often in laboratory experiments and we have to be very careful in applying the results of the tests to the design of practical gas insulation.

V-t characteristic in Pattern III is different from those in Pattern I and II in the following aspects. Negative breakdown voltage is always higher than the positive. This is opposite to the cases in Pattern I and II. Since the pattern is more likely to occur for the negative polarity, as shown in Fig.25, it frequently happens that V-t characteristic is in Pattern III only for negative polarity, while it is in Pattern I or II for positive polarity. From this reason, if negative breakdown voltage is higher than the positive for a given test condition, at least negative V-t characteristic is in Pattern III.

V-t characteristic in Pattern III has its minimum at the time range of around 10 $\mu$s and V-t curve shows V-shape which is well known for a long gap in atmospheric air. The characteristic is more pronounced at higher pressures. Both steep impulse and slow switching surge breakdown voltage increases by the effect of corona stabilization, while the effect is minimum at intermediate duration of applied voltage. At 6 atm, the highest pressure tested on Gap C, breakdown voltage at the minimum is as low as the value expected for the breakdown voltage of the gap in Pattern II.

## §5. Statistical Distribution of Breakdown Field Strength

The experimental data in Fig.70 to 77 are quite limited to discuss the statistical distributuion of breakdown voltages as a function of time t. However, it is noticed that the minimum switching surge voltage is pretty close to that of dc breakdown voltage presented in Chapter III. The fact will suggest that the statistical distribution is also quite similar to that for dc applied voltage. If this is the case, the distribution can be estimat-

ed theoretically by equation 40.

To check the above guess, experimental scattering, the range between the maximum and the minimum breakdown field strength, is compared with the theoretical values calculated by equations III–3 and III–4 in Appendix III for Gap A, B and C in Fig.85 to 87, respectively. The value of m in the theoretical estimation is given by equation 46 and the value of $\lambda_o$ is obtained by multiplying 30 for rough electrode to the value by equation 45. Effective area S for positive and negative polarities are obtained from Fig. IV–2(b) in Appendix IV. The value of $E_d$ is calculated by equation 16 in Chapter II, as a function of gap geometry and gas pressure.

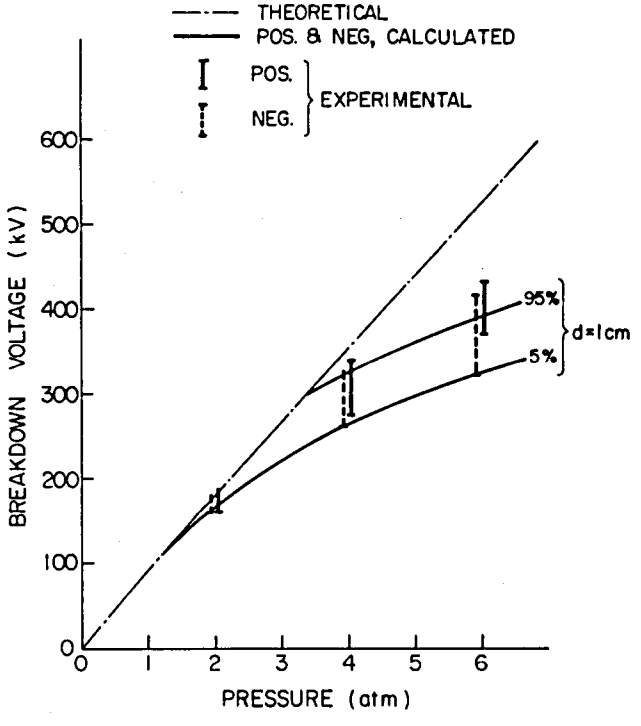


Fig.85 Experimental and Calculated Scattering of Breakdown Voltage for Gap A

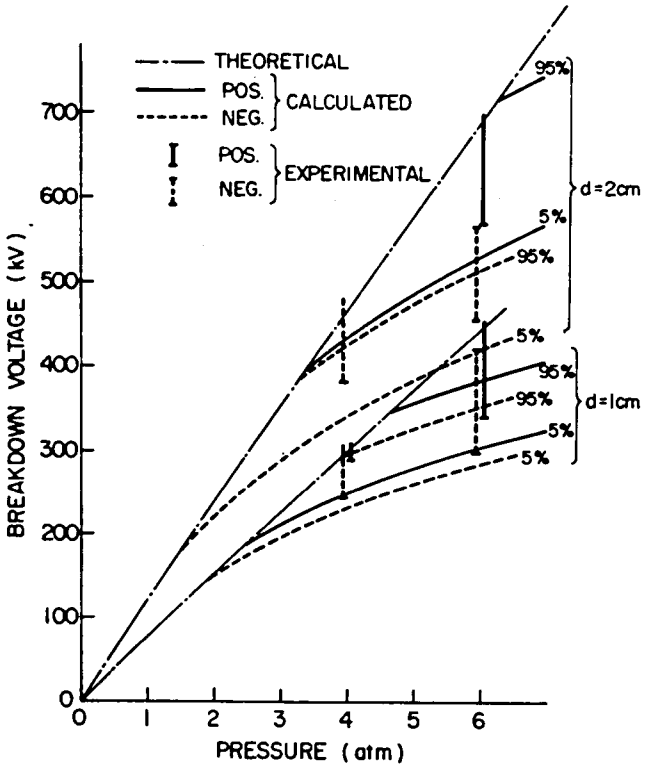


Fig.86 Experimental and Calculated Scattering of Breakdown Voltage for Gap B

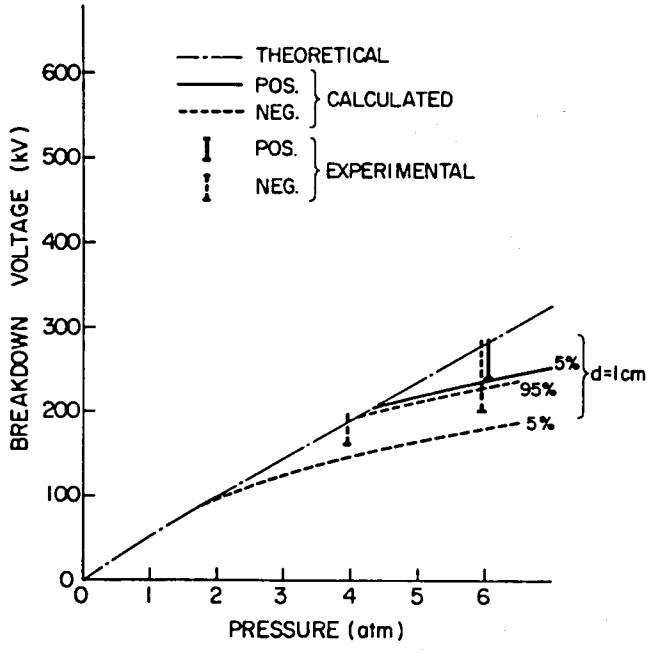


Fig.87 Experimental and Calculated Scattering of Breakdown Voltage for Gap C

The calculated minimum and maximum field strengths are shown by solid and dashed lines for positive and negative polarities, respectively. The ranges of the scattering of experimental switching surge breakdown voltages which are lower than the theoretical estimation by the effect of electrode are shown by the vertical lines in the figures. Since we are only interested in the effect of electrode, all the data higher than the theoretical estimation are omitted from the polots. In spite of the scattering in the experimental data, the coincidence between the theoretical and the experimental results is very good.

The statistical scattering for impulse voltage is also quite similar to that of switching surge applied voltage. No particular evidence of different statistical scattering is observed between impulse and switching surge breakdown field strengths. The indifference in the statistical distributuion by the wave shape of the applied voltage supports the conclusion in Chapter V that the scattering of breakdown voltages are caused by the statistical properties of weak points exist *"a priori"*.

## §6. Conclusion

Voltage-time characteristics of impulse and switching surge breakdown in $SF_6$ are categolized into three patterns depending on the gap conditions. The criterions of these patterns of V-t characteristics are deduced quantitatively from the results of dc experiments in the foregoing chapters.

(1) When the breakdown characteristics are not influenced by the surface of electrode, V-t curve is expressed by equation 55. Constants $\kappa_1$ and $n_1$ are given as a function of the gap conditions in Fig.80 and 81, respectively. The minimum value of switching surge breakdown strength in this pattern coincides to the theoretical estimation by equation 16 and no polarity effect is observed as expected from the theoretical analysis in section 3-4 in Chapter II.

(2) When the switching surge breakdown voltage is lower than the theoretical estimation under the effect of electrode, V-t curve is expressed by equation 59. Constant $\kappa_2$ is independent of the gap condition and the value is about 0.615. The value of $n_2$ is given by equation 61 as a function of the reduction rate of breakdown voltage from the theoretical estimation. In this pattern, positive breakdown voltage is always higher than the negative value.

(3) If a gap is corona stabilized, breakdown voltage is unusually high in the time range from steep impulse to slow switching surge. This pattern of V-t curve has its minimum at the time range of about 10 $\mu$s, particularly at high gas pressures. Negative breakdown voltage is always higher than the positive one in this pattern, which is opposite to the cases in other two patterns.

(4) Statistical distribution of impulse and switching surge breakdown field strength is not particularly different from that for dc applied voltage. The distribution is governed by the statistical property of the weak points exist *"a priori"* on negative electrode, and the distributuion is quantitatively estimable by the light of Weibull statistics.

## VII. CONCLUSION

Electrical breakdown characteristics of $SF_6$ are studied intending to generalize the characteristics in the form to be useful in the design of $SF_6$ gas insulated power substations and other high voltage equipments. The results of the study are summarized in the followings.

(1) The maximum field strength of $SF_6$ at breakdown is expressed theoretically as in equation 16 as a function of gas pressure and the geometrical shape of electrode.

(2) The relation explains experimental results very well at low gas pressures where breakdown characteristics are pure representative of the properties of $SF_6$ gas. At high pressures, however, breakdown voltage is lower than the theoretical estimation due to the effect of electrode rather than the properties of $SF_6$.

(3) In the case of a very non-uniform field gap in relatively low gas pressure, breakdown voltage is sometimes unusually high due to "corona stabilization" of electric field. The condition of the corona stabilization is given in Fig.25. The phenomena is more likely to occur for negative polarity than for positive polarity. In this corona stabilized breakdown of a gap, the inception field strength of the corona is expressed by the theoretical equation 16.

(4) As far as purely electrical discharge concerns, a microscopic protrusion on the surface of electrode will not reduce the breakdown voltage of a gap, unless the height of the protrusion is higher than the critical values shown in Fig.35, provided its shape is not too sharp. However, a sharp protrusion will be effective to reduce the breakdown voltage of the gap by field emission of electrons from its tip and it works as a weak point of the electrical insulation of the gap.

(5) The criterion whether the breakdown characteristics of a given gap is under the effect of electrode roughness or not is expressed as a function of gas pressure and the effective area of negative electrode as shown in Fig.67.

(6) Statistical distribution of cumulative probability of the maximum breakdown field strength obeys in Weibull distribution rather than normal distribution and expres-

sed by equation 40. Constant m in the expression is approximately given as 7.4, independent of gas pressure and the finish of electrode. The value of $\lambda_o$ for fine finished stainless steel laboratory electrode is given by equation 46. For the electrode finished something like a carefully treated surface of a practical gas insulated power equipment and whose surface roughness is the order of $\pm 20\mu$, the value of $\lambda_o$ is about 30 times as large as the value for fine finished electrode, while the value of m is unchanged. The value of $E_o$ is understood as the minimum possible breakdown field strength for infinitely large electrode and the value is experimentally given by equation 44 as a function of gas pressure. Statistical distribution of the breakdown field strength of a given gap can be evaluated by equation 40 using these values of constant and the effect of electrode area is quantitatively explained by the evaluation.

(7) Effective electrode area of a given gap is defined theoretically as in equation 51. The difference of the effective area by the polarity of applied voltage explains the polarity effect of breakdown characteristic.

(8) Voltage-time characteristics of impulse and switching surge breakdown in $SF_6$ are categolized into three patterns I, II and III depending on the gap conditions;
   a. whether dc breakdown voltage is reduced from the theoretical estimation under the effect of electrode or not.
   b. whether dc breakdown voltage is corona stabilized or not.
   These criterions are quantitatively given by Fig.67 and 25, respectively.

(9) V-t characteristics of $SF_6$ gas are formulated in a general expression in equation 59, so that the V-t characteristic of a given gap can be evaluated quantitatively. Insulation coordination and abnormal voltage protection of $SF_6$ gas insulated power equipment can be discussed depending on the type of their patterns of V-t characteristic by the expression

Interest of the present work was limited to the breakdown characteristics of pure $SF_6$ without any detectable foreign particles or solid insulation. In the design of a practical $SF_6$ gas insulated equipment, factors such as solid insulating support to hold live part mechanically from the ground, conducting particles left in an enclosure are very important. Fundamental investigations on these subjects are in due cource as an extension of the present work. Though these factors make the problem much more complicated, the chara-

cteristics of pure gas studied here will be very helpful for the design of a $SF_6$ gas insulated equipment, and also be beneficial as the basis of the future study.

134 項欠

## REFERENCES


1. H. Moissan, P. Lebeau ; Annales de Chemie et Physique 26 145 (1902)

2. E. Charlton, F. S. Cooper ; GE Review 40 438 (1937)

3. F. S. Cooper ; U. S. Patent, No. 2,221.671 (1940)

4. J. F. Ahearn et al ; 5th International Insulation Conference (1963) p-16

5. G. Camilli, G. S. Gordon, R. E. Plump ; Gaseous Insulation for High Voltage Transformer, AIEE TP-52-78 (1952)

6. J. A. Brown ; The Use of Sulfur Hexafluoride as a Gaseous Dielectric, Symposium on Electrical Insulating Gases (1964) pp24-31

7. Allied Chemical Co., General Chemical Division, Catalog TB-85603

8. J. D. Cobine ; Some Electrical and Thermal Characteristics of Helium and Sulfur-Hexafluoride Mixtures, Tr. AIEE, Vol. 74, Pt.I pp. 318-321

9. E. E. Charlton, W. R. Westondorp, L. E. Dempster, G. Hotaling ; Jr. of Applied Physics 10 374 (1939)

10. G. Camilli, J. J. Chapman ; Gaseous Insulation for High-Voltage Apparatus, AIEE TP(PA&S) 66 1463 (1947)

11. T. Nitta, et al ; $SF_6$ Gas Filled Lightning Arrester Gaps for 500 kV Power System, Tr. I.E.E. of Japan, Vol. 92-B, No.9 (1972) pp. 523-530

12. $SF_6$ Switchgear for Transmission and Industrial Applications, Electrical Review, June 4, 1965, pp. 862-863

13. P. Bruckner, H. Floth ; Vollisolierte gekapselte Schaltanlagen für Reihe 110 kV mit sehr kleinem Raumbedarf, ETZ-A, Bd. 86 (1965) pp. 198-204

14. C. Chierichetti, D. Castelli ; High Voltage Metal-Clad Swichgear, CIGRE 123 (1966)

15. J. Raimbault et al ; Electricity Supply to Large Town and Metal Clad Equipment for 225 kV Networks, CIGRE 136 (1966)

16. E. Leimgrubler, H. G. Schutte ; Ein neuer vollisolierter Leistungsschalter für 110 kV Innenraum-Schatanlagen, ETZ–A, Bd. 87 (1966) pp. 102–106

17. H. W. Graybill, J. C. Cronin, E. J. Field ; Testing of Gas Insulated Substations and Transmission Systems, IEEE Tr. T 73 366-2 (1973)

18. K. Morii et al ; Development of 500 kV Gas Insulated Switchgear and its Application, IEEE Tr. T 73 033-8 (1973)

19. J. G. Trump ; Compressed Gas Insulation and Electric Power Systems, Proc. Conf. on Gas Discharges and the Electricity Supply Industry, Leatherhead, (1962)

20. S. Fukuda ; EHV Cables with Compressed $SF_6$, IEEE Tr. Vol. PAS-86 No. 1 (1967) pp. 60-66

21. S. Fukuda ; Current Carrying and Short-Circuit Tests on EHV Cables Insulated with $SF_6$ Gas, IEEE Tr. Vol. PAS-88, No.2 (1969) pp. 147-156

22. H. W. Graybill, J. A. Williams ; Underground Power Transmission with Insulated Phase Gas-Insulated Conductors, IEEE Tr. Vol. PAS-89 (1970) pp. 17-23

23. J. A. Williams et al ; Installation of 345 kV $SF_6$ Insulated Phase Isolated Underground Bus, IEEE PES, Conference Paper C 72 117-5 (1972)

24. G. Supplee et al ; Insulation of a 230 kV Compressed Gas Insulated Bus, IEEE Tr. T 73 364-7 (1973)

25. H. C. Pollock, F. S. Cooper ; The Effect of Pressure on the Positive Point-to-Plane Discharge in $N_2$, $O_2$, $CO_2$, $SO_2$, $SF_6$, $CCl_2F_2$, A, He and $H_2$, Physical Review, Vol. 56 (1939) pp. 170-175

26. T. R. Foord ; Some Experiments on Positive Point-to-Plane Corona and Spark Breakdown of Compressed Gases, Proc. of IEE, Vol. 100, Pt. II, No. 78 (1953) pp. 585-590

27. C. N. Works, T. W. Dakin ; Dielectric Breakdown of Sulfur Hexafluoride in Nonuniform Fields, AIEE Tr. Vol. 72, Pt. I, (1953) pp. 682-689

28. D. Berg, C. N. Works ; Effect of Space Charge on Electric Breakdown of Sulfur Hexafluoride in Nonuniform Fields, IEEE Tr. PAS (1958) pp. 820-823

29. T. Nitta et al ; AC Breakdown Characteristics of Nonuniform Field Gaps in $SF_6$, Joint Meeting of IEE of Japan (1965) Paper No. 102 (in Japanese)

30. J. Hara, T. Nitta ; Dielectric Breakdown Characteristics of $SF_6$, Joint Meeting of Kansai Branch of IEE of Japan (1965) Paper No. 2.1-6 (in Japanese)

31. E. Steiniger ; Durchschlagsverhalten von Schwefelhexafluorid bei Gleich-, Wechsel- und Stossspannungsbeanspruchung, ETZ-A Bd. 86, H. 18 (1965) pp. 583-590

32. N. R. McCormick, J. D. Craggs ; Some Measurements of the Relative Dielectric Strength of Gases, British Jr. of App. Phy. Vol. 5, (1954) p-171

33. R. Geballe, M. L. Reeves ; A Condition on Uniform Field Breakdown in Electron Attaching Gases, Phy. Rev., Vol. 92 (1953) pp. 867-868

34. E. H. Cohen ; The Electric Strength of Highly Compressed Gases, Proc. of IEE, 103, Pt. A (1956) pp. 57-68

35. P. R. Howard ; Insulation Properties of Compressed Electronegative Gases, Proc. of IEE Vol. 104, Pt. A, (1957) pp. 123-138

36. P. Narbut et al ; Factors Controlling Electric Strength of Gaseous Insulation, AIEE Tr. PAS, Vol. 78, Pt. III, (1959) pp. 545-550

37. S. F. Philip ; Compressed Gas Insulation in the Million-Volt Range : A Comparison of $SF_6$ with $N_2$ and $CO_2$, AIEE Tr. PAS (1963) pp. 356-359

38. T. Nitta, K. Kawane, N. Yamada, "Electrical Breakdown characteristics of sulphur hexafluoride", Mitsubishi Denki Giho Vol.39, No.8, pp. 941-946, 1965. (in Japanese)

39. H. C. Doepken ; Compressed-Gas Insulation in Large Coaxial Systems, IEEE Tr. Vol. PAS-88, No.4 (1969) pp. 364-369

40. K. Itaka, G. Ikeda ; Dielectric Characteristics of Compressed Gas Insulated Cables, IEEE Tr. PAS, Vol. PAS-8 (1970) pp. 1986-1994

41. Y. Kawaguchi, K. Sakata, S. Menju ; Dielectric Breakdown of Sulphur Hexafluoride in Nearly Uniform Fields, IEEE Tr. 70 TP 577-PWR (1970)

42. Y. Kawaguchi, S. Menju ; Breakdown Characteristics of Sulfur Hexafluoride in Coaxial Cylinder Electrodes, JIEE of Japan, Vol. 90, No. 10 (1970) pp. 211-218

43. T. Nitta, Y. Shibuya, Y. Fujiwara ; Dielectric Breakdown Characteristics of Long Gaps in $SF_6$ Gas, Joint Meeting of IEE of Japan (1969) Paper No. 127 (in Japanese)

44. I. M. Bortnik, B. A. Gorjunov ; Breakdown Characteristics in Compressed $SF_6$, 9th Int'l Conf. on Phen. in Ion Gases, Bucharest (1969)

45. A. Pedersen ; Criteria for Spark Breakdown in Sulfur Hexafluoride, IEEE Tr. 70 TP 115-PWR (1970)

46. T. Takuma, T. Watanabe ; Discharge Characteristics of Long Gaps in High Pressurized $SF_6$, JIEE of Japan, Vol. 90, No. 6 (1970) pp. 173-182

47. T. Nitta, Y. Shibuya ; Electrical Breakdown of Long Gaps in Sulfur Hexafluoride, IEEE Tr. PAS 70 TP 582-PWR (1970)

48. J. Blackett, J. M. Mattingley, H. M. Ryan ; Breakdown Voltage Estimation in Gases Using a Semi-Empirical Concept, Int'l Conf. on Gas Discharge, London (1970)

49. J. M. Mattingley, H. M. Ryan ; Correlation of Breakdown Gradients in Compressed Air and $SF_6$ for Non-Uniform Fields, Conf. on Elect. Insul. and Dielect. Phenom., Quebec, Canada (1973)

50. H. C. Doepken Jr. ; Compressed-Gas Insulation in Lange Coaxial Systems, IEEE Tr. PAS, 68 TP 630-PWR (1968)

51. A. Diessner, J. G. Trump ; Free Conducting Particles in a Coaxial Compressed-Gas-Insulated System, IEEE Tr. Vol. PAS-89, No. 8 (1970) pp 1970-1974

52. A. H. Cookson, O. Farish ; Particle Initiated Breakdown in Compressed $SF_6$, Conf. on Insul. and Dielect. Phenomena, (1970)

53. A. H. Cookson et al ; Effect of Conducting Particles on AC Corona and Breakdown in Compressed $SF_6$, IEEE Tr. PAS 71 TP 508-PWR (1971)

54. A. H. Cookson, O. Farish ; Particle-Initiated Breakdown between Coaxial Electrodes in Compressed $SF_6$, IEEE Tr. PAS T 72 533-8 (1972)

55. H. Kuwahara et al ; Effect of Solid Impurities on Breakdown in Compressed $SF_6$ Gas, IEEE Tr. T 74 189-7 (1974)

56. S. Menju et al ; Electric Potential and Field of Conical Insulators for $SF_6$ Metal-clad Switchgear, IEEE Tr. PAS 71 TP 554-PWR (1971)

57. J. C. Cronin, E. R. Perry ; Optimization of Insulators for Gas-Insulated Systems, IEEE Tr. PAS, T 72 498-4 (1972)

58. P. Greenwood ; Surface Flashover in Compressed $SF_6$, 2nd Int'l Conf. on Gas Discharges, London (1972)

59. C. M. Cooke, J. G. Trump ; Post-Type Support Spacers for Compressed Gas-Insulated Cables, IEEE Tr. PAS, T 73 121-1 (1973)

60. M. S. Naidu, A. N. Prasad ; Jr. of Physics D. 951 (1970)

61. R. W. Crowe, J. C. Devins ; NRC Conf. on Electrical Insulation, NRC Publication 396 (1956)

62. M. S. Bhalla, J. D. Craggs ; Proc. of Phys. Soc. 80 151 London (1962)

63. W. S. Boyle, P. Kisliuk ; Departure from Paschen's Law of Breakdown in Gases, Physical Review, Vol. 97, No. 2 (1955) pp. 255-259

64. I. D. Chalmers, D. J. Tedford ; Proc. of IEE 118 No. 12, p-1893 (1971)

65. A. Pedersen et al ; Anomalous Breakdown in Uniform Field Gaps in $SF_6$, IEEE Conference Paper, C 73 448-8 (1973)

66. J. M. Meek, J. D. Craggs ; Electrical Breakdown of Gases, Oxford, Clarendon Press (1953)

67. H. Raether ; Electron Avalanche and Breakdown in Gases, London, Butterworths (1962)

68. L. B. Loeb ; Basic Processes of Gaseous Electronics, University of California Press (1955) p-415

69. H. McL. Ryan, C. A. Walley ; Field Auxilliary Factors for Simple Electrode Geometries, Proc. of IEE, Vol. 114, No. 10 (1967) pp. 1529-1536

70. M. S. Abou-Seada, E. Nasser ; Digital Computer Calculation of the Electric Potential and Field of a Rod Gap, Proc. of IEEE, Vol. 56, No. 5, (1968) pp. 813-820

71. T. Nitta, Y. Shibuya ; Closure of "Electrical Breakdown of Long Gaps in Sulfur Hexafluoride" IEEE Tr. Vol. PAS-90, No.3 (1971) pp. 1070-1071

72. T. Nitta, N. Yamada, Y. Arahata, "Characteristic of Sulphur hexafluoride as an insulating medium", Mitsubishi Denki Giho Vol.44, No. 9, pp. 1133-1142, 1970. (in Japanese)

73. T. Nitta et al ; The prebreakdown Phenomena of Atmospheric Air and the Influence of Humidity, Jr. IEE of Japan, Vol. 86-4, No. 931 (1966) pp. 131-140

74. Y. Shibuya, T. Nitta ; Calculation of Electric Field of Rod Gaps in an Earthed Chamber, Jr. IEE of Japan, Vol. 91, No. 10 (1971) pp. 195-203

75. T. Nitta, Y. Shibuya, Y. Fujiwara ; Voltage-Time Characteristic of Electrical Breakdown in $SF_6$, IEEE Transactions, T 74 465-1 (1974)

76. T. Takuma et al ; Flashover Characteristics of Compressed $SF_6$ at Very Long Gaps for Various Impulse Waves, IEEE Conf. Paper, C 72 534-6 (1972)

77. T. Nitta et al ; Effect of Electrode Surface on the Electrical Breakdown of Compressed $SF_6$, Joint Meeting of Kansai Branch of IEE of Japan (1974) (in Japanese)

78. T. Nitta, N. Yamada, N. Ueno ; A Consideration on the Effect of the Surface Roughness of Electrode in the Electrical Breakdown of Compressed $SF_6$, Joint Meeting of Kansai Branch of IEE of Japan (1973) Paper No. G 1-19 (in Japanese)

79. Y. Shibuya, N. Yamada, T. Nitta ; Electrical Breakdown and Prebreakdown Dark Current in Compressed $SF_6$, 2nd Int'l Conference on Gas Discharge, London (1972)

80. N. Yamada, Y. Fujiwara, T. Nitta ; Electrical Breakdown and Prebreakdown Dark Current in Compressed $SF_6$, Jr. of IEE of Japan, Vol. 93-A, No. 1 (1973) pp. 37-44

81. A. H. Cookson ; Electrical Breakdown for Uniform Fields in Compressed Gases, Proc. IEE, Vol. 117, No. 1 (1970) pp. 269-280

82. I. M. Bortnik, C. M. Cooke ; Electrical Breakdown and the Similarity Law in $SF_6$ at Extra-High Voltages, IEEE Tr. PAS T 72 116-7 (1972)

83. T. Nitta, N. Yamada, Y. Fujiwara, "Area Effect of Electrical Breakdown in Compressed $SF_6$, IEEE PES Summer Meeting Paper T 73 449-6 (1973)

84. T. Nitta ; Breakdown Characteristics of Compressed Electronegative Gases, Symposium on Compressed Gas Insulation, Jr. of IEE of Japan, Vol. 87-9, No. 948 (1973) pp. 1635-1639

85. T. Nitta, Y. Fujiwara, Y. Shibuya ; Effective Electrode Area in the Electrical Breakdown of $SF_6$, Symposium on Electrical Discharge of IEE of Japan, ED-74-16 (1974) (in Japanese)

86. G. F. Goldspink et al ; Erratic Spark Breakdown of Gases at High Pressures, Proc. of the 7th Int'l Conf. on Phen. in Ionized Gases, Beograd (1966)

87. E. J. Gumbel ; Statistical Theory of Extreme Values and Some Practical Applications, NBS Applied Mathematics, No. 33, U. S. Gov't Printing Office (1954)

88. K. H. Weber, H. S. Endicott ; Area Effect and its Extremal Basis for the Electric Breakdwon of Transformer Oil, IEEE Tr. PAS Paper No. 56-139 (1956)

89. I. M. Bortnik et al ; Reliability of Gas Insulation at High Pressure, 2nd Int'l Conf. on Gas Discharge, London (1972)

90. S. Menju et al ; Statistical Considerations on the Breakdown of Transformer Oil, IEEE, Conference Paper, C 73 029-6 (1973)

91. P. V. Birke, J. Lackey, S. Palmer ; Determination of Highly Stressed Volume in Oil Dielectrics, IEEE Tr. Vol. EI-7, No.3 (1972)

92. H. W. Anderl, C. L. Wagner, T. H. Dodds; Insulation Coordination for Gas Insulated Substation , IEEE Trans. Vol. PAS-92, No.5, (1973) pp. 1622-1630

93. V. N. Borin; Voltage-Time Characteristics of Compressed Sulphur Hexafluoride Discharge , 2nd International Conference on Gas Discharges, London, (1972) pp. 329-331

94. S. Menju et al; Dielectric Breakdown of High Pressure $SF_6$ Gas between Spheres and Coaxial Cylinders , Trans. I.E.E. of Japan Vol. 93-B, No.11 (1973) pp. 551-558

95. S. Masuda, J. Ozawa; Flashover characteristic of long gap in $SF_6$ , Conf. on Electrical Discharge of Japan ED-73-30, (1973)

96. J. Hara, T. Nitta; Voltage Divider for the Measurement of Rapidly Changing Impulse Waves, Mitsubishi Denki Giho, Vol.37 No.2 (1963) pp. 83-89 (in Japanese)

97. CIGRE study committee; Procedure for the Determination of the Error of Measuring Systems for Impulse Voltages, CIGRE Paper No.344, Appendix II, 1958

98. D. F. Binns; Calculation of Field Factor for a Vertical Sphere Gap, Taking Account of Surrounding Earthed Surfaces, Proc. of IEE, Vol. 112, No.8 (1965) pp. 1575-1582

99. Y. Kawaguchi et al; Effect of a Grounded Cylinder Enclosure on the Breakdown Gradient of Rod Gaps in $SF_6$, IEEE Tr. Paper, 70 TP 583-PWR (1970)

100. H. Isa; Field Analysis of Sphere-Sphere and Rod-Rod Gaps and its Application of Breakdown Voltage, Jr. of IEE of Japan, Vol.91, No.9 (1971) pp. 1730-1742 (in Japanese)

101. T. Watanabe, T. Takuma ; Calculation of Electric Field between the Hemi-Spherically Capped Rod and Plane Electrodes under Various Conditions, and its Application to the Experimental and Insulation Design in the Compressed Gas Insulation, Jr. IEE of Japan, Vol. 91 No.12 (1971) pp. 2288-2298

102. J. J. Thwaites ; The Electric Field at Any Point of a Sphere-Gap, Proc. of IEE, Monograph No.525M (1962)

103. J. Hara, T. Nitta et al ; Electrical Breakdown of Non-Uniform Gaps in Atmospheric Air, Mitsubishi Denki Giho, Vol.37, No.7, 1963 (in Japanese)

ACKNOWLEDGEMENT

The author wishes to express his sincere thanks to Professor Shinsuke Uenosono of Kyoto University for helpful advice, the encouragement and his careful reading of the manuscript.

The author also wishes to express his deep appreciation to Professor Muneaki Hayashi of Kyoto University, Dr. Jingo Hara, Dr. Toshio Itoh and Mr. Shoji Hirabayashi of the Central Research Laboratory of Mitsubshi Electric Corporation for their continuous encouragement, their interest on the present work and helpful advice in the course of the research.

The author is indebted to all his associates in High Voltage and Plasma Physics Group of the Central Research Laboratory of Mitsubshi Electric Corporation, particularly to Messrs. Yoshikazu Shibuya, Naoya Yamada and Yukio Fujiwara for their discussions and co-studies throughout the present work. He is also profited from Messrs. Noboru Ueno and Akiyoshi Yoshioka and grateful for their assistnace in some experimental works, calculations and in preparing the figures in the text.

Thanks are also due to the interest shown by the members of the Switchgear Department of Itami Works of Mitsubishi Electric Corporation in the progress of the work.

146項欠

## APPENDIX I

## ELECTRIC FIELD OF SPHERE AND ROD GAPS [74]

Sphere-plane and sphere-sphere gaps and rod-plane and rod-rod gaps having spherical tips are used widely in the sutdy of electrical breakdown phenomena. It is necessary to know the precise electric field distribution of these gaps to investigate the breakdown phenomena quantitatively using these gaps. Specifically, the maximum field strength at the tip of the electrode is the most important factor in the electrical breakdown of $SF_6$ gas. Minimum field strength in the gap plays important role in the critical condition for corona stabilized breakdown as discussed in Chapter III in the text. The ratio of the maximum field strengths on both electrode, $E_{op}/E_{max}$ and the distribution of field strength on the surface of electrode determines the effective area of the gap.

Though there are some papers on the field distributuion along the axis of symmetry, [69, 70, 74, 98–101] very limited data are available on the field distributuion on the surface of electrode. [102] Electric field of sphere and rod gaps were analyzed by over relaxation method using an electronic computer. The results are sumarized in this appendix, so that we can get a good idea of the electric field of these gaps. These gaps are usually set in a grounded metal tank in the breakdown experiments of gas dielectrics. The effect of side and bottom wall of the tank are also discussed.

### Field Distributuion

Fig.I–1 and I–2 show the examples of the calculated equipotential lines for rod-plane gap at d/R = 1, and for rod-rod gap at d/R = 2. Attention should be paid to the fact that the field distribution of rod-rod gap is not symmetrical with regard to high voltage and grounded electrdoe, since the potential of the grounded electrode is set to be zero, that is equal to the potential at infinity. This asymmetry of electric field distributuion is also exist for sphere-sphere gap, even if the gap is in infinite space. It is this asymmetry of electric field that is the cause of the polarity effect of breakdown phenomena of rod-rod and sphere-sphere gaps.

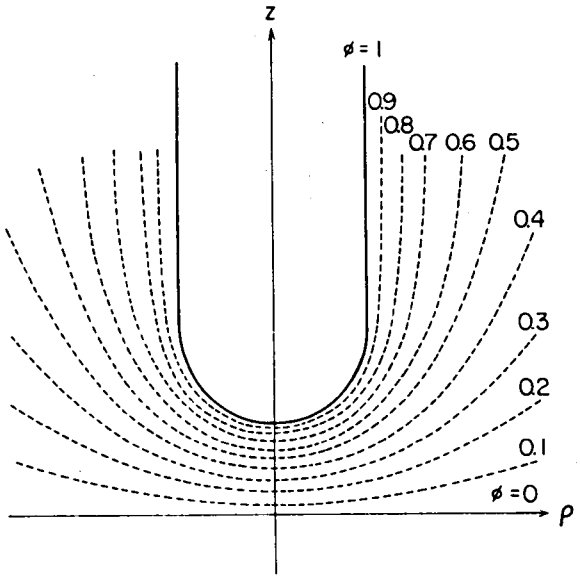


Fig.I–1 Example of Potential Distribution of Rod-Plane Gap (d/R=1)

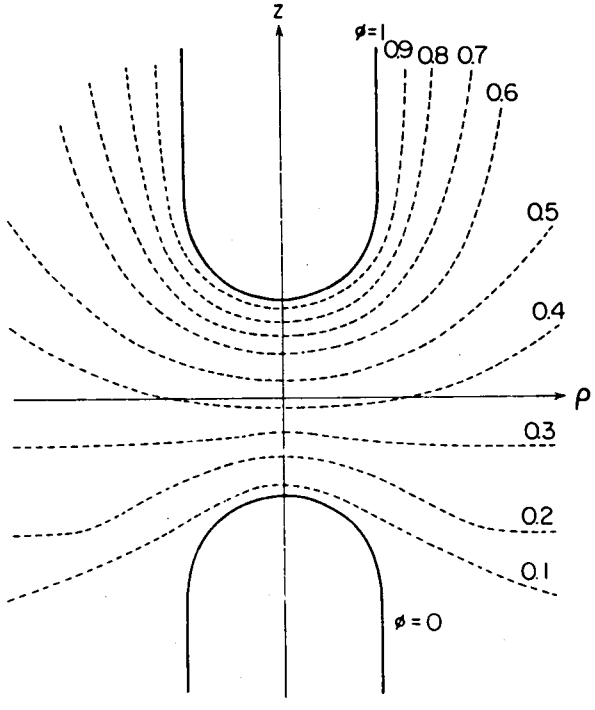


Fig.I–2 Example of Potential Distribution of Rod-Rod Gap (d/R=2)

Maximum Field Strength

The maximum field strength in the gap is the most important factor in breakdown or discharge inception of $SF_6$. The ratio of the average field $E_{av}$ and the maximum field strength $E_{max}$ is called as field utilization factor of the gap and the value is dependent only of the geometrical configuration of the gap.

$$u = E_{av}/E_{max} \tag{I-1}$$

The value of u is unity for uniform field and it approaches to zero with the non-uniformity of field. The value of u for nearly uniform field gap is very close to unity and the difference in the non-uniformity of field is not presented in good accuracy by plotting the value of u in a figure. From this reason, "field non-uniformity factor" $\xi$ is introduced to present the non-uniformity of electric field of a given gap.

$$\xi = \frac{E_{max} - E_{av}}{E_{av}} = \frac{1 - u}{u} \tag{I-2}$$

Fig.I–3 show the field non-uniformity factors of rod-plane gap calculated by the present author [74] and Abou-Seada and Nasser [70] for larger values of d/R. Dashed line is the value for sphere-plane gap reported by Binns. [98] The same curves for rod-rod and sphere-sphere gaps are shown in Fig.I–4.

From these curves, the maximum field strength of a gap of given geometrical configuration at the applied voltage V is given as;

$$E_{max} = \frac{V}{d} \cdot \frac{1}{u} = \frac{V}{d} \cdot (1 + \xi) \tag{I-3}$$

Field along the Axis of Symmetry

An example of the field distribution along the axis of symmetry of a rod-rod gap is typically shown in Fig.I–5. The ratio of $E_{op}/E_{max}$ and $E_{min}/E_{max}$ are functions of d/R. The values for sphere-sphere and rod-rod gaps are given in Fig.I–6. In the case of sphere-plane and rod-plane gaps, $E_{min}$ coincide with $E_{op}$ on the plane electrode. $E_{op}/E_{max}$ of these gaps is plotted in Fig.I–7 as a function of d/R.

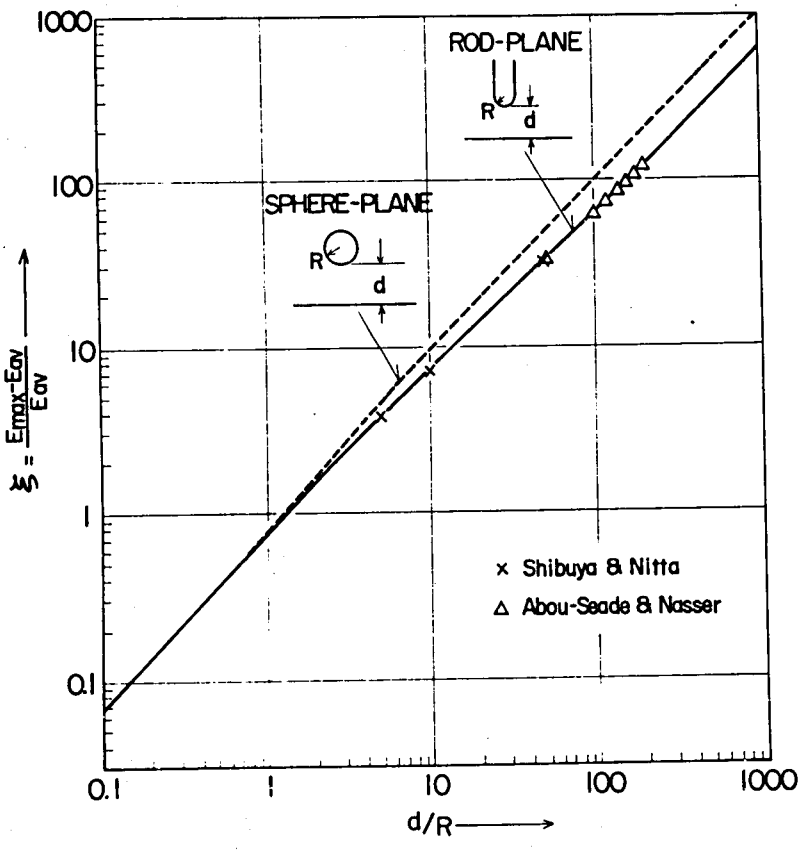


Fig.I–3 Field Non-Uniformity Factor of Sphere-Plane and Rod-Plane Gaps

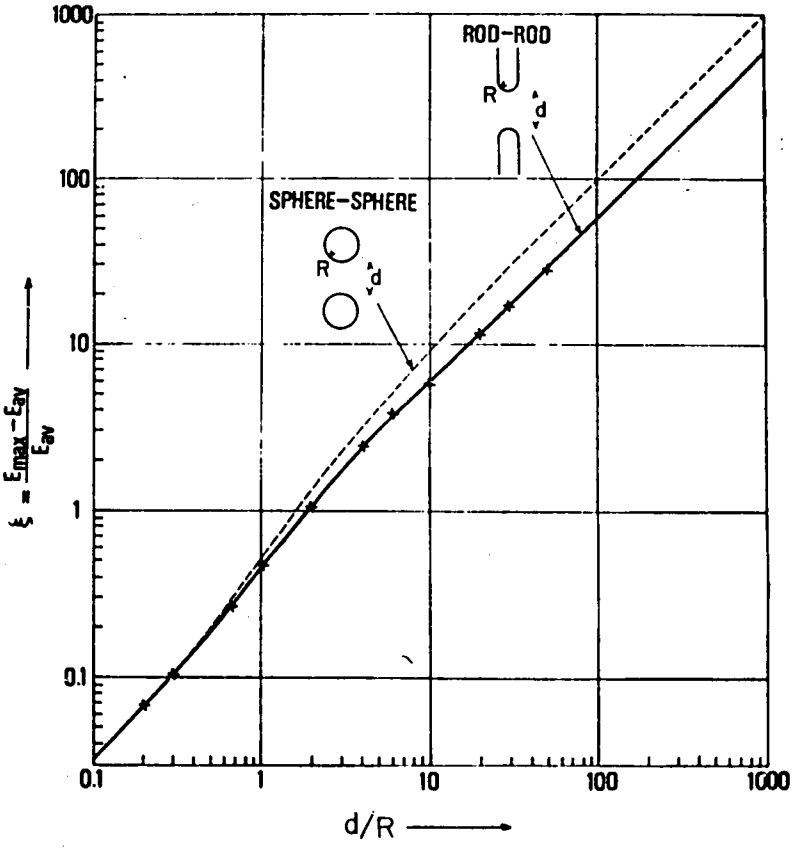


Fig.I–4 Field Non-Uniformity Factor of Sphere-Sphere and Rod-Rod Gaps

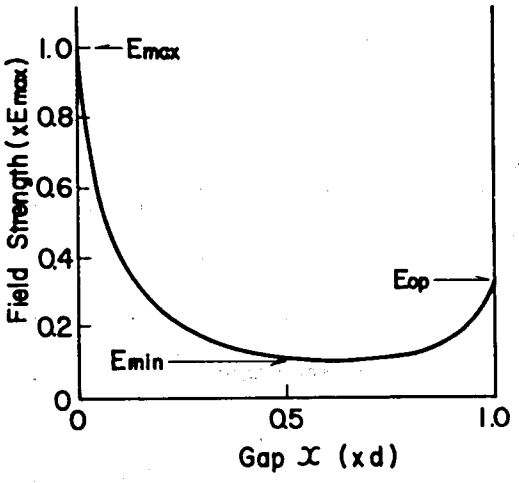


Fig.I–5 An Example of Field Strength Distribution of Rod-Rod Gap for d/R=6

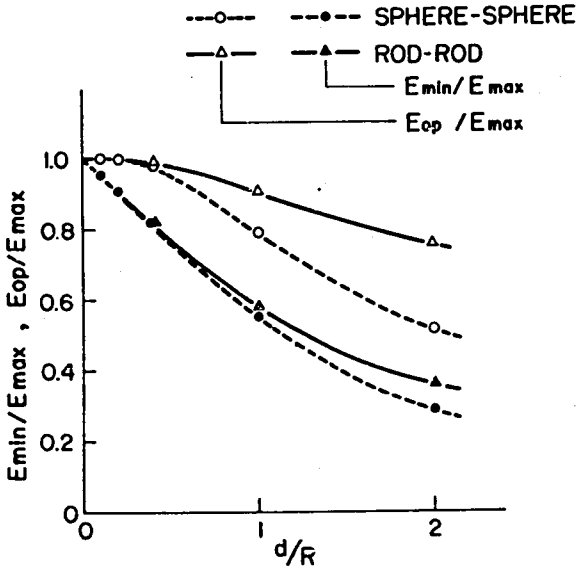


Fig.I–6 $E_{op}/E_{max}$ & $E_{min}/E_{max}$ for Sphere-Sphere and Rod-Rod Gaps

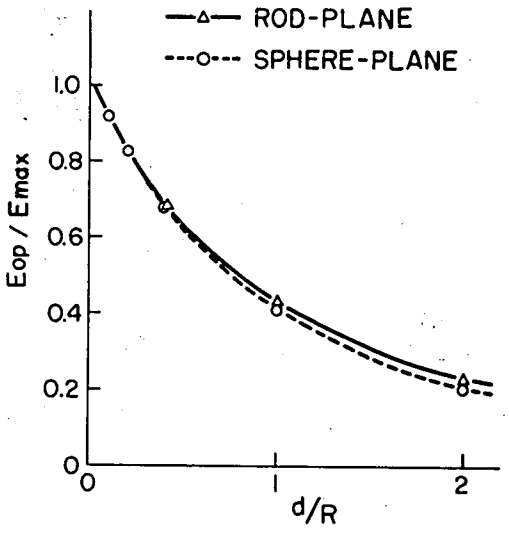


Fig.I–7 $E_{op}/E_{max}$ for Sphere-Plane and Rod-Plane Gaps

Field Distribution on the Surface of Electrode

Field strength E on the surface of floating and grounded electrodes determines the effective area of the gap for negative and positive polarities as discussed in the text. The distribution is expressed as the area on each electrode S(E), where the relative field strength is higher than $E/E_{max}$. The function of S(E) on both floating and grounded electrodes $S^-(E)$ and $S^+(E)$ are plotted in Fig.I–8 to I–11 for sphere and rod gaps, the value of d/R as a parameter. These curves are useful in determining the effective area of those gaps as exampled in Appendix IV.

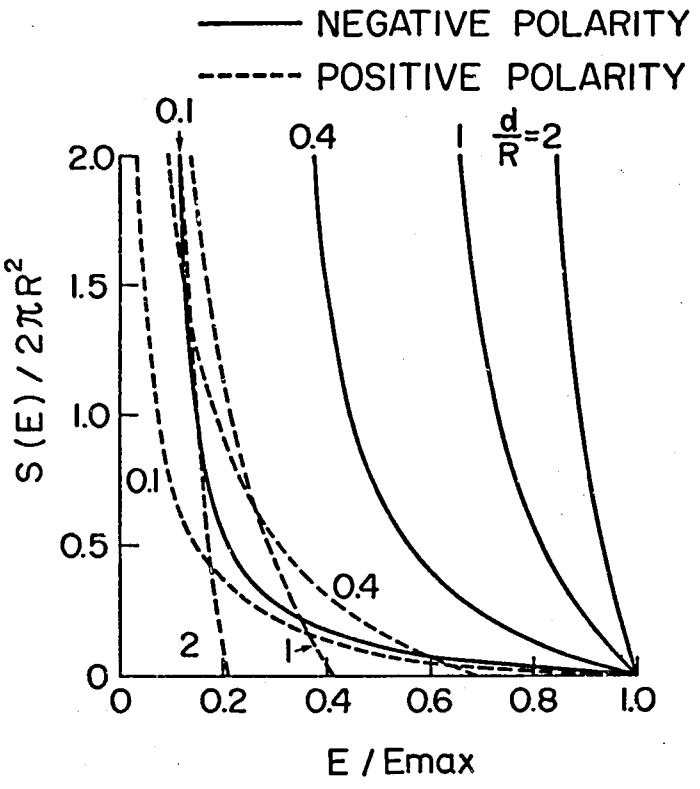


Fig.1–8 Examples of $S^-(E)$ and $S^+(E)$ for Sphere-Plane Gaps

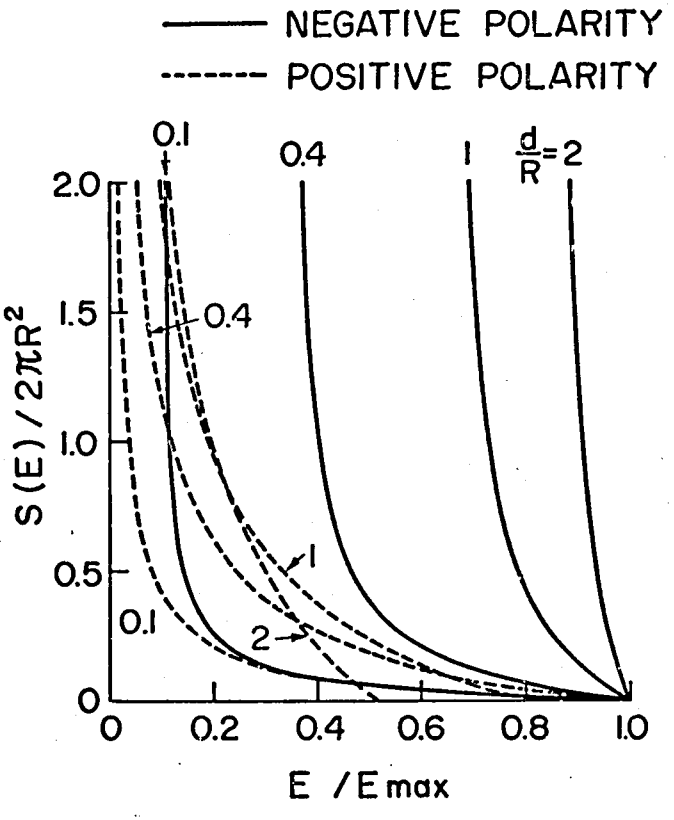


Fig.1–9 Examples of $S^-(E)$ and $S^+(E)$ of Sphere-Sphere Gaps

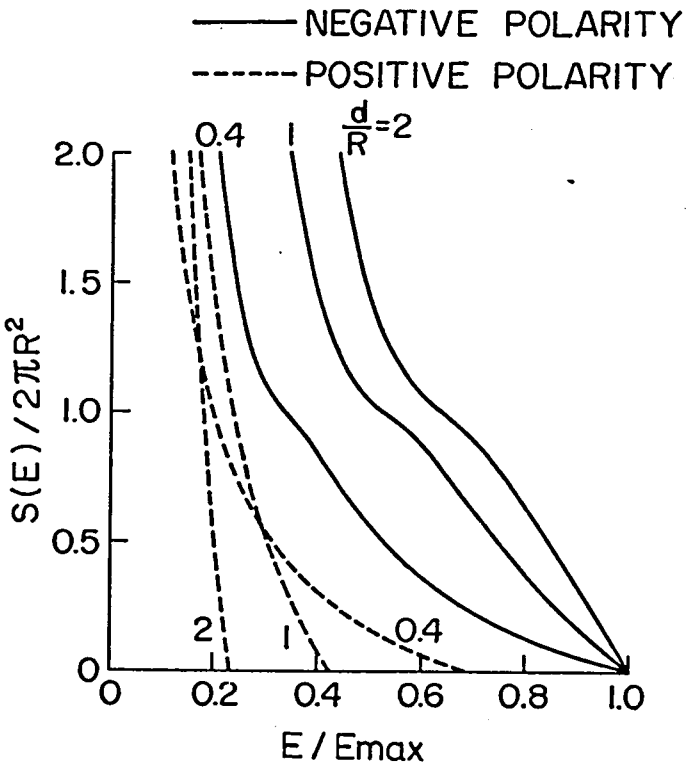


Fig.I–10 Examples of $S^{-}(E)$ and $S^{+}(E)$ for Rod-Plane Gaps

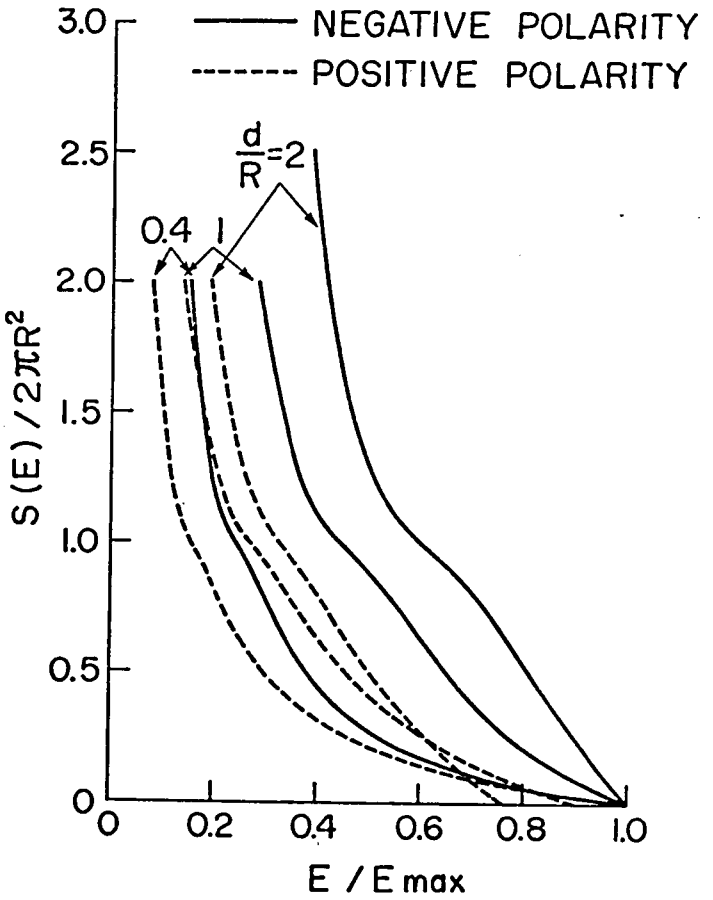


Fig.1–11 Examples of $S^{-}(E)$ and $S^{+}(E)$ for Rod-Rod Gaps

Effect of Tank Wall

If these gaps are set in a grounded metal tank, field distribution of the gap changes under the effect of the wall of the tank. To restrict the effect of the tank within a certain limit, the size of the tank has to be large enough for the limit. The effect of the tank wall on the maximum field strength of rod-rod and rod-plane gaps is evaluated in the followings. The discussions can also be applied to the case of sphere gaps with sufficient accuracy.

When a rod-plane or a rod-rod gap is placed coaxially at the center of a cylinder as in Fig.I–12, the radius of the cylinder G to limit the effect of the wall on the maximum field strength to 1 and 5% of the value without cylinder are roughly estimated in Fig.I–12 based on the results of the field calculation.

The effect of the side wall is more pronounced for rod-rod gap than for rod-plane gap. If the radius of the tank is larger than about 6 and 9 times of gap spacing for rod-plane and rod-rod gaps, respectively, the effect of side wall on the maximum field stress is less

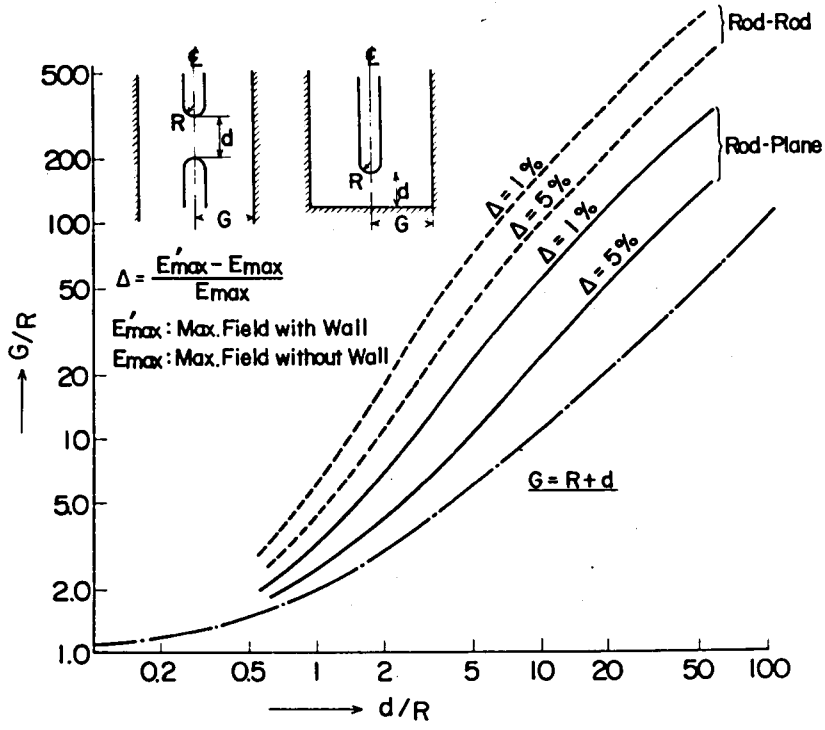


Fig.I–12 Effect of the Tank Wall to the Maximum Field Strength of Rod Gaps

than 1% for any value of d/R.

For smaller values of d/R, field distribution of the gap is quite uniform and side wall has little effect on the non-uniformity of the field as far as G is larger than R + d. If the radius of the tank G is less than R + d, the maximum field will be at the side of rod electrode and the gap has to be considered as a coaxial cylinder gap. The condition G = R + d is shown by a dot-dash curve in Fig.I–12. All the curves which show the effect of tank wall will converge to this curve for very small values of d/R.

For a rod-rod gap, the height or the length of the grounded rod electrode is another very important factor to show the effect of the tank. The effect of the height of the grounded electrode on the maximum field strength of rod-rod gap is estimated and shown in Fig.I–13 as the required height H to limit the increase of $E_{max}$ to 1 and 5% of the value for rod-rod gap in infinite space.

For very large value of d/R, the maximum field of the gap converges to that of a single rod electrode in infinite space. The effect of the opposite electrode is very limited in this region. This is the reason why the required height H converges to zero for large value of d/R.

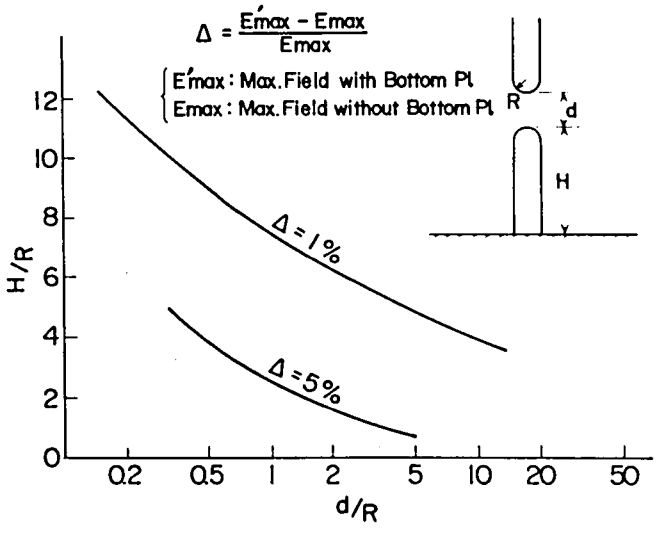


Fig.I–13 Effect of the Height of the Grounded Electrode of Rod-Rod Gap

## APPENDIX II

## ELECTRIC FIELD OF A HEMI-SPHEROIDAL PROTRUSION ON PLANE ELECTRODE

The electric field of a small hemi-spheroidal protrusion attached on the grounded electrode of a parallel plane gap is analyzed. [73, 103]

Potential V in the gap satisfies Laplace equation.

$$\nabla^2 V(\mathbf{r}) = 0 \qquad \text{(II–1)}$$

Boundary condition of the potential field V is equation II–2 as shown in Fig.II–1.

$$\begin{aligned} V(\mathbf{r}) &= +V_o && \text{at } z = +d \\ V(\mathbf{r}) &= -V_o && \text{at } z = -d \\ V(\mathbf{r}) &= 0 && \text{on the spheroid} \end{aligned} \qquad \text{(II–2)}$$

If we put the potential $V(\mathbf{r})$ as;

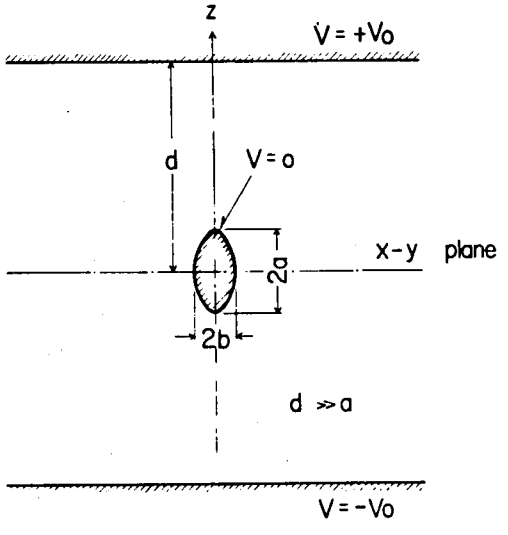


Fig.II–1 Boundary Conditions for the Potential Field

$$V(\mathbf{r}) = \frac{V_o}{d} z + V_1(\mathbf{r}) \qquad \text{(II–3)}$$

Potential $V_1(\mathbf{r})$ also satisfies Laplace equation.

$$\nabla^2 V_1(\mathbf{r}) = 0 \qquad \text{(II–4)}$$

Boundary condition for potential $V_1(\mathbf{r})$ is expressed as;

$$V_1(\mathbf{r}) = 0 \qquad \text{at } z = \pm d$$

$$V_1(\mathbf{r}) = -\frac{z}{d} V_o \qquad \text{on the spheroid} \qquad \text{(II–5)}$$

Since we are dealing with a negligibly small protrusion in comparison with gap spacing ($a \ll d$), the effect of the spheroid will be negligible at $z = \pm d$. Under this circumstance, boundary condition (II–5) can be approximated as;

$$V_1(\mathbf{r}) = 0 \qquad \text{at } \mathbf{r} \longrightarrow \infty$$

$$V_1(\mathbf{r}) = -\frac{z}{d} V_o \qquad \text{on the spheroid} \qquad \text{(II–6)}$$

Prolate Protrusion

When the spheroid is prolate ($a > b$), analytical solution of equation (II–4) under the boundary condition in equation (II–6) is obtained by taking the coordinate system as shown in Fig.II–2(a). Then Cartesian coordinates x, y and z are expressed as;

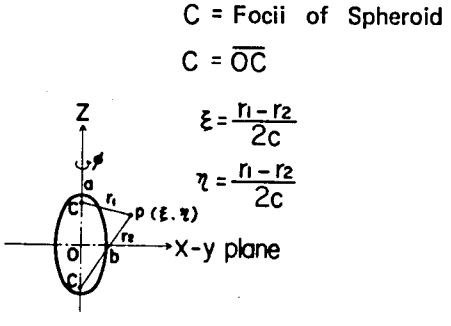


Fig.II–2(a) Coordinate System for Prolate Spheroid

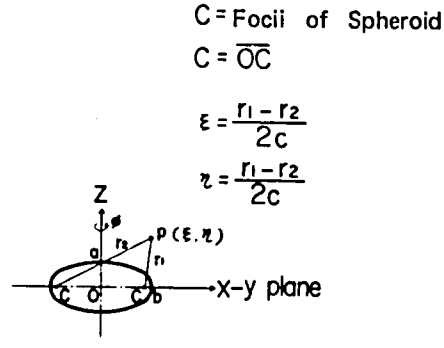


Fig.II–2(b) Coordinate System for Oblate Spheroid

$$x = c\sqrt{(\xi^2-1)(1-\eta^2)}\ \cos\phi$$

$$y = c\sqrt{(\xi^2-1)(1-\eta^2)}\ \sin\phi \quad (\xi \geqslant 1,\ |\eta| \leqslant 1)$$

$$z = c\xi\eta$$

Since $V_1(r)$ is independent of $\phi$, equation (II–4) is;

$$\nabla^2 V_1(r) = \frac{1}{c^2(\xi^2-\eta^2)}\left[\frac{\partial}{\partial\xi}(\xi^2-1)\frac{\partial V_1}{\partial\xi} + \frac{\partial}{\partial\eta}(1-\eta^2)\frac{\partial V_1}{\partial\eta}\right] = 0$$

By putting $V_1(r) = X(\xi)\cdot Y(\eta)$ ;

$$(1-\xi^2)\frac{d^2X}{d\xi^2} - 2\xi\frac{dX}{d\xi} + \lambda^2 X = 0$$

($\lambda$ : const) (II–7)

$$(1-\eta^2)\frac{d^2Y}{d\eta^2} - 2\eta\frac{dY}{d\eta} + \lambda^2 Y = 0$$

These are well known Legendre's equations. They have meaningfull solution when $\lambda^2 = n(n+1)$ (n: integer) and the solutions are;

$$X(\xi) = A_n Q_n(\xi),\quad Y_n(\eta) = B_n P_n(\eta) \qquad (A_n,\ B_n : \text{const})$$

Here, $P_n(\xi)$ and $Q_n(\eta)$ are Legendre polynominals of the first and the second kind, respectively. General solution of $V_1(\xi, \eta)$ is expressed as a linear combination of these plynominals.

$$V_1(\xi, \eta) = \sum_n K_n P_n(\eta) Q_n(\xi) \quad (K_n : \text{const}) \qquad \text{(II–8)}$$

Boundary conditions in equation (II–6) are rewritten as a function of $\xi$ and $\eta$.

$$X(\xi) = 0, \qquad \text{at } \xi \to \infty$$

$$V_1(\xi, \eta) = -\frac{V_o}{d}\, c\cdot\xi\cdot\eta \qquad \text{at } \xi = \xi_o \qquad \text{(II–9)}$$

The function $V_1(\xi, \eta)$ which satisfy equation (II–8) is;

$$V_1(\xi, \eta) = -\frac{V_o}{d}\, c\xi_o \frac{Q_1(\xi)}{Q_1(\xi_o)} P_1(\eta) \qquad \text{(II–10)}$$

Where;

$$P_1(\xi) = \eta, \quad Q_1(\xi) = \frac{1}{2}\xi \, ln \, \frac{\xi+1}{\xi-1} - 1$$

Substituting equation (II–9) and (II–10) into equation II–3

$$V(\xi,\eta) = \frac{V_o}{d} c\xi\eta \left\{ 1 - \frac{ln \sqrt{\frac{\xi+1}{\xi-1}} - \frac{1}{\xi}}{ln \sqrt{\frac{\xi_o+1}{\xi_o-1}} - \frac{1}{\xi_o}} \right\} \qquad \text{(II–11)}$$

Field strength along the axis of the spheroid $E_{ax}(z)$ is obtained by putting $\eta$=1, $\xi$=z/c and $\xi_o$=a/c, and differentiate equation (II–10) by z as;

$$E_{ax}(z) = \frac{V_o}{d} \left\{ 1 - \frac{ln \sqrt{\frac{z+c}{z-c}} - \frac{cz}{z^2-c^2}}{ln \sqrt{\frac{a+c}{a-c}} - \frac{c}{a}} \right\} \qquad \text{(II–12)}$$

Oblate Protrusion

For an oblate spheroid (a<b), coordinate x, y and z are expressed as shown in Fig.II–2(b) as;

$$x = c\xi\eta \cos \phi$$

$$y = c\xi\eta \sin \phi$$

$$z = c \sqrt{(\xi^2-1)(1-\eta^2)}$$

Since $V_1(r)$ is independent of $\phi$, equation (II–4) is

$$\frac{1}{c^2(\xi^2-\eta^2)} \left[ \frac{\sqrt{\xi^2-1}}{\xi} \frac{\partial}{\partial\xi} \xi \sqrt{\xi^2-1} \frac{\partial V_1}{\partial\xi} + \frac{\sqrt{1-\eta^2}}{\eta} \frac{\partial}{\partial\eta} \eta \sqrt{1-\eta^2} \frac{\partial V_1}{\partial\eta} \right] = 0$$

By putting $V_1(\xi, \eta)=X(\xi)\cdot Y(\eta)$,

$$(\xi^2-1) \frac{d^2X}{d\xi^2} + (2\xi - \frac{1}{\xi}) \frac{dX}{d\xi} - \lambda^2 X = 0$$

$$(1-\eta^2)\frac{d^2Y}{d\eta^2} - (2\eta - \frac{1}{\eta})\frac{dY}{d\eta} + \lambda^2 Y = 0$$

We transform these equations by putting $g=i\sqrt{\xi^2-1}$ and $h=\pm\sqrt{1-\eta^2}$,

$$(1-g^2)\frac{d^2X}{dg^2} - 2g\frac{dX}{dg} + \lambda^2 X = 0$$

$$(1-h^2)\frac{d^2Y}{dh^2} - 2h\frac{dY}{dh} + \lambda^2 Y = 0$$

These equations have the same form to equation (II–7) for $\xi$ and $\eta$. Function $V(\xi, \eta)$ can be obtained in the same way as in the case of the prolate spheroid.

$$V_1(\xi,\eta) = -\frac{V_o}{d}\sqrt{\xi^2-1}\sqrt{1-\eta^2}\,\frac{\frac{1}{\sqrt{\xi^2-1}} + \frac{1}{2}\tan^{-1}\frac{2\sqrt{\xi^2-1}}{2-\xi^2}}{\frac{1}{\sqrt{\xi_o^2-1}} + \frac{1}{2}\tan^{-1}\frac{2\sqrt{\xi_o^2-1}}{2-\xi_o^2}}$$

$$V(\xi,\eta) = \frac{V_o}{d}\sqrt{\xi^2-1}\sqrt{1-\eta^2} + V_1(\xi,\eta) \qquad \text{(II–13)}$$

Field strength along the axis of the spheroid $E_{ax}(z)$ is obtained by putting $\eta=0$, $\xi=\sqrt{1+(z/c)^2}$ and $\xi_o=\sqrt{1+(a/c)^2}$, and differentiate equation (II–10) by z:

$$E_{ax}(z) = \frac{V_o}{d}\left[1 - \frac{\frac{cz}{z^2+c^2} + \frac{1}{2}\tan^{-1}\frac{2cz}{c^2-z^2}}{\frac{c}{a} + \frac{1}{2}\tan^{-1}\frac{2ca}{c^2-a^2}}\right] \qquad \text{(II–14)}$$

Spherical Protrusion

When the protrusion is a hemi-sphere (a=b), potential $V_1(r)$ is easily obtained as;

$$V_1(r) = -\frac{V_o}{d}\left(\frac{a}{r}\right)^2$$

Where $r$ is the distance from the origin. Potential $V(r)$ and the field strength along the axis of the sphere are;

$$V(r) = -\frac{V_o}{d}\left\{ z - \left( \frac{a}{r} \right)^2 \right\} \qquad \text{(II-15)}$$

$$E_{ax}(z) = \frac{V_o}{d}\left\{ 1 + 2\left( \frac{a}{z} \right)^3 \right\} \qquad \text{(II-16)}$$

Field Distribution

Field strength along the axis of the protrusion is calculated for several values of a/b and shown in Fig.II-3.

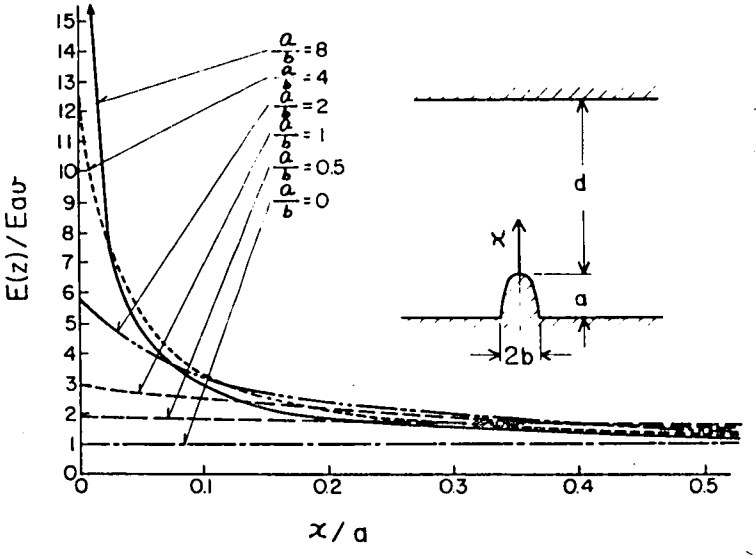


Fig.II-3 Electric Field Strength along the Axis of the Hemi-Spheroidal Protrusion (a≪d)

## APPENDIX III

## PROPERTIES OF WEIBULL DISTRIBUTION

Breakdown field strength of a gap whose negative electrode area is S obeys Weibull distribution in eqution 40 in the text. Some of the basic properties of Weibull distribution are discussed in this appendix.

Breakdown probability density is given by the differentiation of equation 40 of the text with E.

$$p(S,E) = \frac{m\lambda_o}{E_d} \cdot S \cdot \left( \frac{E-E_o}{E_d} \right)^{m-1} \exp\left\{ -S\lambda_o \left( \frac{E-E_o}{E_d} \right)^m \right\} \qquad \text{(III-1)}$$

As a numerical example of the distribution, p(S,E) is plotted in Fig.III-1 as a function of E, effective area S as a parameter. Constants in the equation are set as follows taking the values for fine finished uniform field gaps in 6 atm $SF_6$ gas.

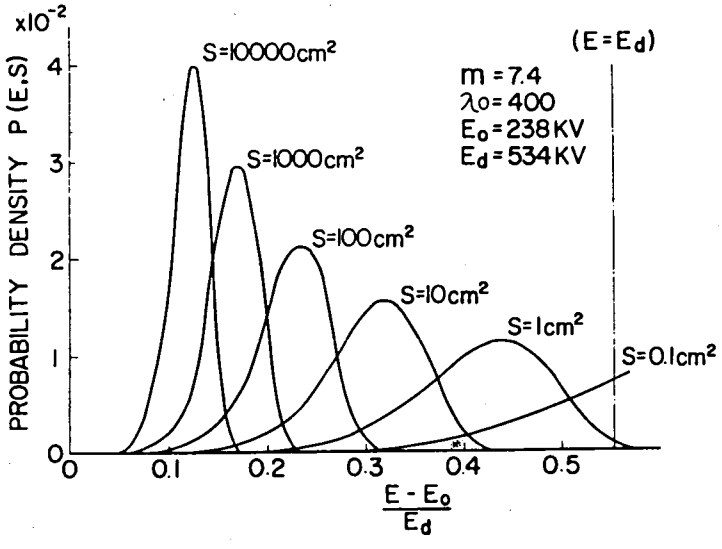


Fig.III-1 Examples of Weibull Probability Density p(E,S)

$$m = 7.4$$

$$\lambda_o = 400$$

$$E_o = 238 \text{ kV}$$

$$E_d = 534 \text{ kV}$$

From these probability density curves, we can get a very good idea on the scattering of breakdown field strength and its dependence on electrode area S.

Modal value of the statistical distribution of breakdown field strength $E_m$ is obtained by putting the differentiation of p(S,E) by E as zero:

$$\frac{E_m - E_o}{E_d} = \left( \frac{m-1}{S \cdot \lambda_o \cdot m} \right)^{\frac{1}{m}}$$

or

$$\frac{E_m}{E_d} = \frac{E_o}{E_d} + \left( \frac{m-1}{S \cdot \lambda_o \cdot m} \right)^{\frac{1}{m}} \qquad \text{(III-2)}$$

The value of $E_m$ will be one of the best representatives of the breakdown field strength of a given gap. The field strength decreases with the increase of the effective area of the gap. The property explains the area effect of electrode in the breakdown characteristics in compressed $SF_6$ as shown in Fig.64 in the text.

If we consider 5% breakdown field strength, $F(S, E_{5\%}) = 0.05$, as a typical representative of the minimum breakdown field strength, approximate value of $E_{5\%}/E_d$ is obtained from eqution 40 of the text as;

$$\lambda_o S \cdot \left( \frac{E_{5\%} - E_0}{E_d} \right)^m = 0.053$$

or

$$\frac{E_{5\%}}{E_d} \cong \frac{E_o}{E_d} + \left( \frac{0.053}{\lambda_o \cdot S} \right)^{\frac{1}{m}} \qquad \text{(III-3)}$$

The value of $E_{5\%}/E_d$ will show a good estimation of the minimum breakdown field strength as a function of area S.

In the same way, if we take the field strength which satisfy the relation F(S,E)=0.95 as a representative of the maximum non-breakdown field strength of the gap, the field is given as;

$$\frac{E_{95\%}}{E_d} \cong \frac{E_0}{E_d} + \left(\frac{3.0}{\lambda_o \cdot S}\right)^{\frac{1}{m}} \qquad \text{(III-4)}$$

The relation between $ln\ ln \dfrac{1}{1-F(S,E)}$ and $ln\ \left(\dfrac{E-E_o}{E_d}\right)$, that is Weibull probability plot, is linear. The curves for electrodes whose area $S_1$ and $S_2$ are parallel to each other and the vertical distance between the two curves is $ln\ S_2/S_1$.

## APPENDIX IV

## NUMERICAL EXAMPLES OF EFFECTIVE AREA OF ELECTRODE

Effective area of a given gap $S_{eff}$ is defined by equation 51 in the text. Numerical value of $S_{eff}$ is obtained by the field analysis of the gap as follows. The ratio $\delta = E_{op}/E_{max}$ and the areas of electrode whose field strength is higher than E, $S^-(E)$ on the electrode which gives the maximum field in the gap and $S^+(E)$ on the opposite electrode, are given as the results of the field analysis. Constants $E_o$, m and $\lambda_o$ in the equations are given by equations 44, 45 and 46, respectively. Then, the effective area for positive and negative polarities, $S^+_{eff}$, $S^-_{eff}$ are calculated by solving equations 51 and 53, simultaneously by the aid of an electronic computer. Some numerical examples of the effective area of the gaps used in the present work are summarized in this appendix.

Parallel Plane Gap

If the effect of electrode edge is negligible, both electrodes of a parallel plane gap are stressed at constant field which coincides to the maximum field of the gap, $E_{max}$. That means,

$$E_{op} = E_{max}$$

The integral in equation 51 on each of these electrodes is:

$$S^+_{eff} = S^-_{eff} = -\int_{E_o}^{E_{max}} \frac{dS(E)}{dE}\, dE = S_o \qquad \text{(IV–1)}$$

which is equal to the surface area of each electrode. If the rounded edge of the plane electrodes is not negligible, the effect has to be evaluated by the precise field analysis on individual gap.

Coaxial Cylinder Gap

Effective area of a coxial cylinder gap whose inner and outer radii and length are $R_1$, $R_2$ and L can be evaluated neglecting end effect as follows.

The ratio $E_{op}/E_{max}$ of the gap is equal to the ratio of the inner and the outer radii, $R_1/R_2$. The internal cylinder is streassed at constant field which is $E_{max}$. $S^-_{eff}$ in equation 51 is deduced as:

$$S^-_{eff} = 2\pi R_1 \cdot L \qquad \text{(IV–2)}$$

Effective area for positive polarity is expressed by equation 51 as:

$$S^+_{eff} = 2\pi R_2 \cdot L \left( \frac{\frac{R_1}{R_2} - \frac{E_o}{E_{max}}}{1 - \frac{E_o}{E_{max}}} \right)^m \qquad \text{(IV–3)}$$

The value of $S^+_{eff}$ is obtained by solving equation IV–3 with equation 53 in the text as a function of gas pressure. Examples of the values for Gap G and F used in the text are presented in Table IV–1. Effective area for positive polarity is very small in comparison with $S^-_{eff}$ because of the asymmetry of electric field of these coaxial cylinder gaps.

| Press. | GAP F | | GAP G | |
|---|---|---|---|---|
| (atm. abs.) | $S^-_{eff}$ ($cm^2$) | $S^+_{eff}$ ($cm^2$) | $S^-_{eff}$ ($cm^2$) | $S^+_{eff}$ ($cm^2$) |
| 1 | 480 | 39.5 | 3000 | 523.7 |
| 2 | 〃 | 39.5 | 〃 | 522.1 |
| 4 | 〃 | 33.8 | 〃 | 460.4 |
| 6 | 〃 | 25.5 | 〃 | 372.6 |
| 8 | 〃 | 17.7 | 〃 | 275.4 |

Table IV–1 Effective Electrode Area of Coaxial Cylinder Gaps F and G as a Function of Gas Pressure

Sphere and Rod Gaps

The values of $E_{op}/E_{max}$ and S(E) for positive and negative polarities are given in Appendix I for sphere and rod gaps. Using these data, effective area of sphere-sphere, sphere-plane, rod-rod and rod plane gaps are calculated as a function of gap configuration

and gas pressure. Examples of the effective area of Gap A, B and C used in the text are presented in Fig. IV–1 (a) and (b) as a function of gap spacing, gas pressure as a parameter, for fine and rough finished electrodes, respectively. The difference of the effective area by gas pressure and the finish of electrode is not so significant. Since the logarithm of $S_{eff}$ is operative to the discharge field strength of $SF_6$, we are interested in the order of magnitude of the effective area. From this point, the effect of these factors is not so significant within the range of surface finish and gas pressure of practical interest.

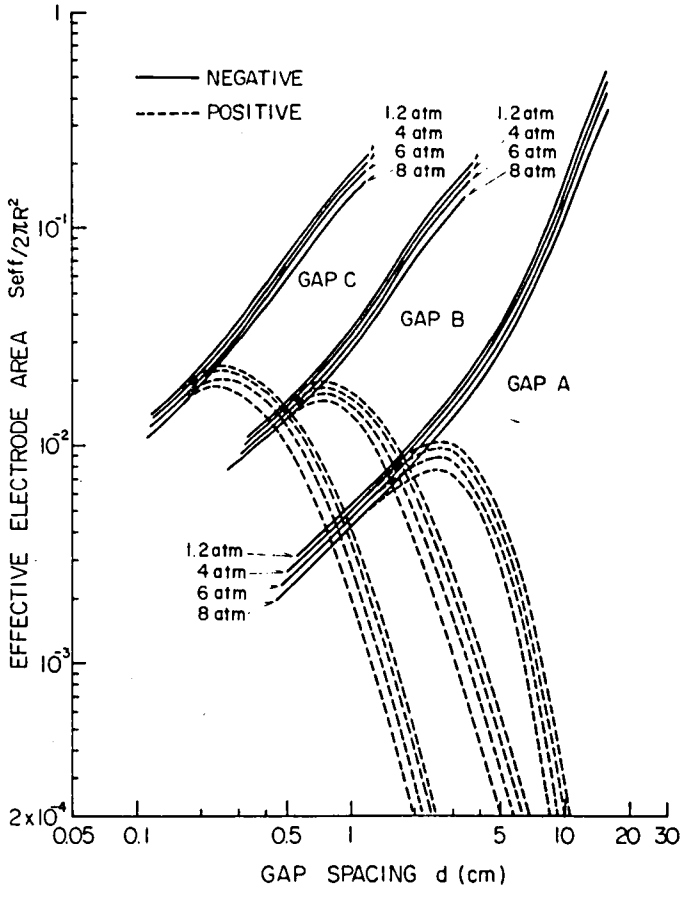


Fig.IV–1(a) Effective Electrode Area of Fine Finished Gap A, B and C Gas Pressure as a Parameter

It should be noted that positive effective electrode area of these gaps converges to zero at a certain value of d/R. At the gap spacing larger than this critical value, the effect of electrode on positive discharge in $SF_6$ will be negligible. On the contrary, the effective electrode area for negative polarity increases with d/R. This difference in the effective area of positive and negative polarities explains the polarity effect of discharge characteristics in $SF_6$.

Examples of the effective electrode areas for fine finished sphere-plane and rod-plane gaps D and H are shown in Fig. IV–2. The values of $S_{eff}$ are very small for these gaps because of the strong asymmetry of the electric field.

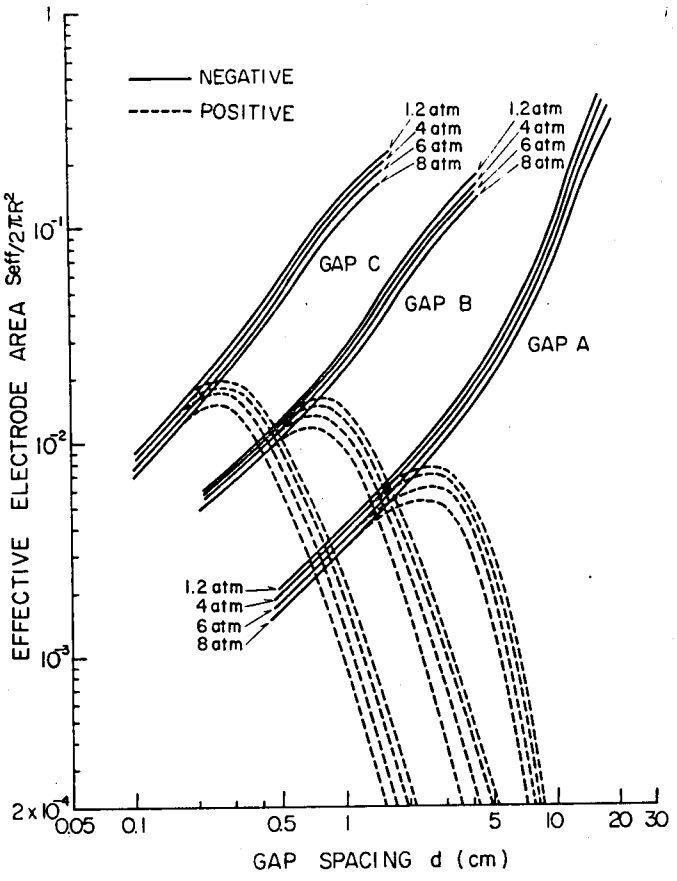


Fig.IV–1(b) Effective Electrode Area of Rough Finished Gap A, B and C, Gas Pressure as a Parameter

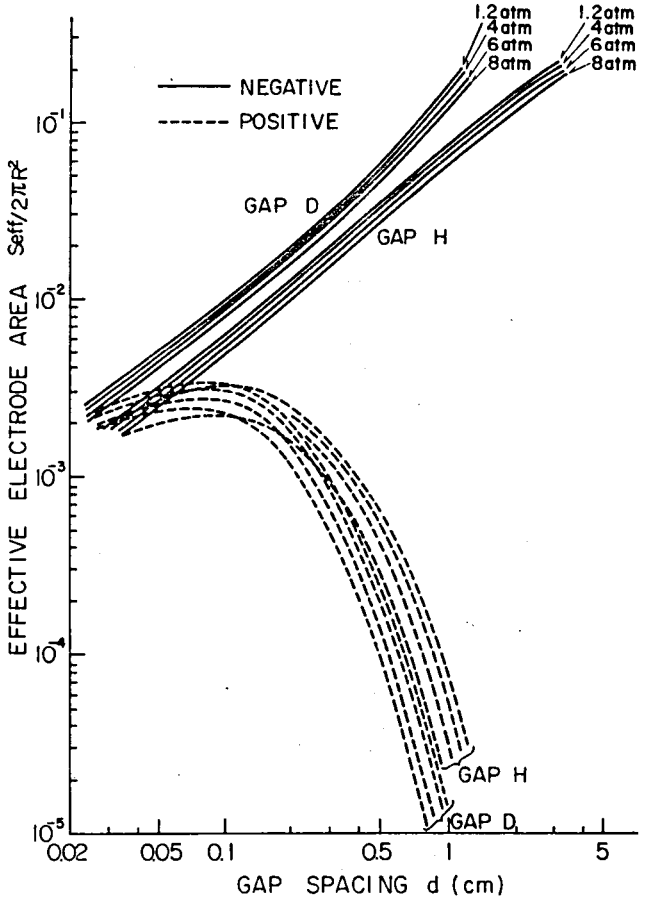


Fig.IV–2 Effective Electrode Area of Fine Finished Gap D and H, Gas Pressure as a Parameter